

AD A031644

REPORT JTCG/AS-74-T-015

FIELD OF INTEREST: 03  
16

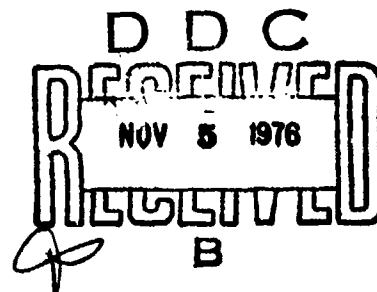


# FLUID DYNAMIC ANALYSIS OF HYDRAULIC RAM III (RESULT OF ANALYSIS)

FINAL REPORT

E.A. Lundstrom  
W.K. Fung

September 1976



Approved for public release; distribution unlimited; statement applied September 1976.

Prepared for

JOINT TECHNICAL COORDINATING GROUP  
FOR  
AIRCRAFT SURVIVABILITY

## FOREWORD

This report summarizes the results of research performed by the Naval Weapons Center, China Lake, CA. The work was conducted between July 1972 and December 1974, and Dr. E. A. Lundstrom and Mr. W. K. Fung were the Project Engineers.

The work was sponsored by JTCG/AS and Naval Air Systems Command Air Tasks A303-510A/216C/OW436-0000 and A330-330E/216B/IF32-432-308, as part of a 3-year TEAS (Test and Evaluation Aircraft Survivability) program. The TEAS program was funded by DDR&E/ODDT&E. The effort was conducted under the direction of the JTCG/AS Technology R&D Subgroup as part of TEAS element 5.1.1.11, *Hydraulic Ram Program*. Current effort in this area supported by JTCG/AS includes *Hydraulic Ram Fluid-Structure Interaction* study and *Hydraulic Ram Damage Prediction* analysis.

## DISCLAIMER

The estimates in this report are not to be construed as an official position of any of the Services or of the Joint AMC/NMC/AFLC/AFSC Commanders.

## NOTE

Information and data contained in this document are based on the reports available at the time of preparation, and the results may be subject to change.

ACCESSION for		
NTIS	White Section	<input checked="" type="checkbox"/>
DDC	Buff Section	<input type="checkbox"/>
UNANNOUNCED		<input checked="" type="checkbox"/>
JUSTIFICATION .....		
BY .....		
DISTRIBUTION/AVAILABILITY CODES		
Dist.	AVAIL.	and/or SPECIAL
A		

UNCLASSIFIED

SECURITY CLASSIFICATION OF THIS PAGE (When Data Entered)

REPORT DOCUMENTATION PAGE		READ INSTRUCTIONS BEFORE COMPLETING FORM
1. REPORT NUMBER (14) JTCG/AS-74-T-015	2. GOVT ACCESSION NO.	3. RECIPIENT'S CATALOG NUMBER (rept.)
4. TITLE (and Subtitle) (6) Fluid Dynamic Analysis of Hydraulic Ram III (Result of Analysis)	(9)	5. TYPE OF REPORT & PERIOD COVERED Final July 1972-December 1974
6. AUTHOR(s) (10) E.A. Lundstrom W.K. Fung		7. PERFORMING ORGANIS REPORT NUMBER
8. PERFORMING ORGANIZATION NAME AND ADDRESS Naval Weapons Center China Lake, CA 93555		9. CONTRACT OR GRANT NUMBER(s) A303-510A/216C/OW436-0000 A330-330E/216B/IF32-432-308
10. CONTROLLING OFFICE NAME AND ADDRESS JTCG/AS Central Office, AIR-5204J Naval Air Systems Command Washington, D.C. 20361	(11)	11. REPORT DATE September 1976
12. MONITORING AGENCY NAME & ADDRESS (if different from Controlling Office) (12) 128p.		12. NUMBER OF PAGES 134
		13. SECURITY CLASS. (of this report) Unclassified
14. DISTRIBUTION STATEMENT (of this Report) Approved for public release; distribution unlimited; statement applied September 1976.		14a. DECLASSIFICATION/DOWNGRADING SCHEDULE
15. DISTRIBUTION STATEMENT (of the abstract entered in Block 20, if different from Report)		
16. SUPPLEMENTARY NOTES		
17. KEY WORDS (Continue on reverse side if necessary and identify by block number) Hydraulic ram      Tumbling projectiles Aircraft survivability      Vulnerability Fuel system      Penetration		
18. ABSTRACT (Continue on reverse side if necessary and identify by block number) See reverse side.		

DD FORM 1 JAN 73 1473

EDITION OF 1 NOV 65 IS OBSOLETE  
S/N 0102-014-6601

UNCLASSIFIED

SECURITY CLASSIFICATION OF THIS PAGE (When Data Entered)

390990

1/B


UNCLASSIFIED

SECURITY CLASSIFICATION OF THIS PAGE(When Data Entered)

Naval Weapons Center

*Fluid Dynamic Analysis of Hydraulic Ram III (Result of Analysis)*, by E. A. Lundstrom and W. K. Fung. China Lake, CA, for Joint Technical Coordinating Group/Aircraft Survivability, September 1976, 134 pp. (Report JTCG/AS-74-T-015, publication UNCLASSIFIED.)

This report presents an analysis of the tests results of pressure waves generated by a penetrating projectile in fluid and verifies a theory modeling the pressure waves. The method of data reduction and verification also is presented.



UNCLASSIFIED

SECURITY CLASSIFICATION OF THIS PAGE(When Data Entered)

## TABLE OF CONTENTS

Introduction .....	1
Test Setup .....	1
Theoretical Considerations .....	2
Method of Analysis .....	5
Ballistic Testing .....	7
12.7 MM API .....	7
14.5 MM API .....	15
.50 Caliber API .....	18
.30 Caliber AP .....	23
Conclusions and Recommendations .....	120
Figures:	
1. Test Tank; (a) Side View and (b) Front View .....	3
2. Variation of the Velocity Decay Coefficient .....	4
3. Experimental Trajectory for Shot 1HR5 .....	25
4. Experimental Trajectory for Shot 1HR8 .....	25
5. Experimental Trajectory for Shot 1HR9 .....	26
6. Experimental Trajectory for Shot 1HR10 .....	26
7. Experimental Trajectory for Shot 1HR11 .....	27
8. Tumbling Distance Distribution; 0 Degree Obliquity, 0 Degree Yaw .....	28
9. Tumbling Distance Distribution; 30 to 45 Degrees Obliquity, 0 Degree Yaw .....	29
10. Peak Pressure—Theory Versus Experiment; 0 Degree Obliquity, 0 Degree Yaw .....	30
11. Impulse—Theory Versus Experiment; 0 Degree Obliquity, 0 Degree Yaw .....	30
12. Pressure Versus Time Plot for Shot 1HR8 .....	31
13. Pressure Versus Time Plot for Shot 1HR9 .....	34
14. Pressure Versus Time Plot for Shot 2HR11 .....	38
15. Pressure Versus Time Plot for Shot 2HR13 .....	42
16. Pressure Versus Time Plot for Shot 2HR14 .....	46
17. Pressure Versus Time Plot for Shot 2HR15 .....	50
18. Peak Pressure—Theory Versus Experiment; 0 Degree Obliquity, Tumbled .....	54
19. Impulse—Theory Versus Experiment; 0 Degree Obliquity, Tumbled .....	54
20. Pressure Versus Time Plot for Shot 2HR1 .....	55
21. Pressure Versus Time Plot for Shot 2HR5 .....	58
22. Peak Pressure—Theory Versus Experiment; 30 to 45 Degrees Obliquity, 0 Degree Yaw .....	62
23. Impulse—Theory Versus Experiment; 30 to 45 Degrees Obliquity, 0 Degree Yaw .....	62
24. Pressure Versus Time Plot for Shot 3HR2 .....	63

# JTCG/AS-74-T-015

25. Pressure Versus Time Plot for Shot 3HR10 .....	67
26. Peak Pressure—Theory Versus Experiment; 15 to 25 Degrees Obliquity, 0 Degree Yaw .....	71
27. Peak Pressure—Theory Versus Experiment; 0 to 0 Degree Obliquity, 0 Degree Yaw .....	71
28. Tumbling Distance Distribution; 0 Degree Obliquity, 0 Degree Yaw .....	72
29. Experimental Trajectory for Shot 4HR6 .....	73
30. Experimental Trajectory for Shot 4HR7 .....	73
31. Experimental Trajectory for Shot 4HR8 .....	74
32. Experimental Trajectory for Shot 4HR9 .....	74
33. Experimental Trajectory for Shot 4HR10 .....	75
34. Experimental Trajectory for Shot 4HR11 .....	75
35. Experimental Trajectory for Shot 4HR12 .....	76
36. Peak Pressure—Theory Versus Experiment; 0 Degree Obliquity, 0 Degree Yaw .....	77
37. Impulse—Theory Versus Experiment; 0 Degree Obliquity, 0 Degree Yaw .....	77
38. Pressure Versus Time Plot for Shot 4HR8 .....	78
39. Pressure Versus Time Plot for Shot 4HR9 .....	83
40. Pressure Versus Time Plot for Shot 4HR12 .....	88
41. Pressure Versus Time Plot for Shot 4HR12 .....	93
42. Peak Pressure—Theory Versus Experiment; 30 to 45 Degrees Obliquity, 0 Degree Yaw .....	98
43. Impulse—Theory Versus Experiment; 30 to 45 Degrees Obliquity, 0 Degree Yaw .....	98
44. Peak Pressure—Theory Versus Experiment; 15 to 25 Degrees Obliquity, 0 Degree Yaw .....	99
45. Peak Pressure—Theory Versus Experiment .....	99
46. Impulse—Theory Versus Experiment .....	100
47. Pressure Versus Time Plot for Shot 1HR3 .....	101
48. Pressure Versus Time Plot for Shot 1HR13 .....	105
49. Experimental Trajectory for Shot 4HR2 .....	109
50. Experimental Trajectory for Shot 4HR3 .....	109
51. Experimental Trajectory for Shot 4HR4 .....	110
52. Experimental Trajectory for Shot 4HR5 .....	110
53. Peak Pressure—Theory Versus Experiment .....	111
54. Impulse—Theory Versus Experiment .....	111
55. Pressure Versus Time Plot for Shot 4HR3 .....	112
56. Pressure Versus Time Plot for Shot 4HR5 .....	116

## Tables:

1. Experimental Conditions .....	8
2. Characteristics of the 12.7-mm API Round .....	8
3. Tumbling Distances .....	9
4. Pressure Pulse Summary .....	11
5. Experimental Conditions .....	16
6. Characteristics of the 14.5-mm API Round .....	16
7. Tumbling Distances .....	17

JTCG/AS-74-T-015

8. Pressure Pulse Summary .....	19
9. Experimental Conditions .....	21
10. Characteristics of the .50-Caliber API Round .....	21
11. Tumbling Distances .....	21
12. Pressure Pulse Summary .....	22
13. Experimental Conditions .....	23
14. Characteristics of the .30-Caliber AP Round .....	24
15. Tumbling Distances .....	24
16. Pressure Pulse Summary .....	24

## INTRODUCTION

During penetration of an incompressible fluid, bullets and other high speed projectiles generate intense pressure waves. Response of the fuel cell walls to these pressure waves can be catastrophic failure. This phenomenon, termed hydraulic ram, is of particular importance to the survivability of U.S. military aircraft. A simple model of the fluid mechanics<sup>1</sup> of hydraulic ram was developed and can be used to calculate fluid pressure due to a penetrating projectile.

To adequately model the pressure waves, the tumbling behavior of bullets must be specified along their trajectory. The model predicts that pressure waves generated by a bullet in a fully tumbled attitude will be approximately five times more intense than those generated by the same bullet in its normal, 0-degree yaw attitude.

Tumbling behavior is also of importance in calculating the bullets residual velocity after exiting the fuel cell. However, the tumbling is largely random in nature since it is initiated by small perturbations of the bullet attitude at impact.

The model was compared with an actual measurement of pressure generated by tumbling API (armor-piercing incendiary) rounds. Agreement between theory and experiment was reasonable, but it was recommended by NWC (Naval Weapons Center) that further gunfire tests be performed under rigid conditions to enhance confidence in the model predictions and to provide sufficient data to diagnose bullet tumbling distances.

## TEST SETUP

Fifty-three rounds\* of ammunition were fired into a water-filled test cell instrumented with five Kistler 601A pressure transducers. Ammunition used in these shots were .30 caliber AP (armor piercing), .50 caliber API, and 12.7 and 14.5 mm API. The rounds were fired at a 0-, 30-, or 45-degree obliquity angle and impacted on entrance panels of different materials and thicknesses. High speed motion pictures were taken of 23 of these shots.

The test cell was a 5-foot cube (Figure 1a) constructed of 1/8-inch-thick steel plates with angle iron reinforcements at the edges. A 1/2-inch steel plate at the rear wall prevented projectile exit of the cell. Entrance panels were 2 ft<sup>2</sup> and were held in place by compression between two rubber gaskets around the edges. Two 1-inch-thick plexiglass windows were placed on opposite sides of the cell to allow for high speed photography. The windows provided a 30-inch-high and 36-inch-long field-of-view. One window was sandblasted and, thus, acted as a diffusing screen for back-lighted photography.

---

<sup>1</sup>Naval Weapons Center. *Fluid Dynamic Analysis of Hydraulic Ram* by E. A. Lundstrom. China Lake, CA, NWC, July 1971. (NWC TP 5227, publication UNCLASSIFIED.)

\*One .30-caliber AP round (shot 4HR1) was not recorded due to transducer difficulties.



The pressure transducers were mounted onto one end of five 1/2-inch-diameter pipes extending beyond the open end of the cell. The other pipe ends, in turn, were mounted onto a separate frame isolated from shock and vibration in the test cell. The transducers were placed 6 inches above the expected trajectory at 6-inch intervals. Coordinates of the transducers with respect to the test cell are presented in Figure 1b.

The pressure transducer signals were recorded analog on magnetic tape and were digitized at 80 points/msec and calibrated. Digitizing rate was consistent with the 20-kHz response of the magnetic tape recorder.

Bullet velocity and impact point coordinates were measured. The coordinates of a second point on the trajectory were obtained from the bullet hole location in a thin, flexible plastic sheet installed behind the last transducer station (Figure 1a).

### THEORETICAL CONSIDERATIONS

To accurately predict hydraulic ram pressure due to ballistic projectiles, the theory (see Footnote 1) requires delineation of trajectory and rate of kinetic energy loss.

The decay of bullet velocity along the trajectory can be expressed as:

$$\frac{dV}{dX_b} = -\beta V \quad (1)$$

where

$X_b$  = bullet position

$V$  = bullet velocity

and the velocity decay coefficient is given by

$$\beta = \frac{1}{2m} \rho C_D A \quad (2)$$

where

$m$  = bullet mass

$A$  = presented area

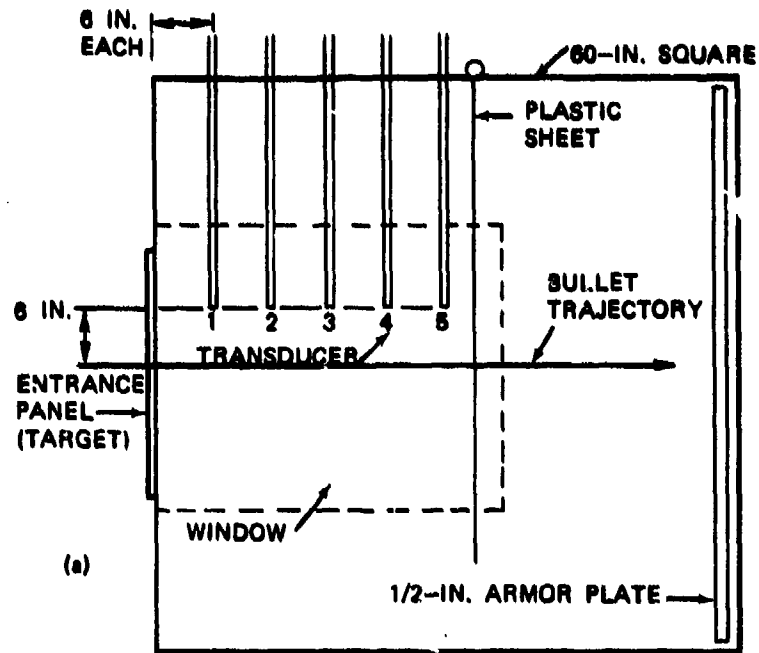
$C_D$  = drag coefficient

$\rho$  = fluid density

The rate at which the bullet kinetic energy,  $E$ , is lost is given by

$$\frac{dE}{dX_b} = m\beta V^2 \quad (3)$$

For tumbling bullets,  $\beta$  is a function of  $X_b$ .



DISTANCE ALONG AXIS, IN.

	TRANSDUCER				
AXIS	1	2	3	4	5
X	36	36	36	36	36
Y	30	30	30	30	30
Z	6	12	18	24	30

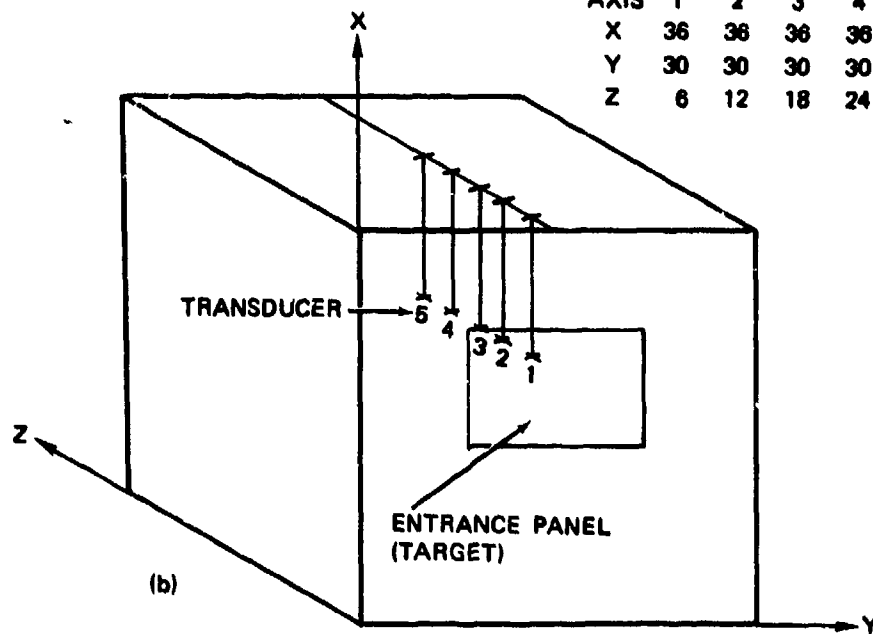


Figure 1. Test Tank; (a) Side View and (b) Front View.

In a previous report (NWC TP 5227), a simple model of the tumbling behavior was presented. The bullet is presumed to enter the test cell with 0 degree yaw and continue in this attitude with a constant drag coefficient until it reaches a distance,  $X_1$ , along its trajectory where it begins to tumble. The bullet becomes fully tumbled at a distance,  $X_2$ , and continues in this attitude with a constant drag coefficient.

For this simple tumbling model, the variation of  $\beta$  along the trajectory is shown in Figure 2. The coefficients  $\beta_1$  and  $\beta_2$  are associated with the 0- and 80-degree yaw and tumbled attitudes, respectively. Variation of  $\beta$  during bullet tumble is described by the relation

$$\beta(X_b) = \beta_1 + (\beta_2 - \beta_1) \left\{ \frac{1}{2} - \frac{1}{2} \cos \left[ \frac{X_b - X_1}{X_2 - X_1} \right] \right\}^n \quad (4)$$

A value of the exponent  $n = 3$  is used.

Evidence from high speed motion pictures of bullet penetration showed the simple tumbling model was incomplete. A bullet impacting the cell with 0 degree yaw continues to tumble along its trajectory for a number of cycles before assuming a stable attitude. To account for this, the model for the variation of  $\beta$  was extended to allow for continuous tumbling of the bullet, as shown by the broken line in Figure 2. The value  $\beta_3$  is associated with the drag coefficient of the bullet when it is in the stern-first attitude. For simplicity, it was assumed that the tumbling proceeds at a constant rate along the trajectory; that is

$$X_2 - X_1 = X_3 - X_2 = X_4 - X_3 = \dots$$

Equation 4 is used for the functional form of  $\beta(X_b)$  with the substitution of  $\beta_3$  for  $\beta_1$  when appropriate. The effect of the continuous tumbling model on the pressure traces is to sharply decrease the fall time. Substituting the continuous tumbling model for the simple tumbling model improved the agreement with the experimental pressure records.

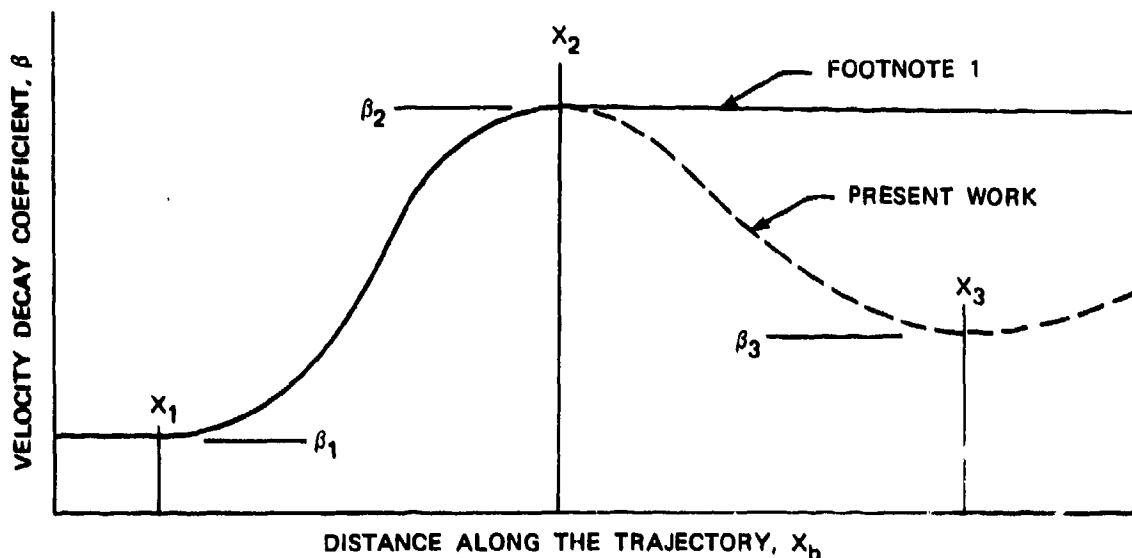


Figure 2. Variation of the Velocity Decay Coefficient.

During several of the tests it was noted that the jackets were stripped from the AP core of the API ammunition. The kinetic energy of the jacket and incendiary was approximately 40% of the kinetic energy of the complete round. Deposition of this energy into the fluid was evidenced by a distinct pulse on the experimental pressure records.

To account for the pressure pulse, a crude method for incorporating the jacket energy deposition into the hydraulic ram model was developed. The projectile penetrates the fluid in a normal fashion for a distance,  $X_s$ , where the jacket strips. The kinetic energy of the jacket and incendiary material is calculated at this point. The energy deposition of the AP core is calculated in the normal manner except that values of  $\beta$  appropriate to the core must be used. The energy deposition of the jacket is assumed to be exponential and is added to that of the core. The equation for total energy deposition is

$$\frac{dE}{dX_b} = m_c \beta_c V^2 + \frac{a E_{js}}{\beta_j} \cdot -\beta_j (X_b - X_s) \quad (5)$$

where  $c$  indicates properties of the core, and  $E_{js}$  is the kinetic energy of the jacket at  $X_s$ . The parameter  $\beta$  dictates the distance the jacket energy is deposited in the fluid. A reasonable value can be obtained from equation 2 using the jacket and incendiary mass (the area of the tumbled round) and a drag coefficient of 1. The factor  $a$  in equation 5 was included to allow for adjustment of the pulse height to agree with the experiment. A constant value of  $a = 1/3$  was used throughout the analysis and resulted in a reasonable description of the stripping pulse for most of the shots.

## METHOD OF ANALYSIS

A computer program was written which calculates pressures according to the theory with modifications to the trajectory behavior described in this report. Experimental pressure data were read into the program, and an rms error between experimental and theoretical pressures was calculated. The program was used as a subroutine which calculated the rms error as a function of tumbling distances  $X_1$  and  $X_2$ . The subroutine was incorporated into a computer program which calculated the particular values of the tumbling distances which, in turn, gave the minimum value of the rms error.

The size of the test cell was sufficiently large so pressure waves reflecting from the cell walls did not arrive at the transducer stations until approximately 1 msec after bullet impact. To avoid the complicating effects of wall reflections, the analysis included only the 1-msec interval. Wave reflections from the impact wall could not be ignored. Because of the lightweight construction of the entrance panel, it was assumed that the reflected pressure waves were reflected from a free surface. Then, the reflected pressure waves were calculated using the method of images. The use of free surface approximation and method of images is documented in NWC TP 5227.

Initial drag coefficient values for bullets in the 0-degree yaw attitude ( $C_D = 0.05$ ) and in the tumbled attitude ( $C_D = 0.30$ ) were obtained from a report<sup>2</sup> by McDonnell Douglas Corporation. The drag coefficient used for a bullet traveling in a stern-first attitude was  $C_D = 0.82$  corresponding to a circular disk. Using these drag coefficients, the tumbling distances were calculated by the computer program. The theoretical trajectories were compared with experimental trajectories measured from high speed motion pictures of the shots. Based on this comparison, the .30-caliber AP drag coefficient was doubled to  $C_D = 0.60$  for the fully tumbled attitude. The accuracy of the experimental trajectory measurements was not sufficient to obtain direct verification for the 0-degree yaw drag coefficient. Therefore, the initial part of the pressure pulse generated by the bullet in its 0-degree yaw attitude in theory and in experiment was compared.

Agreement was improved when the 0-degree yaw drag coefficient was doubled to  $C_D = 0.10$  for the .30-caliber AP and 14.5-mm API rounds. However, the 0-degree yaw drag coefficient was sensitive particularly to the bullet nose geometry, which can be distorted considerably during impact and penetration of the target panel. Therefore, it is expected that the 0-degree yaw drag coefficient will vary with impact obliquity and velocity as well as with target thickness and material. The drag coefficient for the AP core was taken as identical to that of the complete round.

Parameters governing the pressure pulse due to jacket stripping were obtained from the detailed analysis of several selected shots where the jacket stripping pulses were clear and distinct, and where high speed motion pictures were obtained. The parameter  $\beta_j$  in equation 5 was calculated initially according to equation 2 using the area of the tumbled round and the combined mass of the jacket and incendiary material. The width of the resulting stripping pressure pulse appeared reasonable when compared to experiment. Therefore this method for estimating  $\beta_j$  was followed in further analyses. The parameter  $a$  in equation 5 was chosen to give the correct amplitude for the stripping pressure pulse. The best value for the selected shots was  $a = 1/3$ , which was used in further analyses.

Some pressure records obtained during the tests were not acceptable. During several of the shots the pressure recorded by a gage appeared to "stick" at a finite pressure even after the fluid pressure decreased to zero. The gage became "unstuck" some tens of milliseconds later when the gage signal dropped abruptly to zero. This behavior probably was due to loose cable connectors. Such pressure records were discarded when they were identified.

A further source of error was caused by the unnoticed trapping of large air bubbles on the downward-facing pressure gage surface. The effect of the larger bubbles on the pressure gage response was to decrease the rise time of the gage and to introduce ringing. The magnitude of the effect depended on the air bubble size. The presence of large bubbles was determined easily by examining the rise time of the pressure record. Records with a slow rise time were not included in the analysis. However, the presence of smaller bubbles could not be detected easily, and it is believed that error in the theoretical predictions was due to this effect.

<sup>2</sup>McDonnell Douglas Corporation. *Hydraulic Ram: A Fuel Tank Vulnerability Study* by R. Yurkovich, St. Louis, MO, MDC, September 1969 (Report No. G964, publication UNCLASSIFIED).

The pressure wave model (see Footnote 1, page 1) assumes for simplicity that the bullet travels in a straight line. To obtain two points on the trajectory, a thin, flexible plastic sheet was placed 6 inches behind the last transducer station, and the coordinates of the resulting bullet holes were measured. Initially, the pressure pulse analysis assumed that the bullets traveled in a straight line between the impact point and the penetration point on the plastic sheet. However, it was found that the agreement between experiment and theory was increased if the plastic sheet coordinates were ignored, and it was assumed, instead, that the bullet penetrated the fluid undeflected from its original straight line path. Improved agreement was because the bullet impacted at 0 degree obliquity and did not deflect significantly from its original path until after it had tumbled. Thus, the early portion of the pressure pulse, which contributed the most to the rms error, was not affected by subsequent bullet deflections. There was no observable correlation between the rms error and the measured bullet deflection.

## BALLISTIC TESTING

### 12.7 MM API

Thirty shots were fired at service velocity into the test cell at 0-, 30-, or 45-degree obliquity angles, as shown in Table 1. Four rounds impacted in a tumbled attitude. Entrance panels of the test cell were constructed from rubber used for self-sealing fuel tanks or 7075-T6 aluminum in one of three thicknesses (Table 1).

Physical parameters of the shots are given in Table 2. The drag coefficients presented are those which gave the best overall agreement of experimental data with theory.

The tumbling distances were derived from the pressure pulses and are summarized in Table 3.

Of the 18 shots fired into the test cell at 0 degree obliquity and 0 degree yaw, the jacket was stripped from only one (1HR7). For shots 1HR5, 8, 9, 10, and 11, verification of tumbling distance,  $X_2$ , was obtained from high speed motion pictures. The distance from the impact point to the point on the trajectory with maximum cavity radius was measured and the result is included in Table 3. The experimental and the derived tumbling distance,  $X_2$ , correspond for these five shots. The measured tumbling distance should be slightly less than the derived value because of the cavity radius dependence on bullet velocity.

Experimental trajectories for these five shots are shown in Figures 3 through 7 (page 25) with the theoretical curves. Error in the experimental points is estimated to be  $\pm 1/2$  inch, and no consideration was given for the bullet's departure from a straight line. In general, the agreement is acceptable except at long penetration distances; probably caused by deviations from the assumed straight line path which would give a decrease in velocity.

Due to error in making the trajectory measurements, deceleration of the bullet in its 0-degree yaw attitude could not be determined. However, because of the similarity of the trajectories shown in Figures 3 through 7 and agreement of the detailed pressure pulse shape, it is concluded that the trajectory model used for these shots is valid and the drag coefficients used for the 12.7 mm API are adequate.

Table 1. Experimental Conditions.

Shot	Velocity, ft/sec	Entrance panel		Impact coordinates, in.		Obliquity, deg	Yaw attitude, deg
		Rubber	Al, in.	X	Y		
1HR5	2,897	X	...	...	...	0	0
1HR6	2,762	X	...	...	...	0	0
1HR7	2,717	X	...	...	...	0	0
1HR8	2,733	...	0.063	30.75	31.50	0	0
1HR9	2,725	...	0.063	30.75	31.50	0	0
1HR10	2,729	...	0.160	30.50	30.00	0	0
1HR11	2,701	...	0.160	30.75	31.25	0	0
2HR1	...	...	0.063	31.50	31.00	0	Tumbled
2HR2	2,734	...	0.063	30.00	31.25	0	Tumbled
2HR3	2,736	...	0.063	31.00	31.25	0	0
2HR4	2,734	...	0.190	31.25	31.25	0	Tumbled
2HR5	2,734	...	0.190	31.25	31.00	0	Tumbled
2HR6	2,743	...	0.190	31.50	31.50	0	0
2HR7	2,719	...	0.063	30.25	31.25	0	0
2HR8	2,686	...	0.063	31.25	31.50	0	0
2HR9	2,749	...	0.063	31.25	31.25	0	0
2HR10	2,759	...	0.063	31.75	31.25	0	0
2HR11	2,643	...	0.190	30.75	32.00	0	0
2HR12	2,752	...	0.190	...	...	0	0
2HR13	2,752	...	0.190	31.50	31.75	0	0
2HR14	2,752	...	0.190	31.25	32.00	0	0
2HR15	2,733	...	0.190	31.25	29.25	0	0
3HR1	2,773	...	0.063	32.00	30.50	30	0
3HR2	2,742	...	0.063	32.00	30.75	30	0
3HR3	2,742	...	0.063	32.75	30.25	30	0
3HR4	2,760	...	0.063	31.50	30.25	30	0
3HR9	2,770	...	0.063	31.50	30.00	45	0
3HR10	2,758	...	0.063	30.50	29.50	45	0
3HR11	2,737	...	0.063	31.75	30.25	45	0
3HR12	2,754	...	0.063	31.25	29.25	45	0

Table 2. Characteristics of the 12.7-mm API Round.

Bullet weight = 0.166 pounds; core weight = 0.064 pounds.

Yaw angle, deg	Bullet area, in <sup>2</sup>	Core area, in <sup>2</sup>	Drag coefficient
0	0.2046	0.1432	0.05
90	1.0370	0.7002	0.30
180	0.0855	...	0.82

## JTCG/AS-74-T-015

Table 3. Tumbling Distances.

Shot	X <sub>1</sub> , in.	X <sub>2</sub> - X <sub>1</sub> , in.	X <sub>2</sub> , in.	X <sub>s</sub> , in.	X <sub>2</sub> (experiment), in.
1HR5	7.42	8.29	15.71	...	16
1HR6	7.13	8.44	15.57	...	...
1HR7	0.01	8.94	8.95	1.0	...
1HR8	10.01	7.92	17.93	...	17
1HR9	5.13	10.53	15.66	...	12
1HR10	4.92	11.21	16.13	...	15
1HR11	4.93	11.61	16.54	...	15
2HR3	4.82	9.88	14.70	...	...
2HR6	7.08	12.22	19.30	...	...
2HR7	3.02	13.72	16.74	...	...
2HR8	8.47	9.71	18.18	...	...
2HR9	5.37	11.40	16.77	...	...
2HR10	5.13	11.40	16.53	...	...
2HR11	12.36	10.88	23.24	...	...
2HR12	4.27	9.50	13.77	...	...
2HR13	4.82	9.88	14.70	...	...
2HR14	6.55	9.31	15.86	...	...
2HR15	5.44	10.64	16.08	...	...
Average	5.94	10.30	16.24		
2HR1	-4.93	...	5.13	...	...
2HR2	-2.90	...	4.13	0.6	...
2HR4	-6.35	...	3.15	...	...
2HR5	-6.15	...	3.59	...	...
3HR1	4.81	10.78	15.59	...	...
3HR2	4.11	8.53	12.64	...	...
3HR3	4.11	7.63	11.74	...	...
3HR4	0.32	13.17	13.49	...	...
Average	3.34	10.03	13.37	...	...
3HR9	3.00	10.15	13.15	...	...
3HR10	3.50	7.44	10.94	...	...
3HR11	3.51	7.01	10.52	...	...
3HR12	2.37	8.04	10.41	...	...
Average	3.10	8.16	11.26	...	...



Distribution of  $X_1$  and  $X_2$  is shown in Figure 8 for impact at 0 degree obliquity, 0 degree yaw. Shot 1HR7, where the jacket stripped, is not included. There is a wide distribution for both  $X_1$  and  $X_2$ . Their average values are  $X_1 = 5.94$  inches and  $X_2 = 16.24$  inches. (Note that tumbling distance  $X_2$  varies by as much as a factor of 2.)

Four shots (2HR1, 2, 4, and 5 in Table 3) were tumbled prior to impact at 0 degree obliquity. Analysis of these tumbled shots proceeded in a different manner than those which impacted in the 0-degree yaw attitude. First, it was assumed that, when the shots attained a fully tumbled attitude, they remained in that state. Second, since the exact attitude of the bullet at impact could not be controlled or measured,  $X_1$  was allowed to become negative during the analysis. Tumbling distances minimized the rms deviation of the experimental and theoretical pressure traces. The jacket was stripped from one of the tumbled shots.

Four rounds were fired into the test cell at 30 degrees obliquity and four were fired at 45 degrees. Obliquity angle was obtained by rotation of the test cell. A 1/2-inch-thick steel plate was placed internally on the plate side to protect the plexiglass cell. Therefore motion picture coverage of these shots could not be obtained. There was poor correlation between experimental and theoretical pressure pulses, but the tumbling distances should be accurate. Distribution of the derived tumbling distances is shown in Figure 9. Although there were not enough shots performed to provide adequate statistics of these tumbling distances, it appears that tumbling occurs more rapidly with increased entrance obliquity angle.

Decrease in the tumbling distances with increased obliquity is to be expected since the bullet experiences highly nonsymmetric forces during oblique penetration of the impact plate. Nonzero obliquity shots were performed at velocities which exceeded the ballistic limit. It is expected that the influence of obliquity on tumbling distances will be more pronounced near the ballistic limit.

A summary of the pressure pulse analysis is presented in Table 4, which includes experimental and calculated values of peak pressure and impulse. Also shown in the table is the rms deviation of experimental and theoretical pressure traces.

For impact at 0 degree obliquity and 0 degree yaw, the rms deviation divided by the experimental peak pressure (Table 4) is a good indication that the pressure model is valid.

Theoretical and experimental peak pressure and impulse are plotted in Figures 10 and 11, respectively. Bullet departure from the 45-degree straight line, as shown in both figures, indicates the extent of the error. The amount of scatter in Figures 10 and 11 is not unusual since the transducers were located near the bullet trajectory. A 2-inch deflection of the bullet from a straight line trajectory would give a 30% error in the predicted pressure.

Theoretical and experimental pressure pulses are shown in Figures 12 through 17 for six representative shots with these impact conditions. These shots were selected to have errors ranging from minimum to maximum.

Tumbled entry data for peak pressure and impulse are shown in Figures 18 and 19, respectively. Agreement of theory and experiment is similar to that obtained for impact at 0 degree yaw. Pressure traces from two of these shots (2HR1 and 2HR5) are shown in Figures 20 and 21.

## JTCG/AS-74-T-015

Table 4. Pressure Pulse Summary.

Shot	PGA	Peak pressure, psi		Impulse, psi-msec		rms deviation, psi	rms error parameter
		Experiment	Theory	Experiment	Theory		
1HR5	1	...	...	...	...	...	...
	2	720	740	209	213	46	0.064
	3	815	1,140	195	251	143	0.175
	4	670	910	142	212	150	0.224
	5	520	655	100	140	106	0.204
1HR6	1	...	...	...	...	...	...
	2	870	730	246	248	68	0.078
	3	945	1,100	240	248	90	0.095
	4	750	870	169	206	100	0.133
	5	550	625	105	134	80	0.145
1HR7	1	460	990	140	153	119	0.259
	2	578	720	149	210	115	0.199
	3	...	...	...	...	...	...
	4	378	430	70	122	95	0.251
	5	349	347	55	75	50	0.143
1HR8	1	...	...	...	...	...	...
	2	500	545	191	196	46	0.092
	3	...	...	...	...	...	...
	4	880	940	208	224	76	0.086
	5	640	658	135	142	57	0.089
1HR9	1	255	346	127	142	49	0.192
	2	750	767	223	269	48	0.064
	3	...	...	...	...	...	...
	4	695	810	153	215	113	0.163
	5	510	569	105	134	74	0.145
1HR10	1	...	...	...	...	...	...
	2	640	740	225	236	72	0.113
	3	...	...	...	...	...	...
	4	1,450	800	197	217	379	0.261
	5	510	585	116	136	73	0.143
1HR11	1	...	...	...	...	...	...
	2	930	690	332	232	142	0.153
	3	...	...	...	...	...	...
	4	920	790	256	218	87	0.095
	5	585	555	134	136	59	0.101
2HR1	1	...	...	...	...	...	...
	2	...	...	...	...	...	...
	3	562	545	129	215	141	0.251
	4	442	420	83	121	84	0.190
	5	420	338	65	71	49	0.117

Table 4. Pressure Pulse Summary (Contd).

Shot	PGA	Peak pressure, psi		Impulse, psi-msec		rms deviation, psi	rms error parameter
		Experiment	Theory	Experiment	Theory		
2HR2	1	830	810	203	164	58	0.070
	2	...	...	...	...	...	...
	3	710	595	134	174	82	0.115
	4	480	450	84	108	66	0.138
	5	400	360	62	68	38	0.095
2HR3	1	310	365	120	133	65	0.211
	2	...	...	...	...	...	...
	3	755	1,250	200	263	192	0.254
	4	615	800	153	206	121	0.197
	5	500	530	113	129	70	0.140
2HR4	1	1,350	1,070	177	168	65	0.048
	2	...	...	...	...	...	...
	3	680	620	98	134	95	0.140
	4	780	490	60	74	113	0.145
	5	440	400	48	45	62	0.141
2HR5	1	775	940	220	202	111	0.143
	2	...	...	...	...	...	...
	3	520	520	149	186	66	0.127
	4	405	395	66	104	81	0.200
	5	355	315	53	62	42	0.118
2HR6	1	500	230	102	120	72	0.144
	2	...	...	...	...	...	...
	3	970	1,140	288	319	96	0.099
	4	1,075	1,025	261	278	138	0.128
	5	800	680	170	168	85	0.106
2HR7	1	300	290	137	121	27	0.090
	2	...	...	...	...	...	...
	3	780	920	213	264	107	0.137
	4	870	725	195	213	120	0.138
	5	560	520	114	136	88	0.157
2HR8	1	500	240	78	112	76	0.152
	2	...	...	...	...	...	...
	3	1,050	1,100	292	285	64	0.061
	4	900	950	226	238	213	0.237
	5	690	650	139	145	64	0.093
2HR9	1	580	290	82	130	100	0.172
	2	...	...	...	...	...	...
	3	950	1,190	258	299	142	0.149
	4	845	890	195	238	114	0.135
	5	630	610	132	146	69	0.110

Table 4. Pressure Pulse Summary (Contd.).

Shot	PG <sup>a</sup>	Peak pressure, psi		Impulse, psi-msec		rms deviation, psi	rms error parameter
		Experiment	Theory	Experiment	Theory		
2HR10	1	200	310	98	139	67	0.335
	2	...	...	...	...	...	...
	3	760	1,265	244	321	232	0.305
	4	800	920	185	250	152	0.190
	5	610	610	126	149	83	0.136
2HR11	1	320	165	81	80	36	0.113
	2	...	...	...	...	...	...
	3	550	570	207	216	40	0.073
	4	1,200	950	300	239	130	0.108
	5	970	760	202	159	109	0.112
2HR12	1	240	400	106	129	71	0.296
	2	...	...	...	...	...	...
	3	730	1,050	187	238	169	0.232
	4	600	760	148	189	104	0.173
	5	480	500	108	122	62	0.129
2HR13	1	320	380	116	139	74	0.231
	2	...	...	...	...	...	...
	3	800	1,200	213	278	209	0.261
	4	680	830	159	216	128	0.188
	5	540	580	113	134	81	0.150
2HR14	1	250	320	116	124	66	0.264
	2	...	...	...	...	...	...
	3	1,000	1,200	254	237	95	0.095
	4	770	890	183	221	96	0.125
	5	560	620	125	139	65	0.116
2HR15	1	200	315	90	132	71	0.355
	2	...	...	...	...	...	...
	3	745	1,200	200	292	257	0.345
	4	700	865	170	229	138	0.197
	5	560	590	123	139	67	0.120
3HR1	1	345	310	115	107	50	0.145
	2	1,250	555	368	178	289	0.231
	3	900	587	260	160	169	0.188
	4	720	480	170	123	96	0.133
	5	510	392	116	90	58	0.114

Table 4. Pressure Pulse Summary (Contd).

Shot	PG <sup>a</sup>	Peak pressure, psi		Impulse, psi-msec		rms deviation, psi	rms error parameter
		Experiment	Theory	Experiment	Theory		
3HR2	1	490	460	158	137	59	0.120
	2	1,900	745	500	177	500	0.263
	3	...	...	...	...	...	...
	4	700	500	163	103	99	0.141
	5	510	390	105	76	62	0.122
3HR3	1	622	520	174	144	158	0.254
	2	1,870	795	476	175	457	0.244
	3	...	...	...	...	...	...
	4	790	500	237	98	176	0.223
	5	590	390	126	72	127	0.215
3HR4	1	625	406	179	135	88	0.141
	2	2,050	615	550	181	598	0.292
	3	...	...	...	...	...	...
	4	750	435	192	110	128	0.171
	5	560	340	111	81	79	0.141
3HR9	1	282	295	110	88	64	0.227
	2	1,270	410	338	109	339	0.267
	3	...	...	...	...	...	...
	4	750	317	173	171	193	0.257
	5	560	263	121	57	137	0.245
3HR10	1	460	340	156	75	133	0.289
	2	1,680	445	433	93	546	0.325
	3	...	...	...	...	...	...
	4	740	330	187	58	207	0.280
	5	550	275	114	47	142	0.258
3HR11	1	480	455	149	147	93	0.194
	2	1,575	540	420	200	482	0.306
	3	1,130	445	317	82	362	0.320
	4	740	355	187	59	202	0.273
	5	540	290	113	45	139	0.257
3HR12	1	505	355	146	82	106	0.210
	2	1,340	452	375	95	421	0.314
	3	...	...	...	...	...	...
	4	725	325	204	57	220	0.303
	5	...	...	...	...	...	...

<sup>a</sup>Where information is left blank (...) that particular gage was not working properly and readings were incorrect.

For shots with 30 and 45 degrees obliquity, theoretical predictions of peak pressure and impulse are plotted against experimental values in Figures 22 and 23, respectively. The predicted pulse shape shown in the figures is unsatisfactory as the theory consistently underestimates the pressure.

Plots of the experimental pressure pulses for shots 3HR2 and 3HR10 are shown with the theoretical curves in Figures 24 and 25. In general, the predicted pulse shape is correct; however, the magnitude of the pressure is too low, particularly for PG2. It should be noted that the peak pressures measured at PG2 for the 30- and 45-degree obliquity shots are consistently higher than those recorded for the 0-degree shots. The bullet was presumed to have traveled in an undeflected straight line so higher pressures were recorded when the bullet was far from the transducer. Either the pressure measurements were in error or the assumptions of the trajectory model were incorrect.

Pressures were measured with Kistler 601A pressure transducers. These transducers are not acceleration compensated, and it is possible that the unusually high pressures were due to acceleration effects. In addition, it is possible the calibration of the transducers was in error.

Assuming that the pressure measurements were correct, there are several physical explanations for the nonconformity. Bullets impacting the test cell at nonzero obliquity experience intense nonsymmetric forces while penetrating the aluminum panel. Bullets could be deformed more for the 30- and 45-degree obliquity shots than for the 0-degree shots where the impact forces are symmetric. This premise was tested by performing an analysis of the pressures using doubled drag coefficients. Some improvement was obtained; however, there remained a substantial error.

Also, asymmetric impact forces could produce a deflection in the bullet trajectory. The plastic sheet was placed in the cell for these shots, and the coordinates were recorded. These data could not be used to determine the initial bullet deflection because of the scatter in the data and the possibility of ricochets from the cell walls. The problem of bullet deflection therefore was tested by repeating the pressure wave analysis with assumed deflection angles. The 30-degree obliquity shots were presumed to be deflected to 0 and 15 degrees while the 45-degree shots were presumed to be deflected to 0 and 25 degrees. The same drag coefficients were used as those used for the basic 0-degree obliquity shots. Theoretical predictions of peak pressure are plotted against the experimental values in Figures 26 and 27. Figure 26 assumes the bullets are deflected from 30 and 45 degrees to 15 and 25 degrees obliquity, while Figure 27 assumes deflection to 0 degree obliquity. These figures show substantial improvement in the theoretical predictions when compared to Figure 22 for the undeflected bullet. The average rms error parameter was 0.234 for undeflected bullets, 0.157 for bullets deflected to 15 and 25 degrees, and 0.157 for deflection to 0 degree obliquity. It is concluded that there is a substantial initial deflection of bullets which impact at nonzero obliquities, and that the deflection significantly affects the pressure fields.

#### 14.5 MM API

Twelve shots were fired at service velocity with a 0-degree yaw attitude at impact. The experimental conditions for each shot are shown in Table 5. Physical parameters of the shots are presented in Table 6. The drag coefficients presented are those which gave the best agreement of theory with the 0-degree obliquity shots. Tumbling distances were derived from the pressure pulses and are shown in Table 7.

Table 5. Experimental Conditions.

Shot	Velocity, ft/sec	Entrance panel, in. Al	Impact coordinates, in.		Obliquity, deg	Yaw attitude, deg
			X	Y		
1HR14	3,217	0.063	29.00	31.00	0	0
3HR5	3,172	0.063	31.50	30.00	30	0
3HR6	3,182	0.063	31.50	30.00	30	0
3HR7	3,182	0.063	31.00	28.25	45	0
3HR8	3,185	0.063	31.50	28.50	45	0
4HR6	3,150	0.063	31.00	31.25	0	0
4HR7	3,507	0.063	30.50	30.50	0	0
4HR8	3,464	0.063	30.50	30.25	0	0
4HR9	3,027	0.063	30.13	30.00	0	0
4HR10	3,088	0.063	30.75	30.25	0	0
4HR11	3,112	0.063	30.13	29.75	0	0
4HR12	3,076	0.190	30.50	30.50	0	0

Table 6. Characteristics of the 14.5-mm API Round.

Bullet weight = 0.1376 pounds; core weight = 0.0936 pounds.

Yaw angle, deg	Bullet area, in <sup>2</sup>	Core area, in <sup>2</sup>	Drag coefficient
0	0.280	0.188	0.10
90	1.322	1.050	0.30
180	0.126	...	0.82

The jacket was stripped from six of the 0-degree obliquity shots producing a distinct pulse on the pressure records. Tumbling distance,  $X_2$ , was measured from the point of maximum cavity radius on high speed motion picture frames and the values are shown in the last column of Table 7. Experimental and theoretical values of  $X_2$  are in reasonable correlation except for shot 1HR9. For this shot, the maximum cavity radius corresponded to the point of jacket stripping,  $X_s$ , rather than  $X_2$ . Distribution of  $X_1$  and  $X_2$  is shown in Figure 28. There is no indication that jacket stripping influences tumbling distance distribution.

Table 7. Tumbling Distances.

Shot	X <sub>1</sub> , in.	X <sub>2</sub> - X <sub>1</sub> , in.	X <sub>2</sub> , in.	X <sub>s</sub> , in.	X <sub>2</sub> (experiment), in.
1HR14	3.28	9.76	13.04	5	...
4HR6	7.53	6.73	14.26	...	18.0
4HR7	5.85	11.86	17.71	3	21.0
4HR8	3.53	11.25	14.78	...	17.0
4HR9	1.38	9.59	10.97	4	6.5
4HR10	0.42	10.61	11.03	5	10.0
4HR11	3.30	8.64	11.94	6	10.0
4HR12	4.69	12.20	16.89	4	18.0
Average	3.75	10.08	13.83	...	...
<hr/>					
3HR5	2.53	7.24	9.77	...	...
3HR6	3.09	8.32	11.41	...	...
Average	2.81	7.78	10.59	...	...
<hr/>					
3HR7	2.30	6.67	8.97	...	...
3HR8	1.67	6.48	8.15	...	...
Average	1.99	6.58	8.56	...	...

Trajectories of seven rounds (4HR6, 7, 8, 9, 10, 11, and 12) were measured to confirm the drag coefficient values used in the analysis. Theoretical trajectories are plotted with experimental points in Figures 29 through 35. Error in the trajectory measurements is estimated to be  $\pm 1/2$  inch, assuming that the round traveled in a straight line. Agreement is excellent for shot 4HR9 as shown in Figure 32; but, in general, it appears that the drag coefficient used for the tumbled attitude may be too low. Due to its low magnitude, the drag coefficient in the 0-degree yaw attitude cannot be determined from the trajectory, but was chosen to give the best agreement with the pressure pulses.

Four of the 14.5-mm shots were performed with nonzero obliquity angles, two each at 30 and 45 degrees. The test procedures are identical to those described for the 12.7-mm API, nonzero obliquity shots.

Shots fired at 30 degrees obliquity did not evidence the jacket being stripped. Shots fired at 45 degrees indicated a distinct pressure pulse arising from the jacket stripping, but this was ignored in the analysis. Tumbling distances decreased with increased obliquity, similar to the 12.7 mm API. There were two shots, one each at 30 and 45 degrees, which are exceedingly poor statistical samples. However, the trend agrees with the suggestion that nonsymmetric forces acting on nonzero obliquity shots during impact produce a quicker bullet tumble.



A summary of the pressure pulse analysis for the 14.5-mm API round is presented in Table 8.

For impact at 0 degree obliquity, the low values of the rms error parameter (Table 8) indicate theoretical and experimental pressure pulse shapes are similar. Theoretical and experimental peak pressure and impulse data are compared in Figures 36 and 37. Bullet departure from the 45-degree straight line, as shown in each of these figures, indicates the extent of the error. Good correlation was obtained between experiment and theory.

Theoretical and experimental pressure traces are compared in Figures 38, 39, and 40. Figure 38 gives plots of the pressure traces for shot 4HR8 which had an average rms error parameter of 0.111. The jacket apparently did not strip from this round. The initial pressure spike, which is particularly prominent in PG1, is a common feature of several of the pressure traces. It is due either to overshoot of the recording equipment or it may evidence the shock phase overpressure.

Pressure plots for shots 4HR9 and 4HR12 are shown in Figures 39 and 40, respectively. The jacket was stripped from both of these rounds, and the resulting pressure pulse can be seen. The crudeness of the stripping pressure model is obvious from these figures. However, Figure 41 gives the pressure pulse for shot 4HR12 that would result if the jacket stripping behavior was ignored. Improved agreement of experiment with theory is derived by inclusion of the stripping process, as is evident when Figures 40 and 41 are compared.

For the 30- and 45-degree obliquity shots, theoretical peak pressure and impulse are plotted against experimental values in Figures 42 and 43. The correlation of theory and experiment shown in the figures is inadequate. Both peak pressure and impulse are consistently underestimated by theory. This lack of correlation for the nonzero obliquity shots was discussed in the section on 12.7 mm API. As was stated, the correlation of experiment and theory could be improved if the assumption that the bullet tumbled in an unperturbed straight line was eased. The pressure pulse analysis was repeated assuming that the initial 30- and 45-degree obliquity shots were deflected on impact to 15 and 25 degrees, respectively. Results of the peak pressure are plotted in Figure 44. Experiment and theory agree better when bullets are assumed to deflect (Figures 42 and 44).

#### .50 CALIBER API

Six of the shots were .50-caliber API rounds fired at 0 degree obliquity into rubber or aluminum panels, as shown in Table 9. Four of the rounds impacted in a tumbled attitude. Characteristics of the .50-caliber API round are presented in Table 10.

The tumbling distances (Table 11) were obtained from the pressure pulse analysis. It was determined that the jackets were stripped in each shot. Experimental values of  $X_2$ , obtained from high speed motion pictures, are included in Table 10 for the two 0-degree yaw impact shots. Reasonable agreement exists with the corresponding values obtained from the pressure pulse analysis.

Table 8. Pressure Pulse Summary.

Shot	PG <sup>a</sup>	Peak pressure, psi		Impulse, psi-msec		rms deviation, psi	rms error parameter
		Experiment	Theory	Experiment	Theory		
1HR14	1	815	950	189	161	95	0.116
	2	1,200	1,425	315	251	132	0.110
	3	...	...	...	...	...	...
	4	1,030	975	237	213	76	0.074
	5	820	730	159	152	71	0.087
3HR5	1	1,150	830	257	181	196	0.170
	2	1,800	1,150	425	218	318	0.177
	3	1,270	950	296	181	197	0.155
	4	940	745	196	137	128	0.136
	5	750	585	143	97	112	0.149
3HR6	1	650	660	195	178	84	0.129
	2	1,900	1,020	432	220	335	0.176
	3	1,600	920	338	180	260	0.163
	4	1,200	725	250	136	199	0.166
	5	910	570	179	103	145	0.159
3HR7	1	1,125	670	279	85	314	0.279
	2	1,500	820	412	123	429	0.286
	3	1,100	700	324	103	346	0.315
	4	800	580	190	84	195	0.244
	5	625	490	134	66	151	0.242
3HR8	1	1,470	825	304	106	331	0.225
	2	1,650	930	399	134	412	0.250
	3	1,230	775	270	109	278	0.226
	4	870	635	163	82	167	0.192
	5	675	525	174	57	214	0.317
4HR6	1	490	510	172	173	132	0.269
	2	1,300	1,270	374	298	111	0.085
	3	1,700	1,815	415	312	151	0.089
	4	1,300	1,380	378	273	127	0.098
	5	...	...	...	...	...	...

Table 8. Pressure Pulse Summary (Contd.).

Shot	PG <sup>a</sup>	Peak pressure, psi		Impulse, psi-msec		rms deviation, psi	rms error parameter
		Experiment	Theory	Experiment	Theory		
4HR7	1	1,350	1,800	214	176	196	0.145
	2	1,450	1,700	349	331	155	0.107
	3	1,125	1,525	349	385	220	0.196
	4	880	1,400	292	344	244	0.277
	5	680	1,020	175	251	211	0.310
4HR8	1	560	610	172	206	79	0.141
	2	1,800	1,450	449	366	156	0.087
	3	2,040	2,000	495	386	231	0.113
	4	1,580	1,560	404	333	156	0.099
	5	1,190	1,175	217	252	137	0.115
4HR9	1	1,025	1,170	229	183	117	0.114
	2	1,500	1,200	362	255	158	0.105
	3	1,175	1,060	283	240	90	0.077
	4	920	775	211	186	82	0.089
	5	750	590	129	133	71	0.095
4HR10	1	900	1,320	230	217	150	0.167
	2	1,650	1,640	353	301	149	0.090
	3	1,300	1,240	251	273	99	0.076
	4	960	880	170	206	116	0.121
	5	730	680	109	128	91	0.125
4HR11	1	770	1,200	188	187	101	0.131
	2	1,380	1,470	333	270	152	0.110
	3	1,230	1,350	264	264	105	0.085
	4	920	950	184	217	118	0.128
	5	950	820	112	144	210	0.221
4HR12	1	1,050	1,400	237	171	193	0.184
	2	1,200	1,480	374	300	163	0.136
	3	1,100	1,120	364	320	144	0.131
	4	780	910	269	266	143	0.183
	5	720	670	146	176	138	0.192

<sup>a</sup>Where information is left blank ( . . ) that particular gage was not working properly and readings were incorrect.

JTCG/AS-74-T-015

Table 9. Experimental Conditions.

Shot	Velocity, ft/sec	Entrance panel		Impact coordinates, in.		Obliquity, deg	Yaw attitude, deg
		Rubber	A <sub>g</sub> , in.	X	Y		
1HR1	2,882	X	...	...	...	0	Tumbled
1HR2	2,902	X	...	...	...	0	Tumbled
1HR3	2,928	...	0.063	30.50	31.50	0	Tumbled
1HR4	2,873	...	0.160	31.50	34.50	0	Tumbled
1HR12	3,006	X	...	...	...	0	0
1HR13	3,018	...	0.063	30.25	31.75	0	0

Table 10. Characteristics of the .50-Caliber API Round.

Bullet weight = 0.090 pounds; core weight = 0.064 pounds.

Yaw angle, deg	Bullet area, in <sup>2</sup>	Core area, in <sup>2</sup>	Drag coefficient
0	0.205	0.143	0.05
90	0.736	0.598	0.30
180	0.112	...	0.82

Table 11. Tumbling Distances.

Shot	X <sub>1</sub> , in.	X <sub>2</sub> - X <sub>1</sub> , in.	X <sub>2</sub> , in.	X <sub>s</sub> , in.	X <sub>2</sub> (experiment), in.
1HR1	-5.54	12.34	6.80	0.4	...
1HR2	-0.15	3.80	3.65	0.4	...
1HR3	0.45	1.01	1.46	0.4	...
1HR4	-1.41	3.11	1.70	0.4	...
1HR12	11.68	7.67	19.35	2.0	18
1HR13	5.04	9.39	14.43	6.0	18

Results of the pressure pulse analysis is summarized in Table 12. Low values of the error parameter given in the last column of the table indicate theoretical and experimental pressure pulse shapes are similar. Peak pressure and impulse data presented in Table 12 are shown in Figures 45 and 46. Deviation from the 45-degree straight line in each figure indicates the extent of the error. Agreement between experimental and theoretical peak pressure and impulse is reasonable, although the theory predicts a large impulse.

Table 12. Pressure Pulse Summary.

Shot	PG <sup>a</sup>	Peak pressure, psi		Impulse, psi-msec		rms deviation, psi	rms error parameter
		Experiment	Theory	Experiment	Theory		
1HR1	1	...	...	...	...	...	...
	2	710	700	184	180	52	0.073
	3	610	655	116	151	71	0.116
	4	650	460	80	93	73	0.112
	5	368	375	60	59	34	0.092
1HR2	1	...	...	...	...	...	...
	2	...	...	...	...	...	...
	3	870	860	106	150	143	0.164
	4	...	...	...	...	...	...
	5	465	475	45	61	67	0.144
1HR3	1	1,080	1,100	132	145	136	0.126
	2	1,050	950	145	165	104	0.099
	3	980	770	117	135	84	0.086
	4	...	...	...	...	...	...
	5	800	465	55	50	91	0.114
1HR4	1	...	...	...	...	...	...
	2	840	840	96	151	124	0.148
	3	920	640	81	118	76	0.083
	4	730	490	63	73	46	0.063
	5	556	410	50	46	53	0.095
1HR12	1	660	1,100	140	122	100	0.152
	2	730	855	175	181	81	0.111
	3	...	...	...	...	...	...
	4	1,170	900	135	222	246	0.210
	5	460	660	109	156	192	0.417
1HR13	1	670	775	168	132	104	0.155
	2	950	1,070	249	218	78	0.082
	3	...	...	...	...	...	...
	4	720	735	178	191	85	0.118
	5	535	545	113	130	81	0.151

<sup>a</sup>Where information is left blank (...) that particular gage was not working properly and readings were incorrect.

Theoretical and experimental pressure traces are shown in Figures 47 and 48 for shots 1HR3 and 1HR13, respectively. Shot 1HR3 was partially tumbled prior to impact. The jacket stripped to 0.4 inch along the trajectory. Best agreement with experiment was obtained by assuming that the bullet attained a fully tumbled attitude at 6.8 inches. The theory overestimates the initial pressure peak at PG1 while it systematically underestimates at the downstream transducers. The effect of the jacket stripping is evident particularly for shot 1HR13 (Figure 48).

### .30 CALIBER AP

Four .30-caliber AP rounds were fired at 0 degree obliquity; one tumbled prior to impact, and the remaining three impacted at 0 degree yaw. The experimental conditions are listed in Table 13.

Physical parameters for this round are given in Table 14. The drag coefficients presented are double the values given in a previous report (see Footnote 2, page 6).

A summary of the tumbling distances obtained from the pressure pulse analysis is given in Table 15. The round appears to be quite unstable in water as the bullet starts to tumble almost immediately after impact. However, the distance to become fully tumbled,  $X_2 - X_1$ , is large compared to the higher caliber rounds. The experimental values of  $X_2$  were taken from measurements of high speed motion picture frames and showed excellent correspondence with the theoretical values.

Experimental trajectories were obtained for the four shots. These are plotted with the theoretical curves in Figures 49 through 52. The figures show reasonable correlation between experiment and theory.

Results of the pressure pulse analysis are summarized in Table 16. The error parameter given in the last column of the table indicates satisfactory agreement between experiment and theory. Experimental and theoretical peak pressures and impulses are compared in Figures 53 and 54. The large error indicated in shot 4HR5 for PG2 was caused by the round passing within 2 inches of the transducer. A small error in the trajectory thus gave a large error in pressure.

Two examples of the pressure pulses generated by the .30-caliber AP round are shown in Figures 55 and 56. Experimental and theoretical pressures correspond for shot 4HR3 (Figure 55).

Table 13. Experimental Conditions.

Shot	Velocity, ft/sec	Entrance panel, in. A $\phi$	Impact coordinates, in.		Obliquity, deg	Yaw attitude, deg
			X	Y		
4HR2	2,645	0.063	31.00	28.75	0	Tumbled
4HR3	2,799	0.063	30.25	31.63	0	0
4HR4	2,843	0.063	32.00	31.50	0	0
4HR5	2,828	0.063	29.31	33.00	0	0

JTCG/AS-74-T-015

Table 14. Characteristics of the .30-Caliber AP Round.

Bullet weight = 0.0237 pounds; core weight = 0.0115 pounds.

Yaw angle, deg	Bullet area, in <sup>2</sup>	Core area, in <sup>2</sup>	Drag coefficient
0	0.0745	0.0469	0.10
90	0.3170	0.2600	0.30
180	0.0314	...	0.82

Table 15. Tumbling Distances.

Shot	X <sub>1</sub> , in.	X <sub>2</sub> - X <sub>1</sub> , in.	X <sub>2</sub> , in.	X <sub>s</sub> , in.	X <sub>2</sub> (experiment), in.
4HR2	0.00	0.00	0.00	...	...
4HR3	1.13	11.61	12.74	...	13
4HR4	0.63	14.61	15.24	...	16
4HR5	0.00	14.44	14.44	...	16

Table 16. Pressure Pulse Summary.

Shot	PG <sup>a</sup>	Peak pressure, psi		Impulse, psi-msec		rms deviation, psi	rms error parameter
		Experiment	Theory	Experiment	Theory		
4HR2	1	250	580	41	61	72	0.288
	2	230	450	49	50	56	0.243
	3	180	300	35	25	37	0.206
	4	160	220	22	14	36	0.225
	5	110	180	13	9	22	0.200
4HR3	1	250	260	76	73	19	0.076
	2	500	430	133	100	49	0.098
	3	370	385	96	82	40	0.108
	4	275	300	58	56	37	0.135
	5	...	...	...	...	...	...
4HR4	1	185	245	59	92	51	0.276
	2	410	490	107	131	70	0.171
	3	370	440	85	106	64	0.173
	4	260	310	56	70	44	0.169
	5	...	...	...	...	...	...
4HR5	1	340	250	104	71	61	0.179
	2	930	450	225	109	183	0.197
	3	515	415	163	97	114	0.221
	4	300	305	69	65	36	0.120
	5	...	...	...	...	...	...

<sup>a</sup>Where information is left blank (...) that particular gage was not working properly and readings were incorrect.

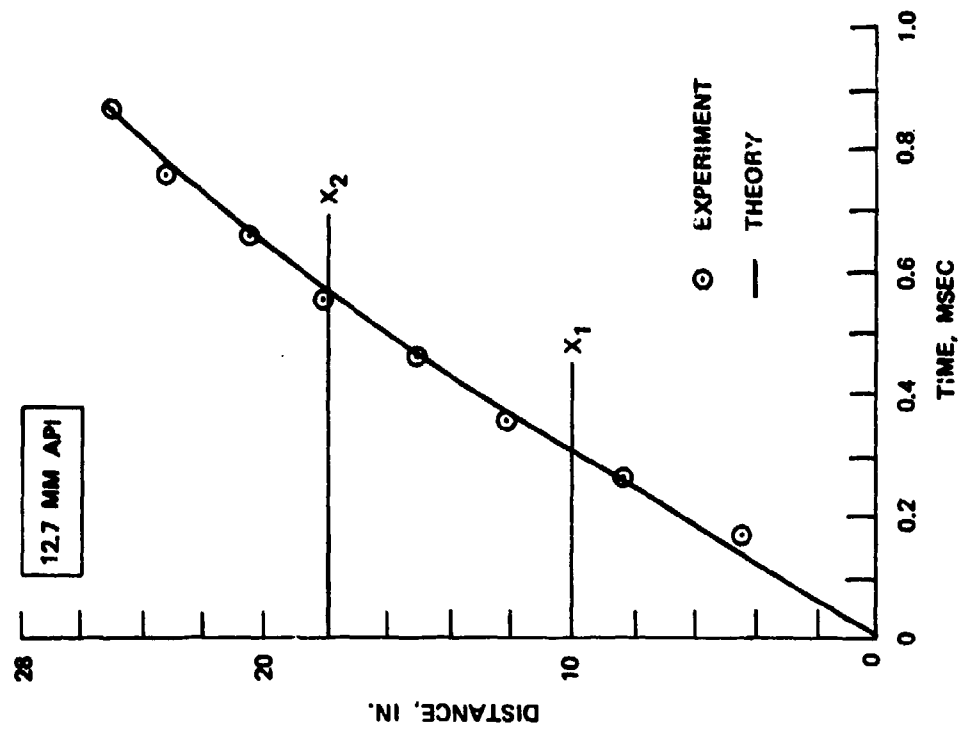


Figure 3. Experimental Trajectory for Shot 1HR5.

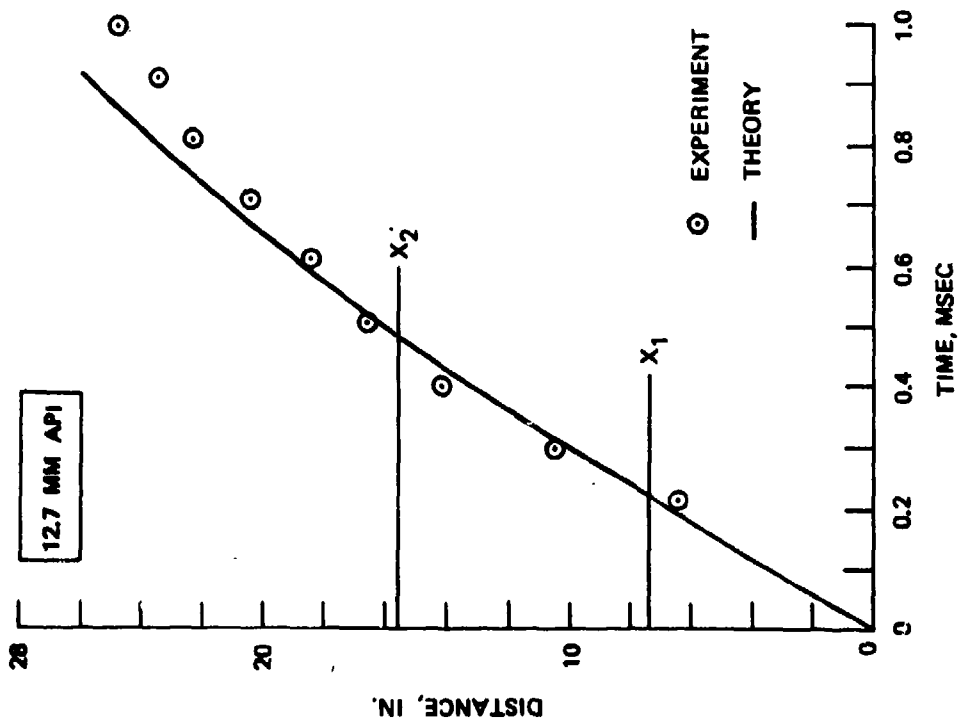


Figure 4. Experimental Trajectory for Shot 1HR8.



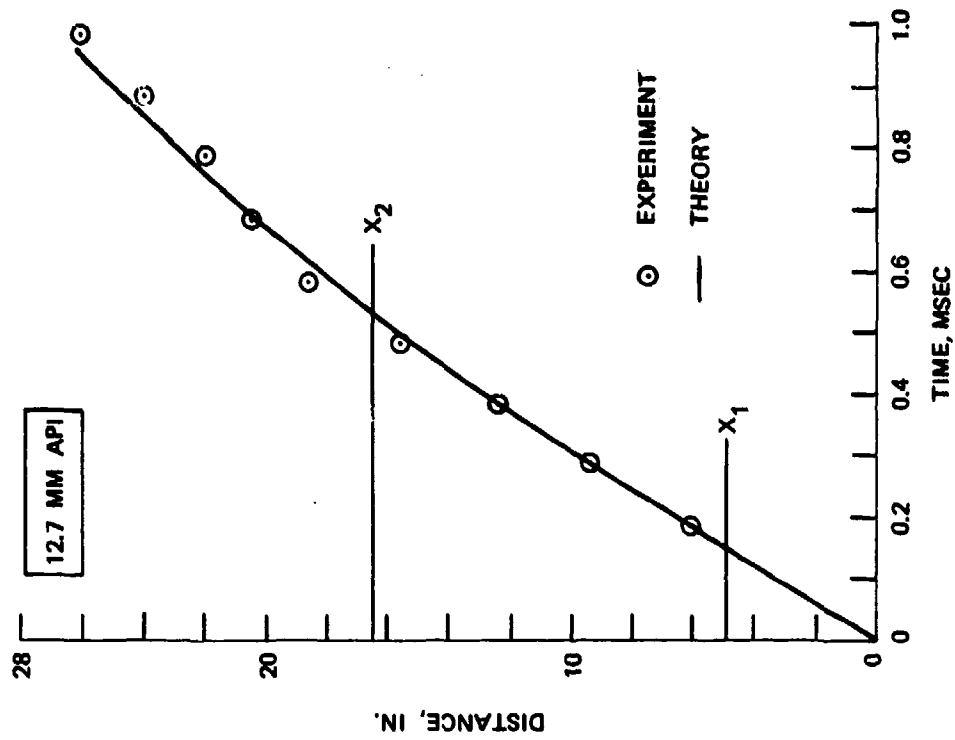


Figure 5. Experimental Trajectory for Shot 1HR9.

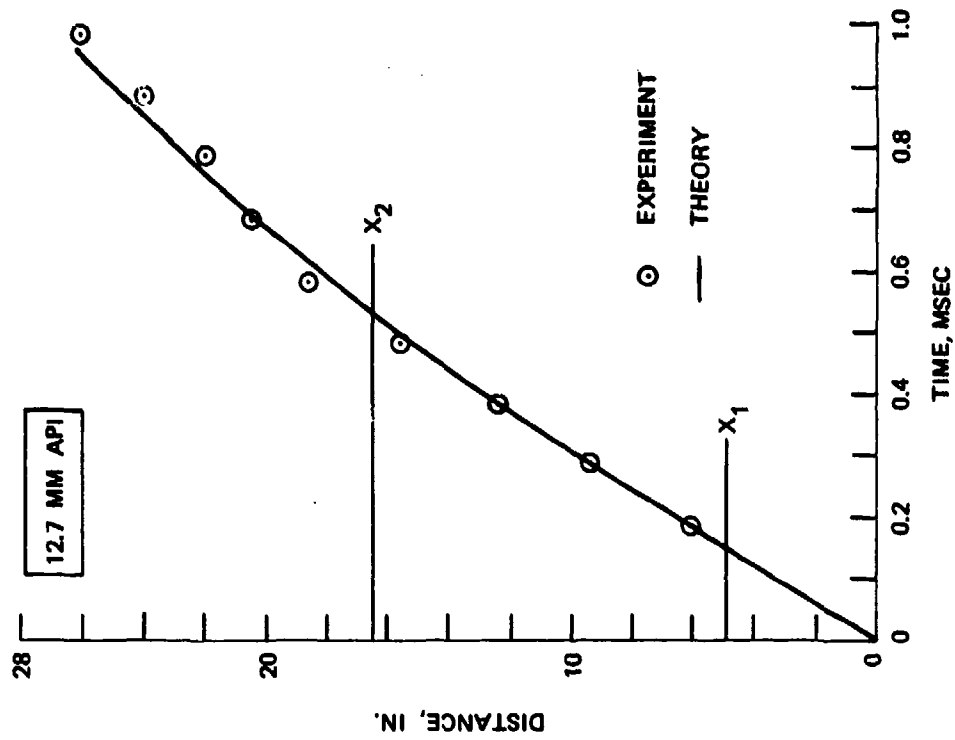


Figure 6. Experimental Trajectory for Shot 1HR10.

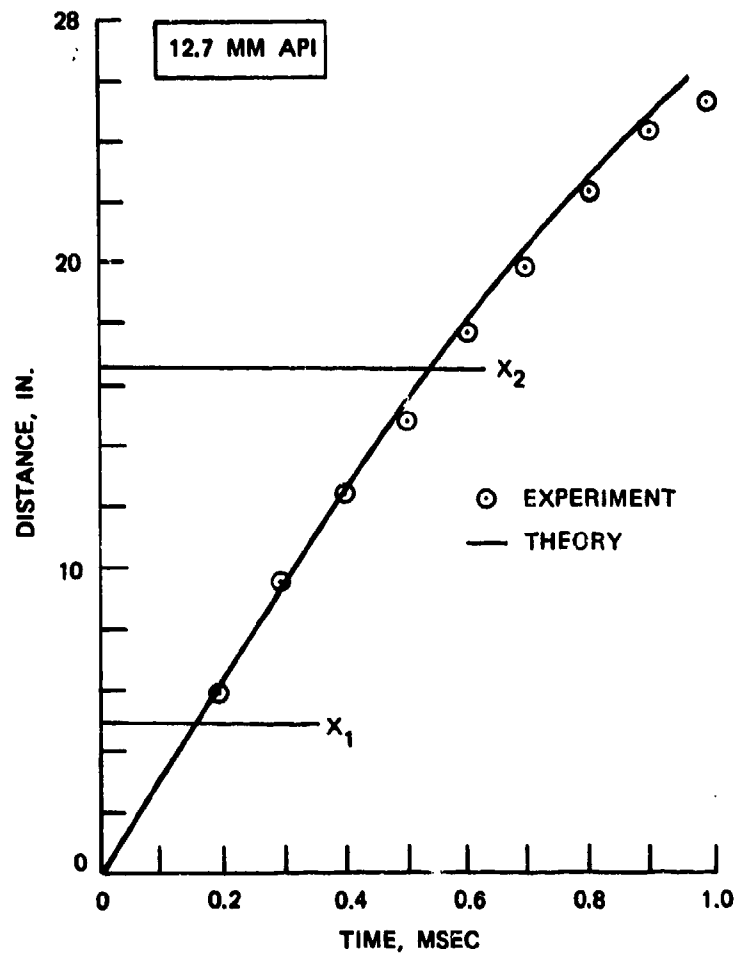


Figure 7. Experimental Trajectory for Shot 1HR11.

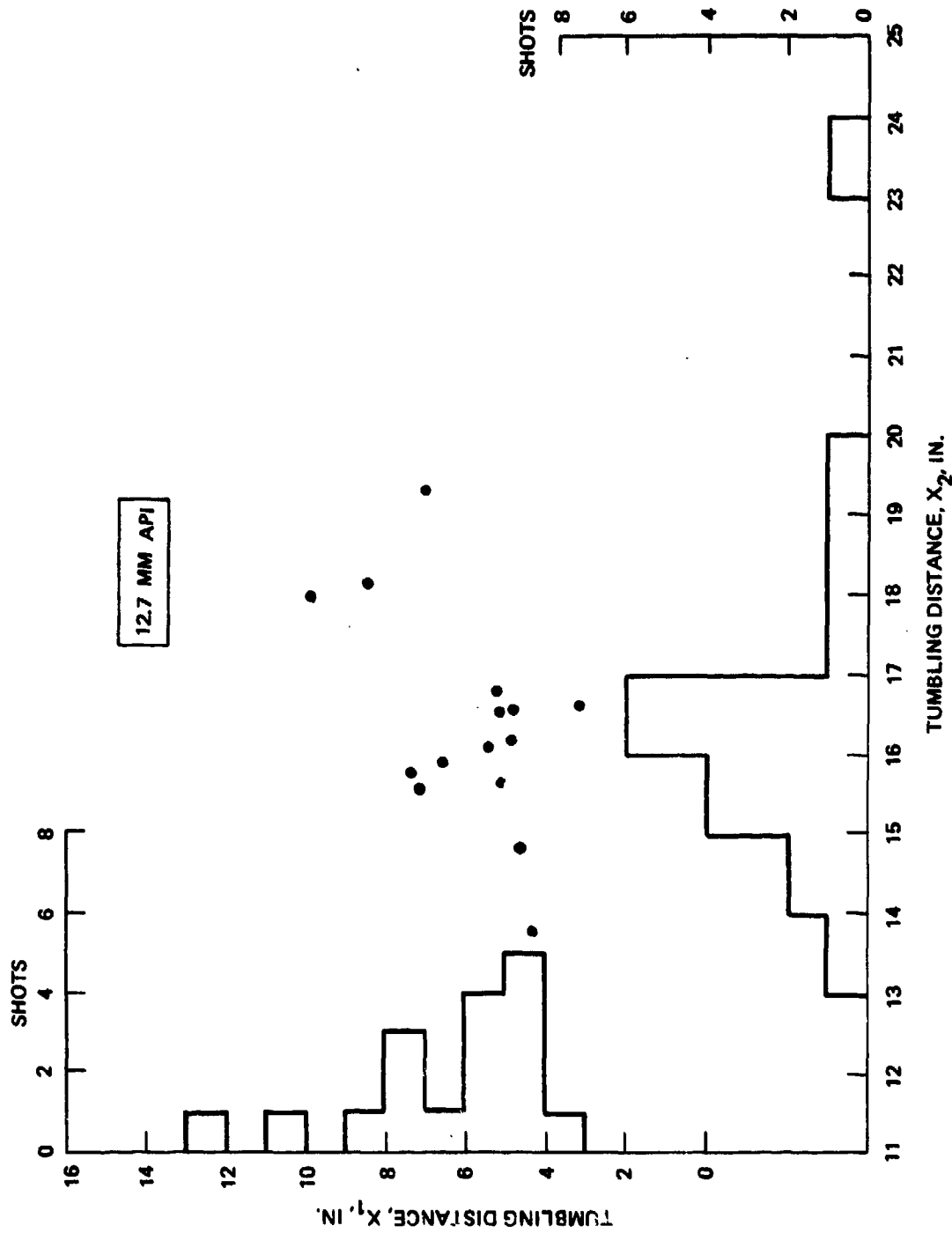


Figure 8. Tumbling Distance Distribution; 0 Degree Obliquity, 0 Degree Yaw.

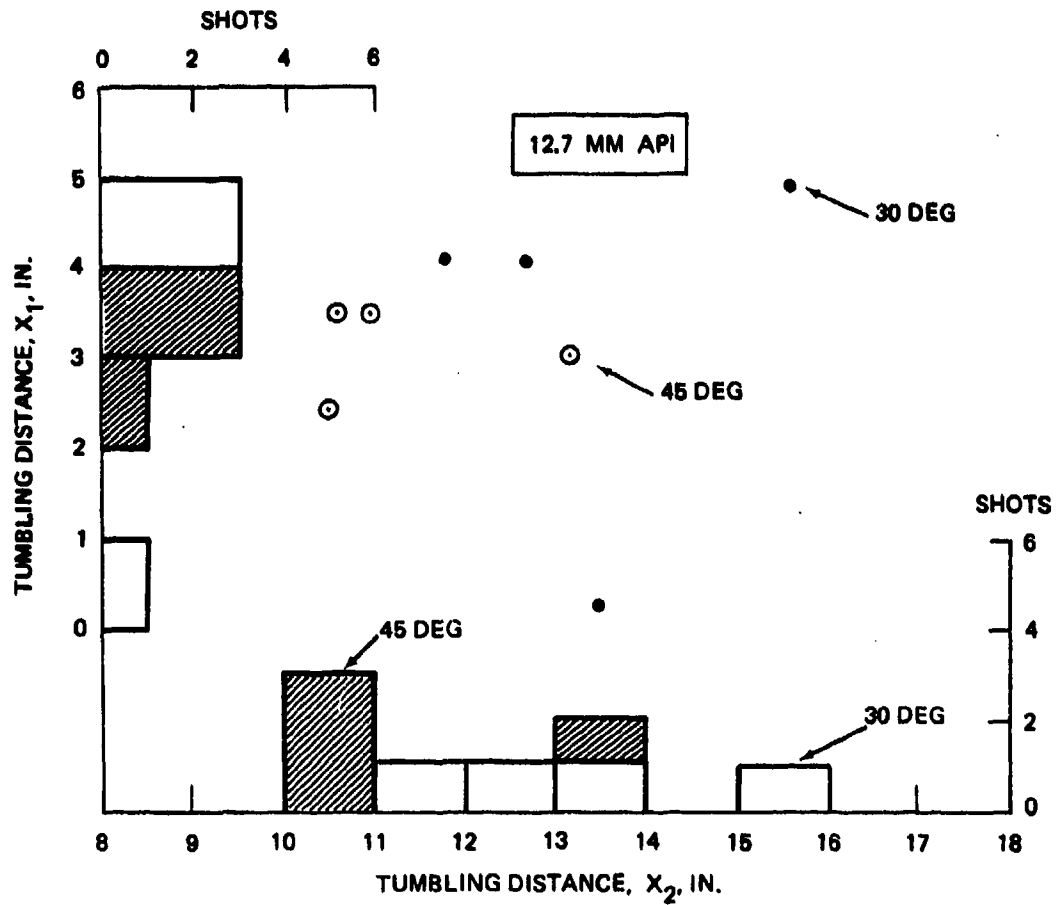


Figure 9. Tumbling Distance Distribution; 30 to 45 Degrees Obliquity, 0 Degree Yaw.

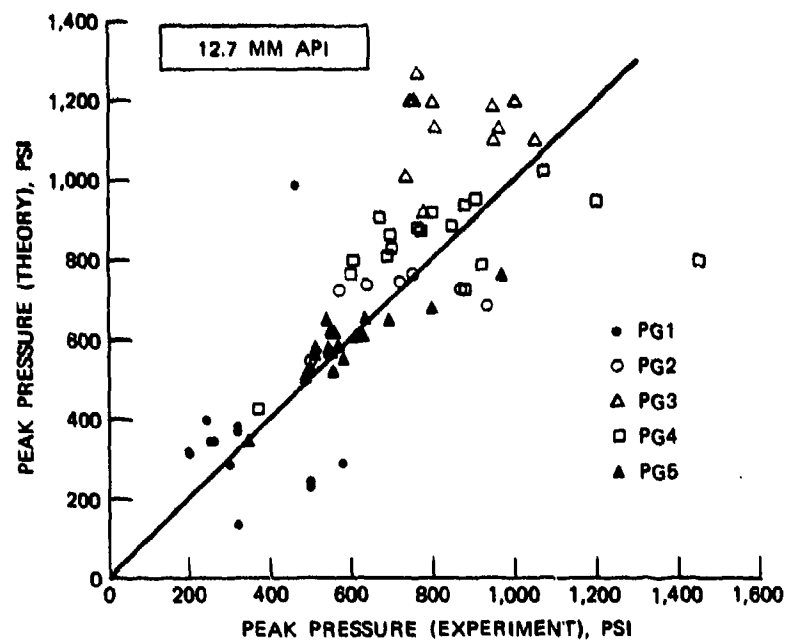


Figure 10. Peak Pressure—Theory Versus Experiment;  
0 Degree Obliquity, 0 Degree Yaw.

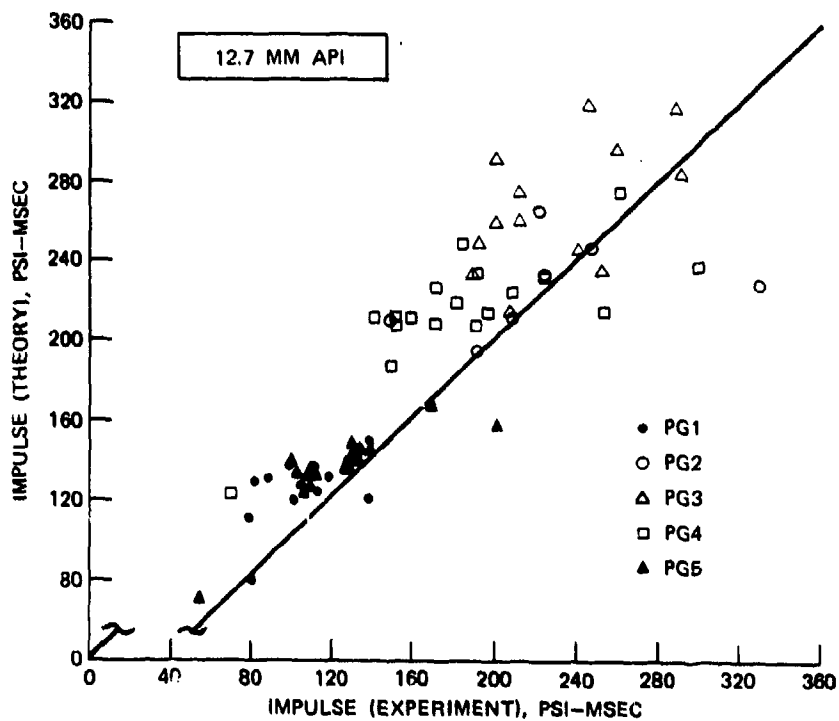


Figure 11. Impulse—Theory Versus Experiment;  
0 Degree Obliquity, 0 Degree Yaw.

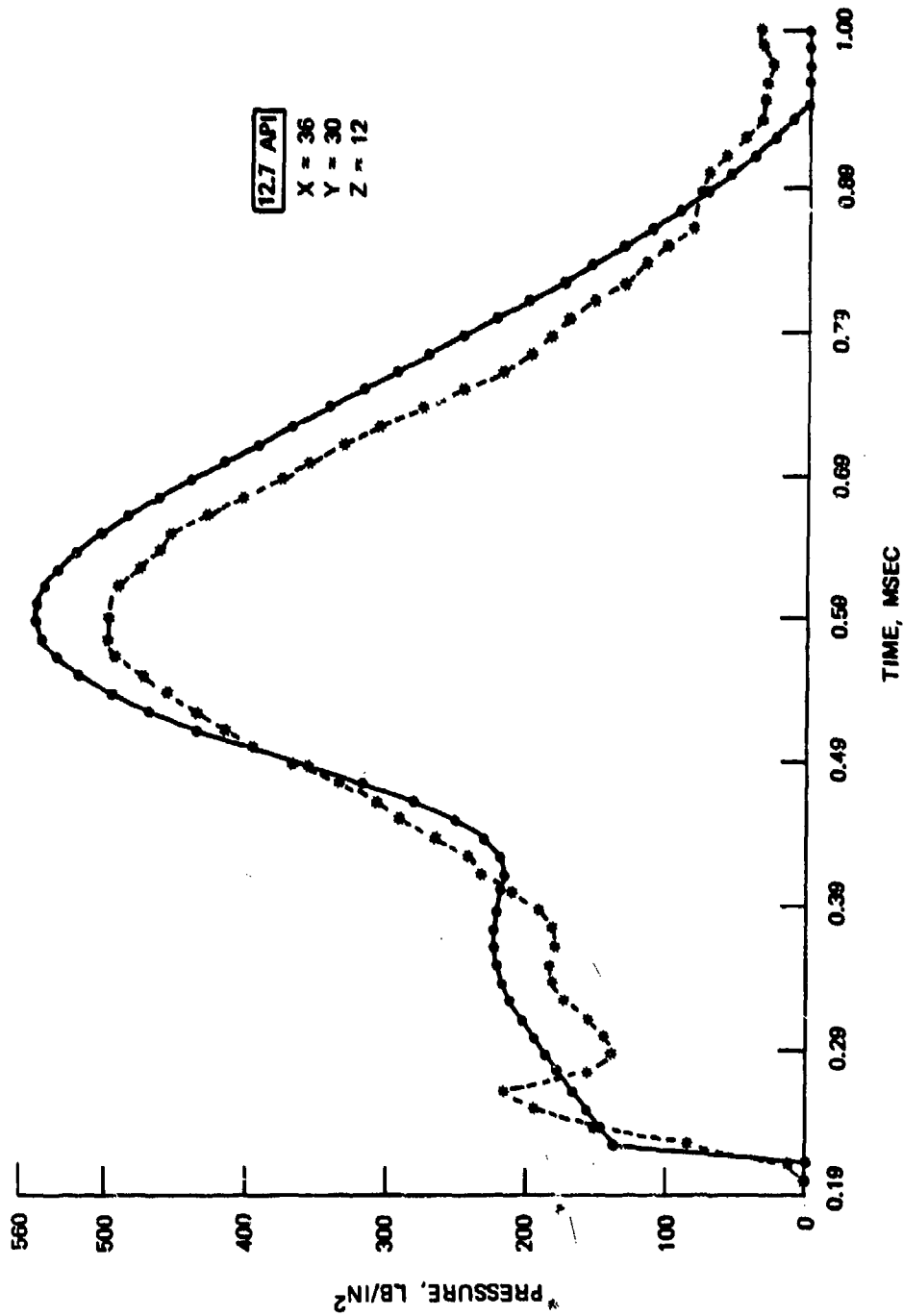


Figure 12. Pressure Versus Time Plot for Shot 1HR8 (Sheet 1 of 3).

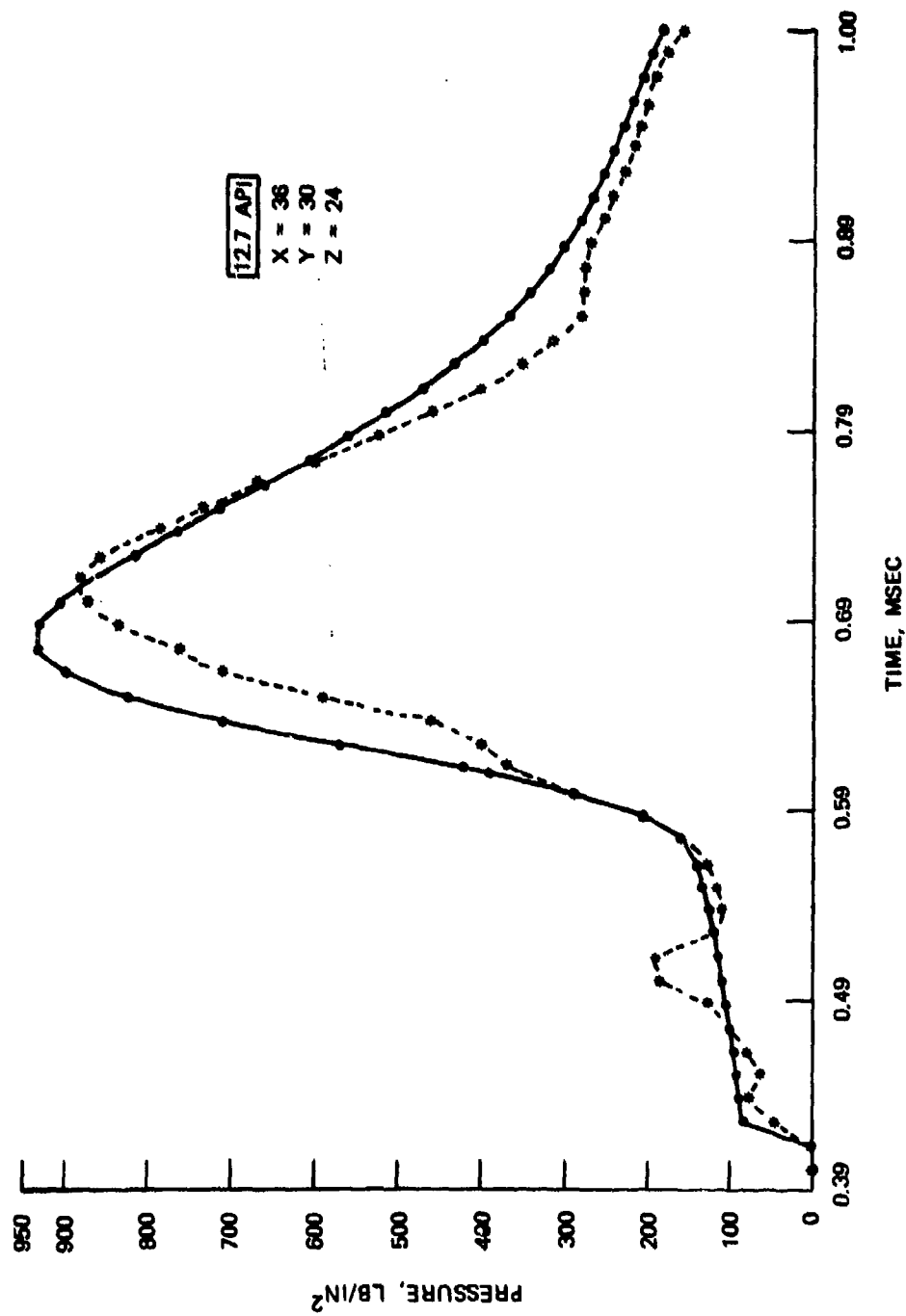


Figure 12. Pressure Versus Time Plot for Shot 1HR8 (Sheet 2 of 3).

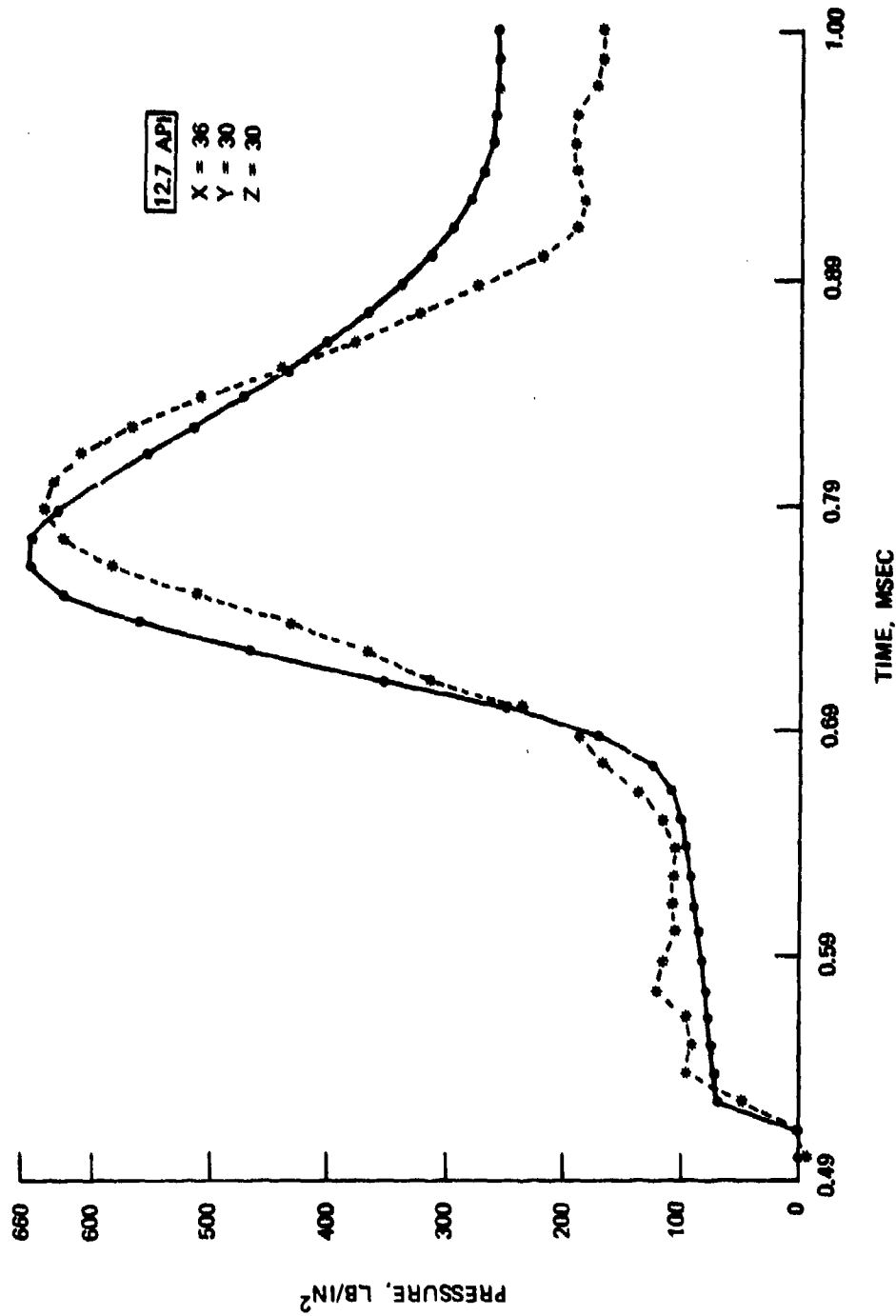


Figure 12. Pressure Versus Time Plot for Shot 1HR8 (Sheet 3 of 3).



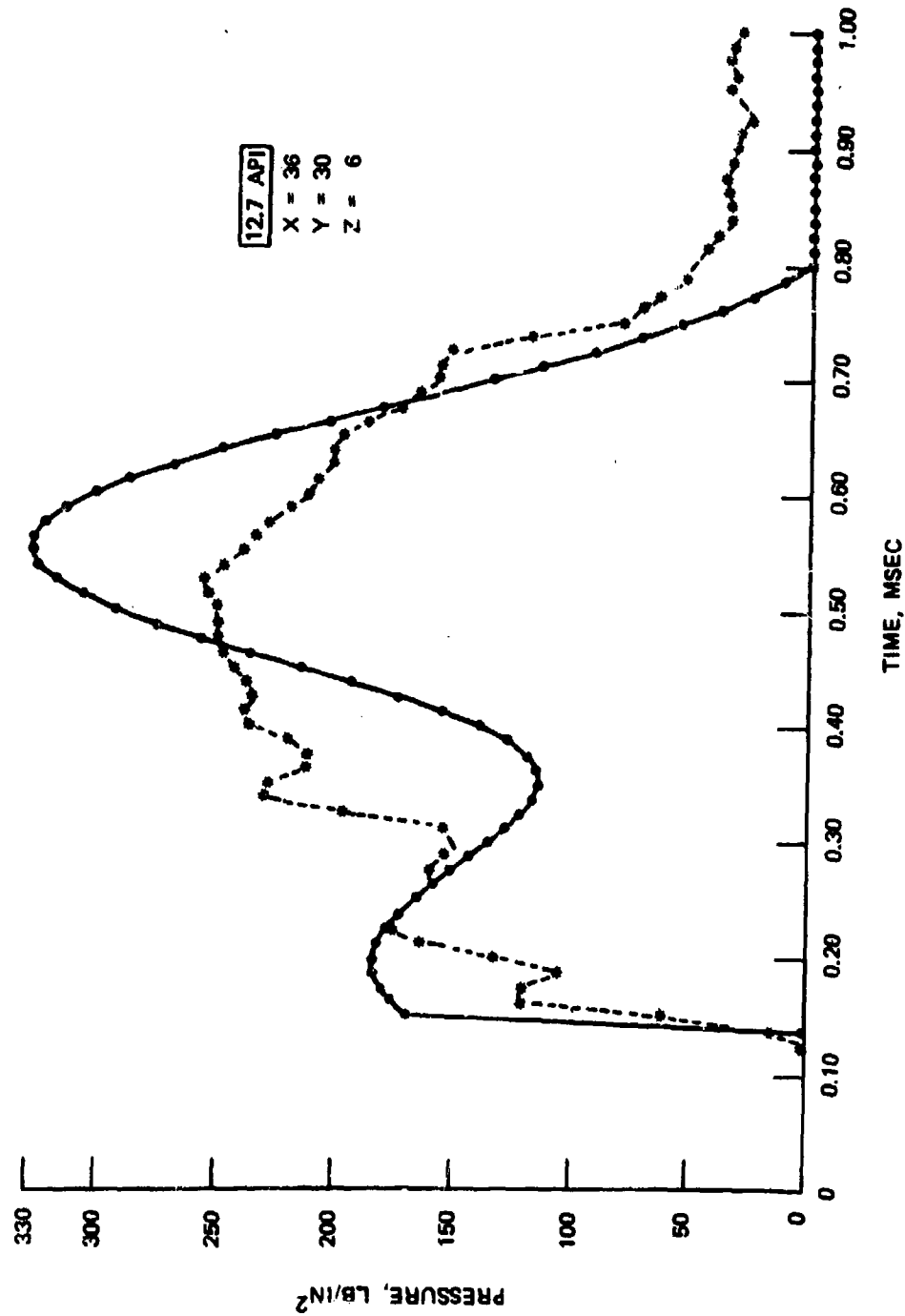


Figure 13. Pressure Versus Time Plot for Shot 1HR9 (Sheet 1 of 4).

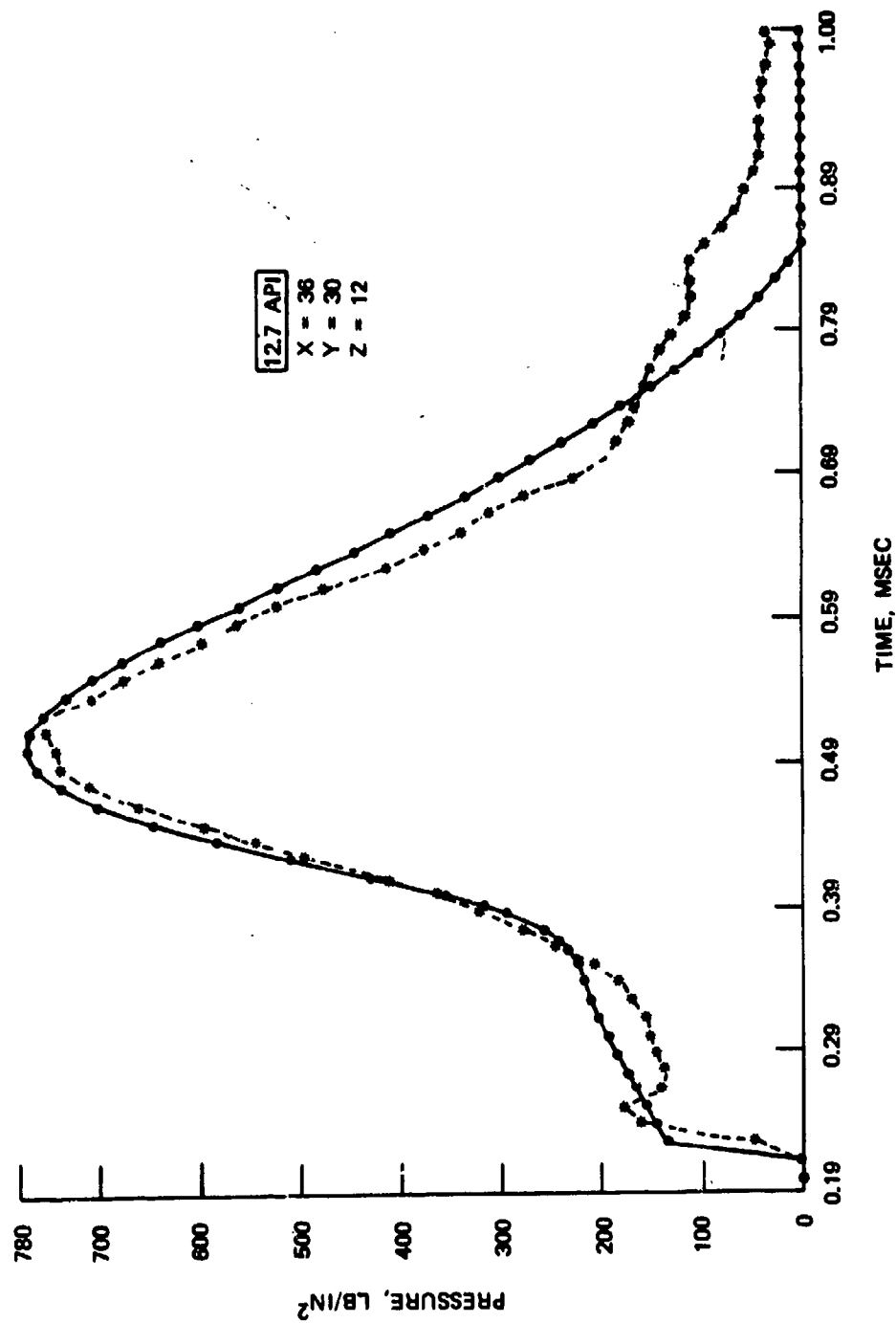


Figure 13. Pressure Versus Time Plot for Shot 1HR9 (Sheet 2 of 4).

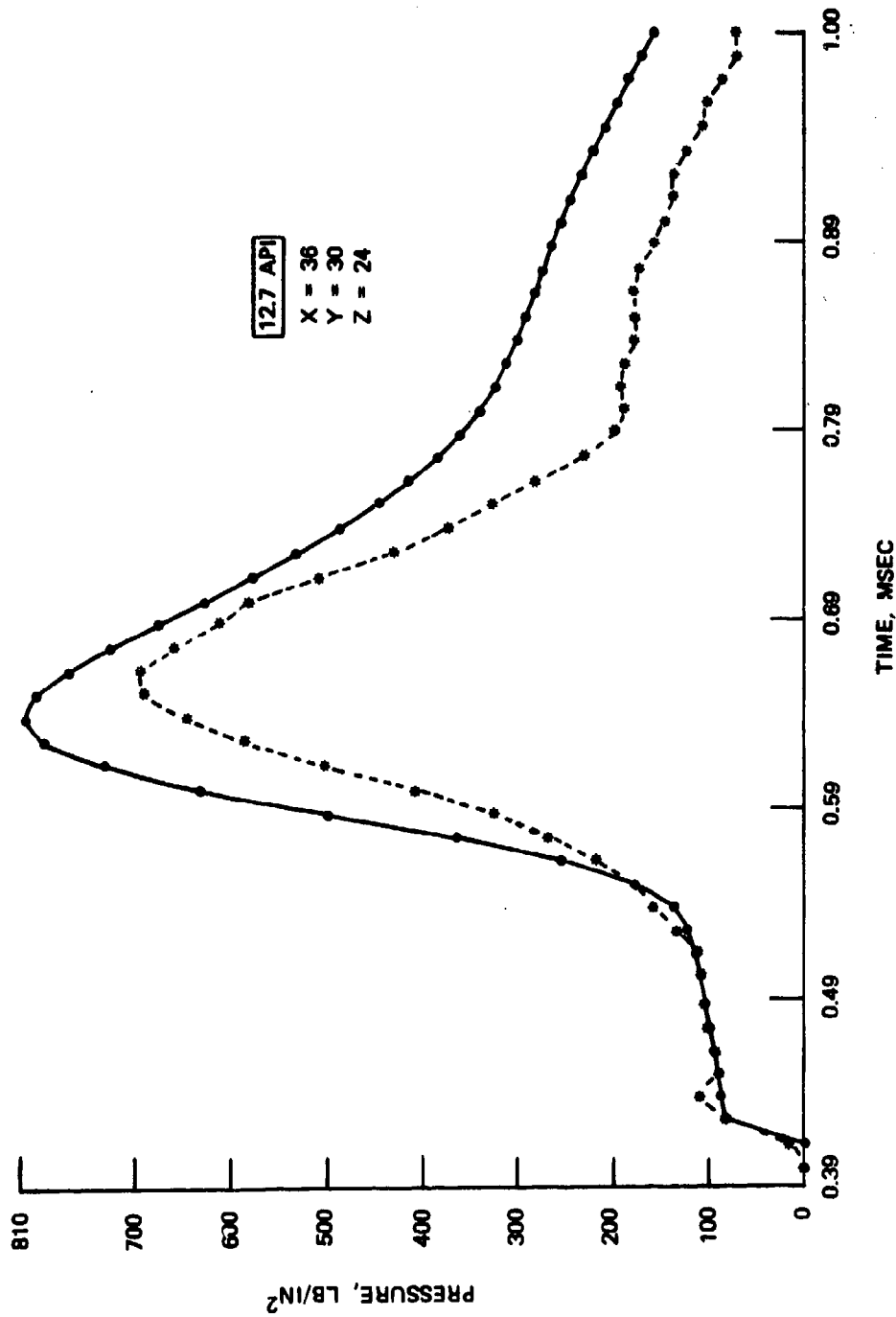


Figure 13. Pressure Versus Time Plot for Shot 1HR9 (Sheet 3 of 4).

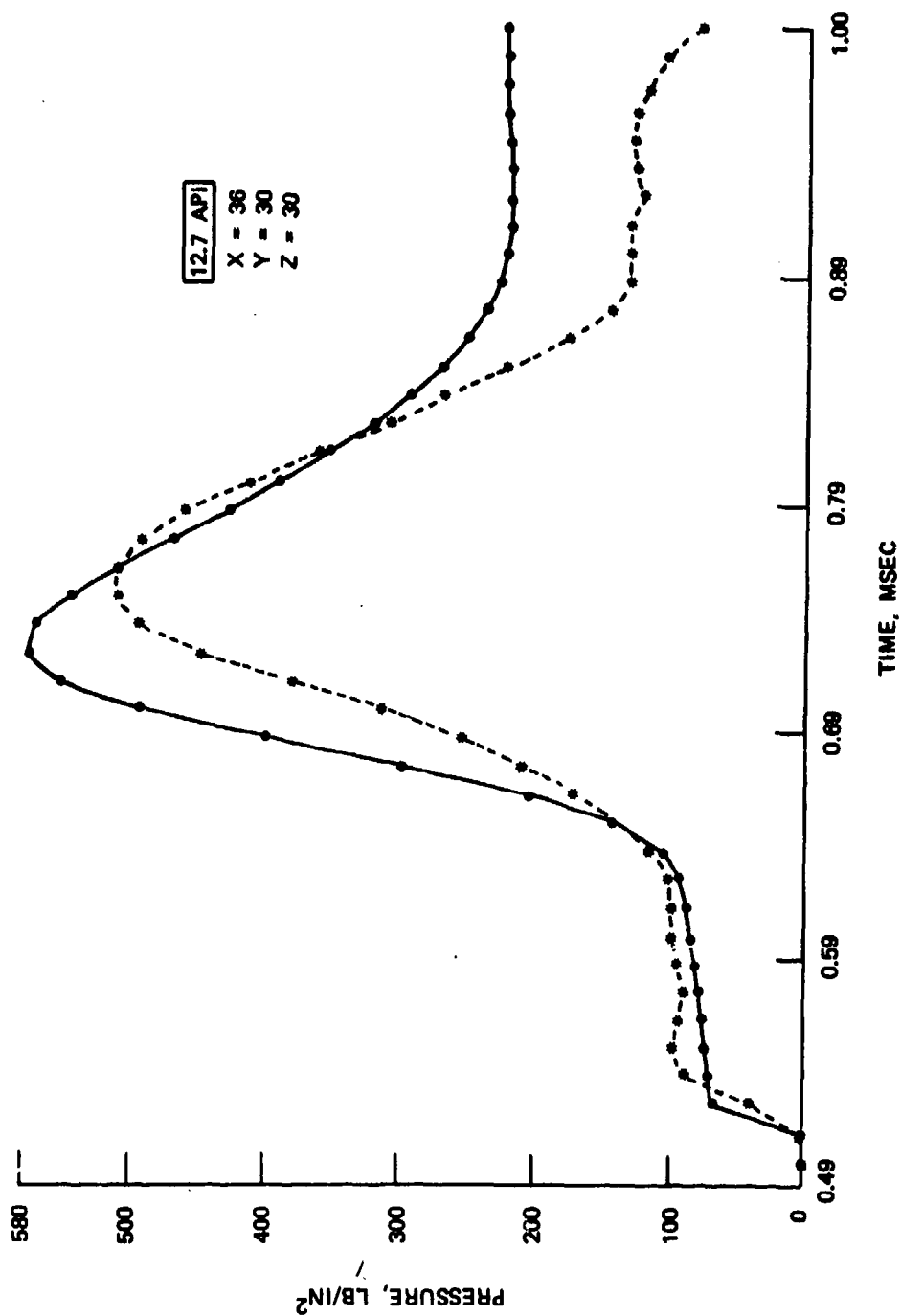


Figure 13. Pressure Versus Time Plot for Shot 1HR9 (Sheet 4 of 4).

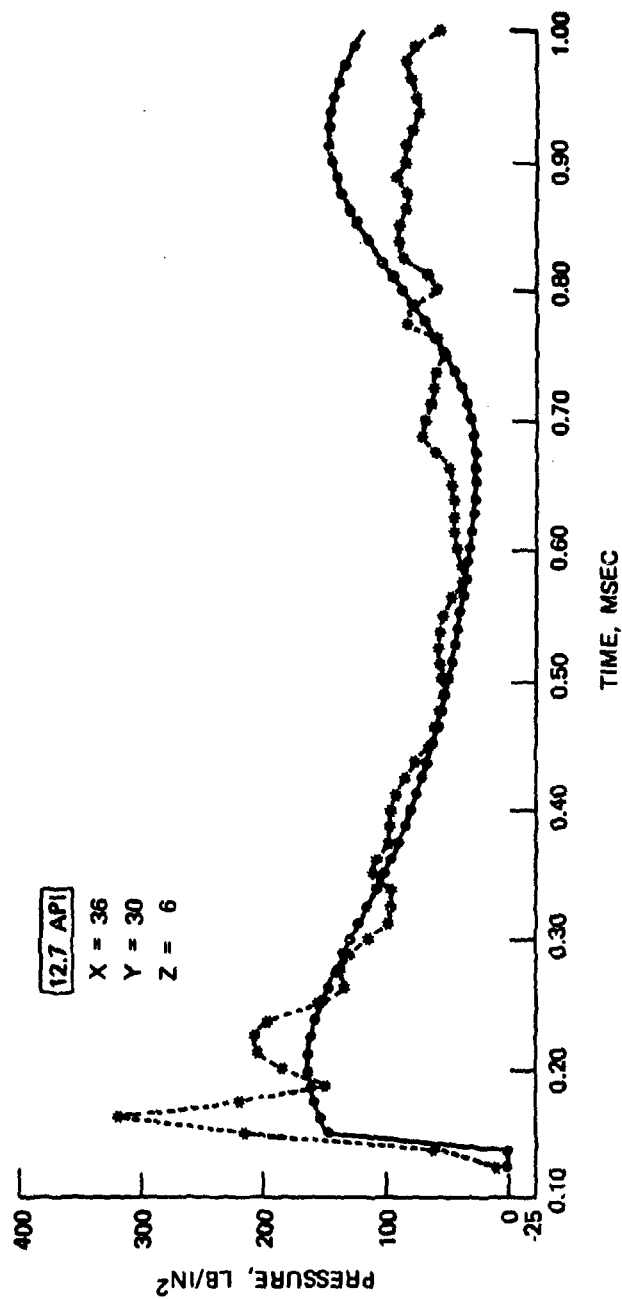


Figure 14. Pressure Versus Time Plot for Shot 2HR11 (Sheet 1 of 4).

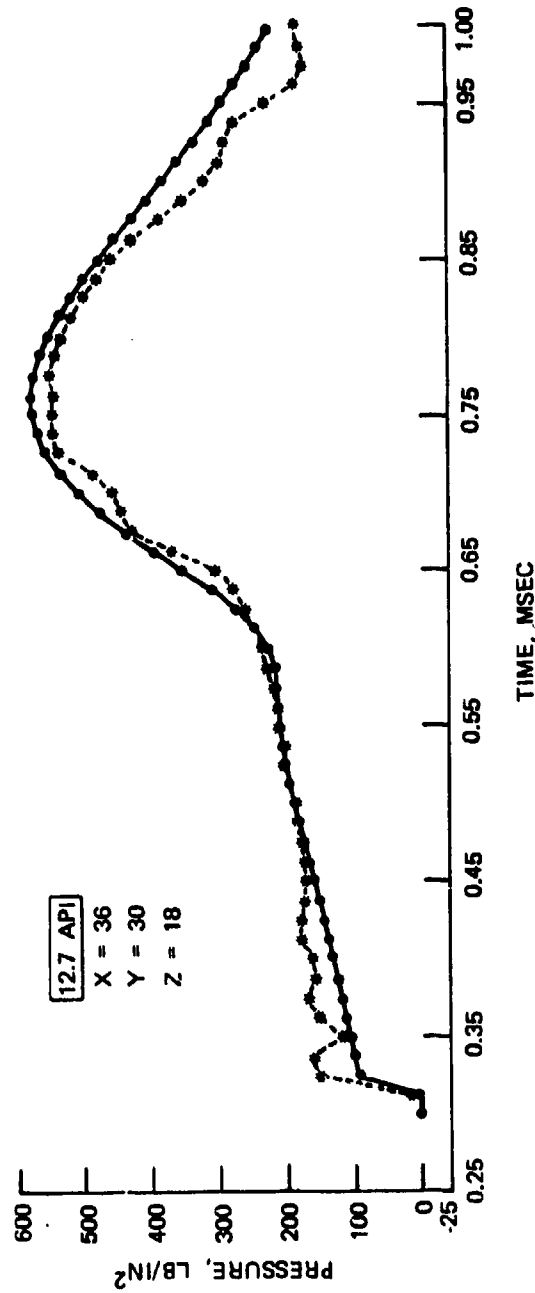


Figure 14. Pressure Versus Time Plot for Shot 2HR11 (Sheet 2 of 4).

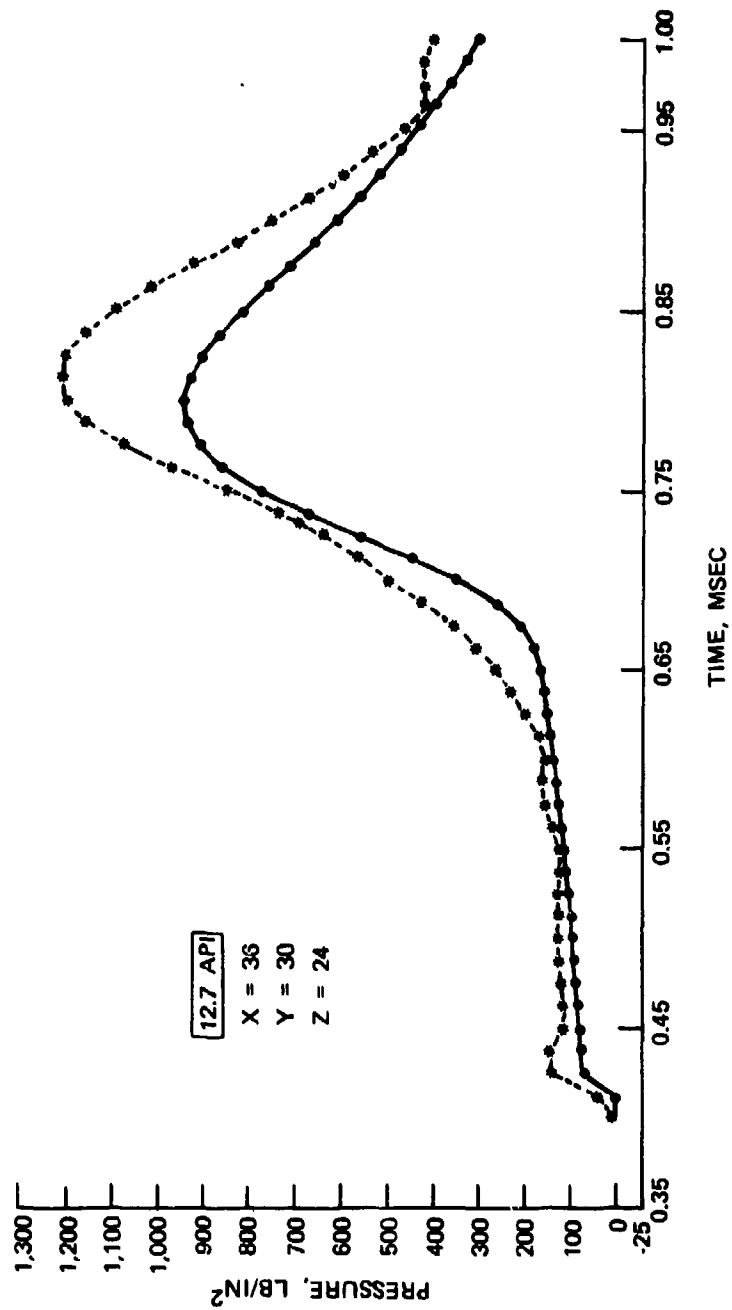


Figure 14. Pressure Versus Time Plot for Shot 2HR11 (Sheet 3 of 4).

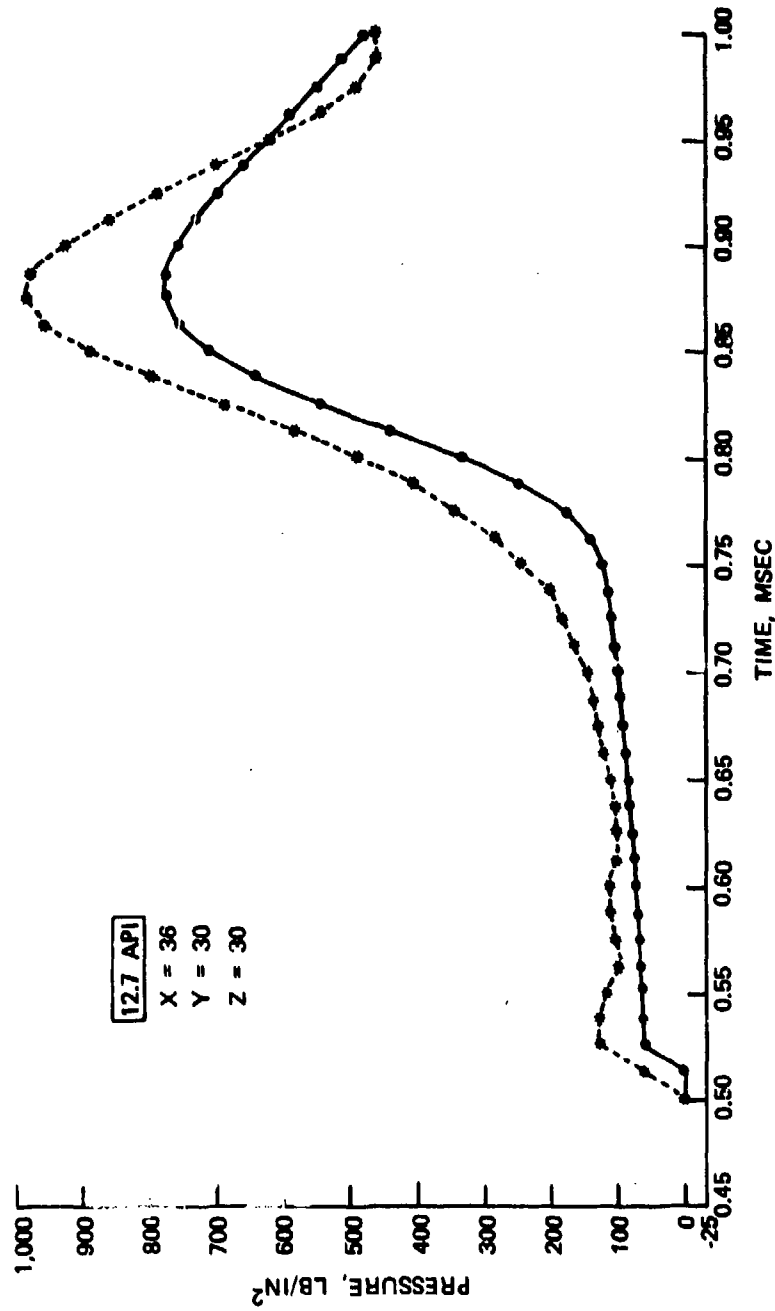


Figure 14. Pressure Versus Time Plot for Shot 2HR11 (Sheet 4 of 4).



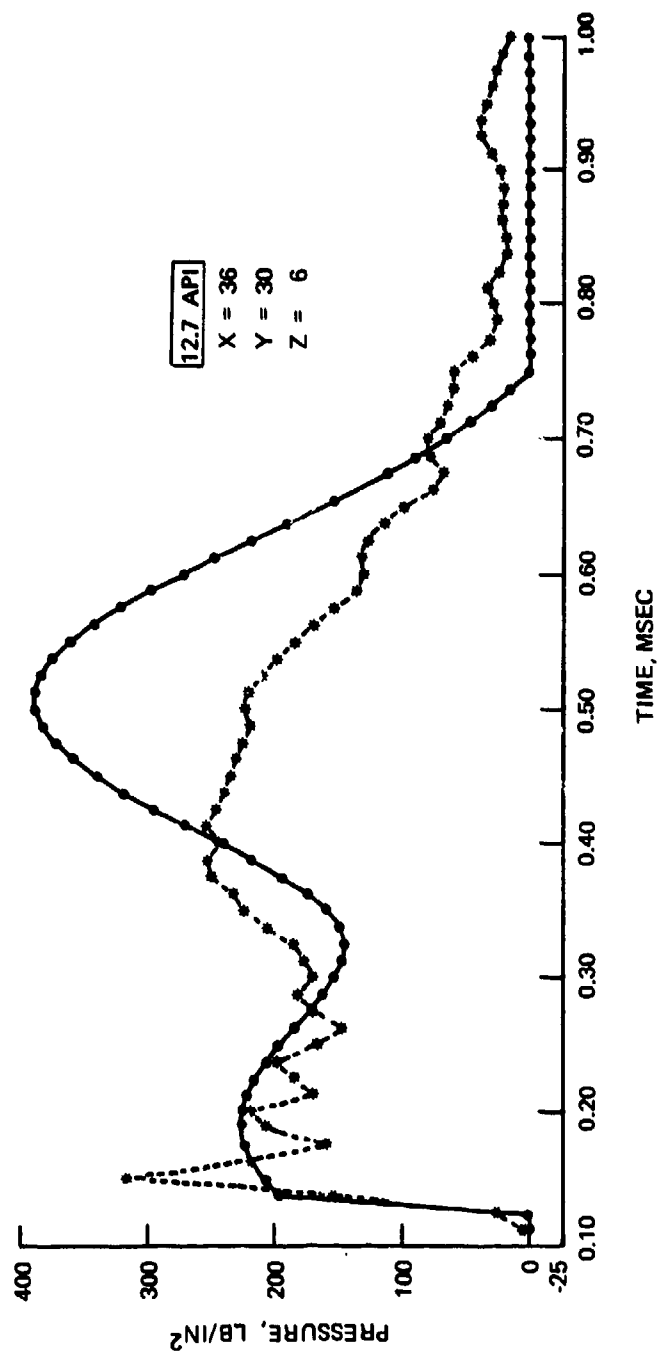


Figure 15. Pressure Versus Time Plot for Shot 2HR13 (Sheet 1 of 4).

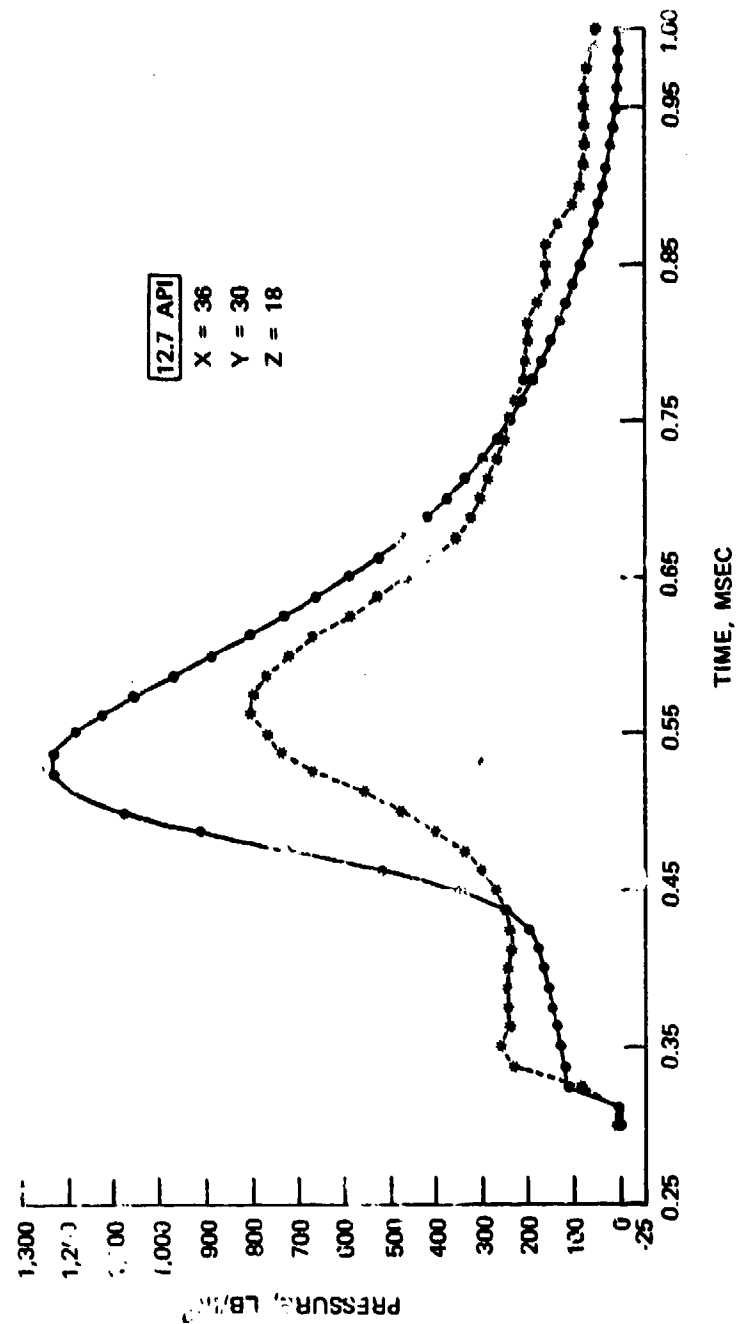


Figure 15. Pressure Versus Time Plot for Hot 2HR17 (Sheet 2 of 4).

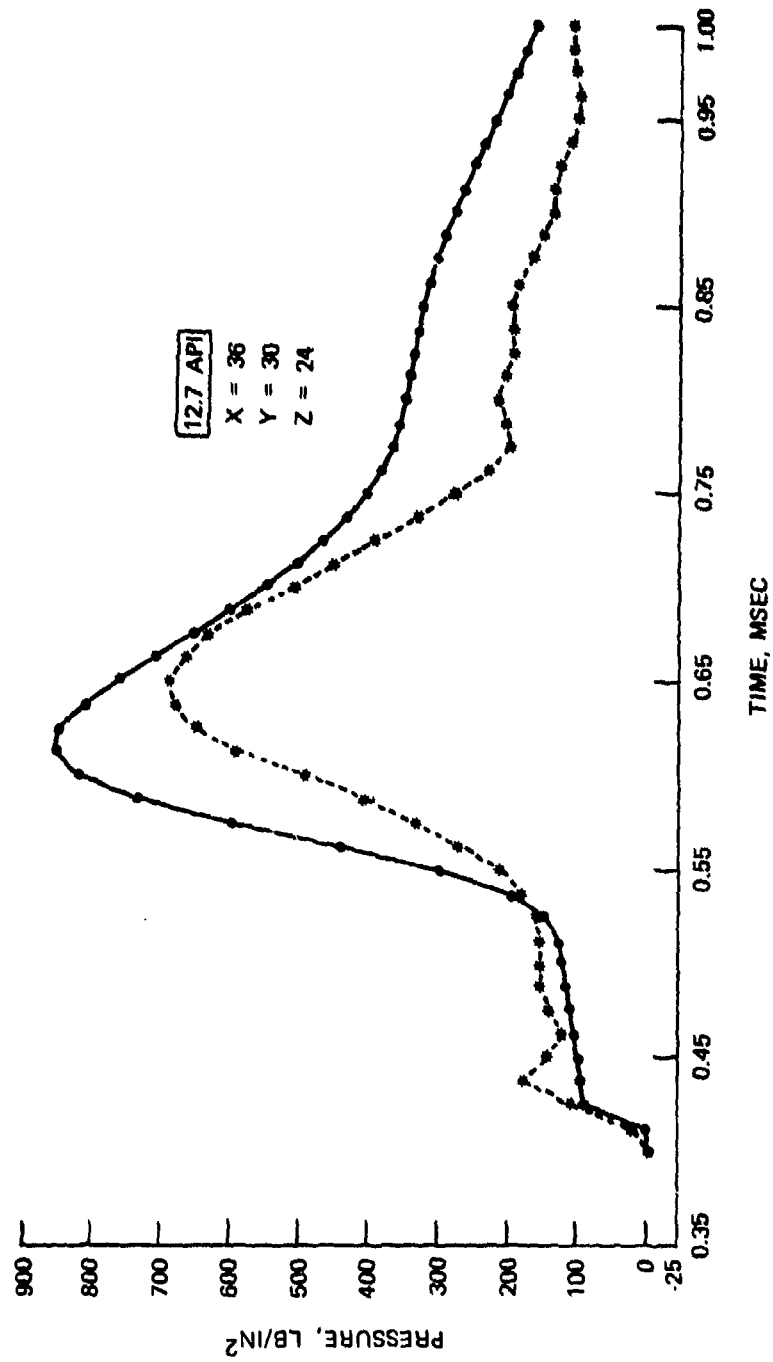


Figure 15. Pressure Versus Time Plot for Shot 2HR13 (Sheet 3 of 4).

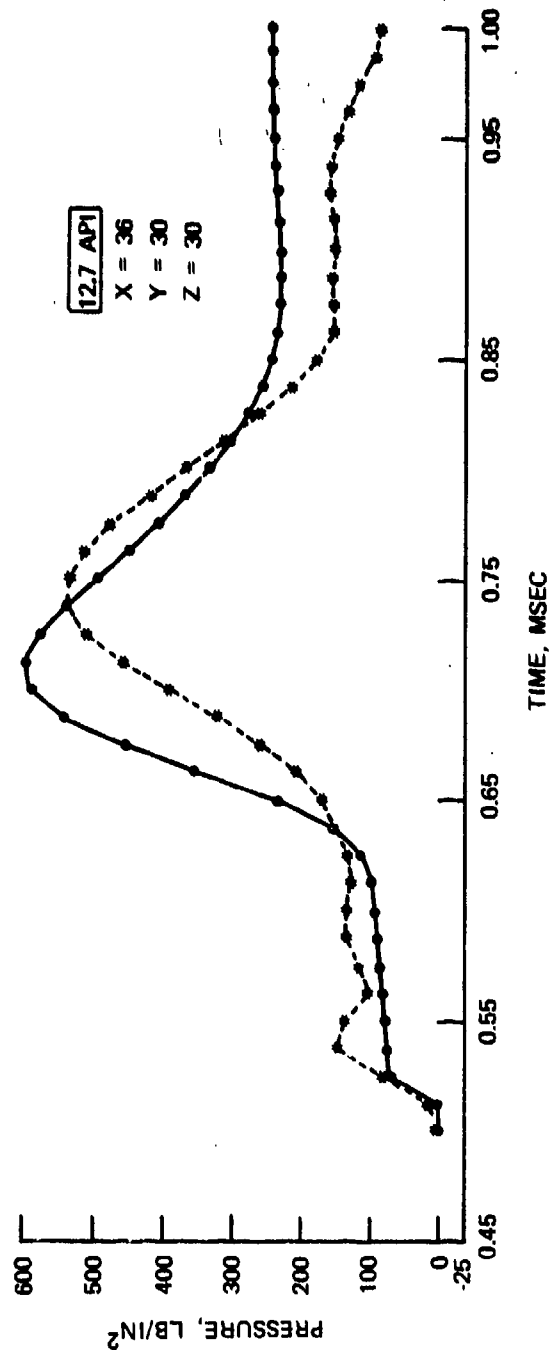


Figure 15. Pressure Versus Time Plot for Shot 2HR13 (Sheet 4 of 4).

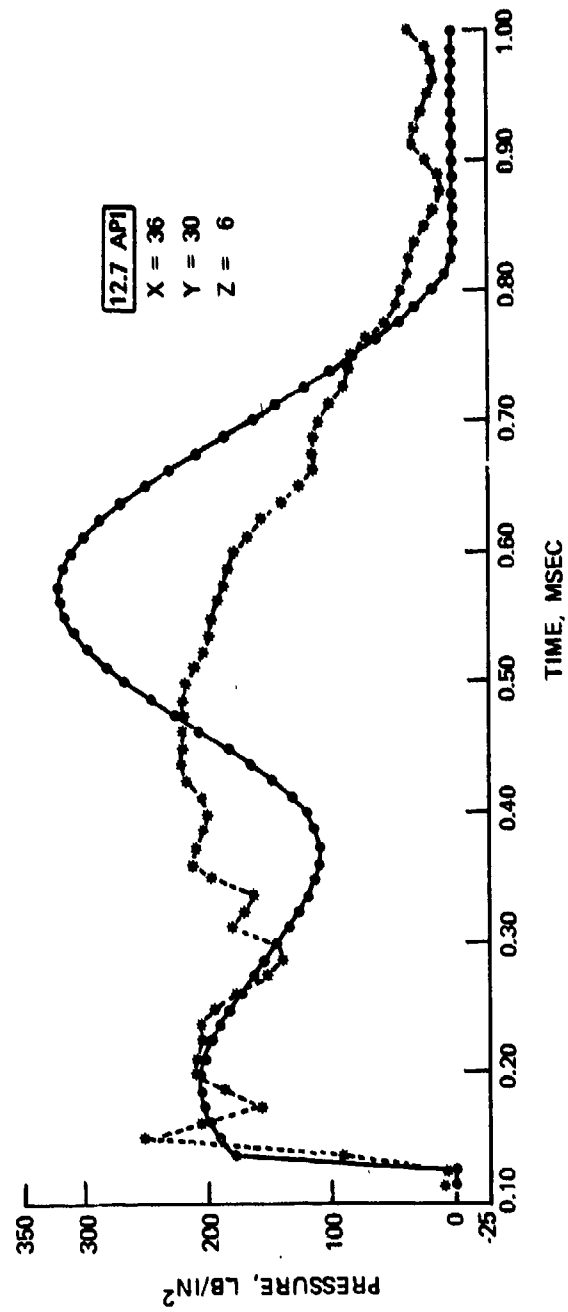


Figure 16. Pressure Versus Time Plot for Shot 2HR14 (Sheet 1 of 4).

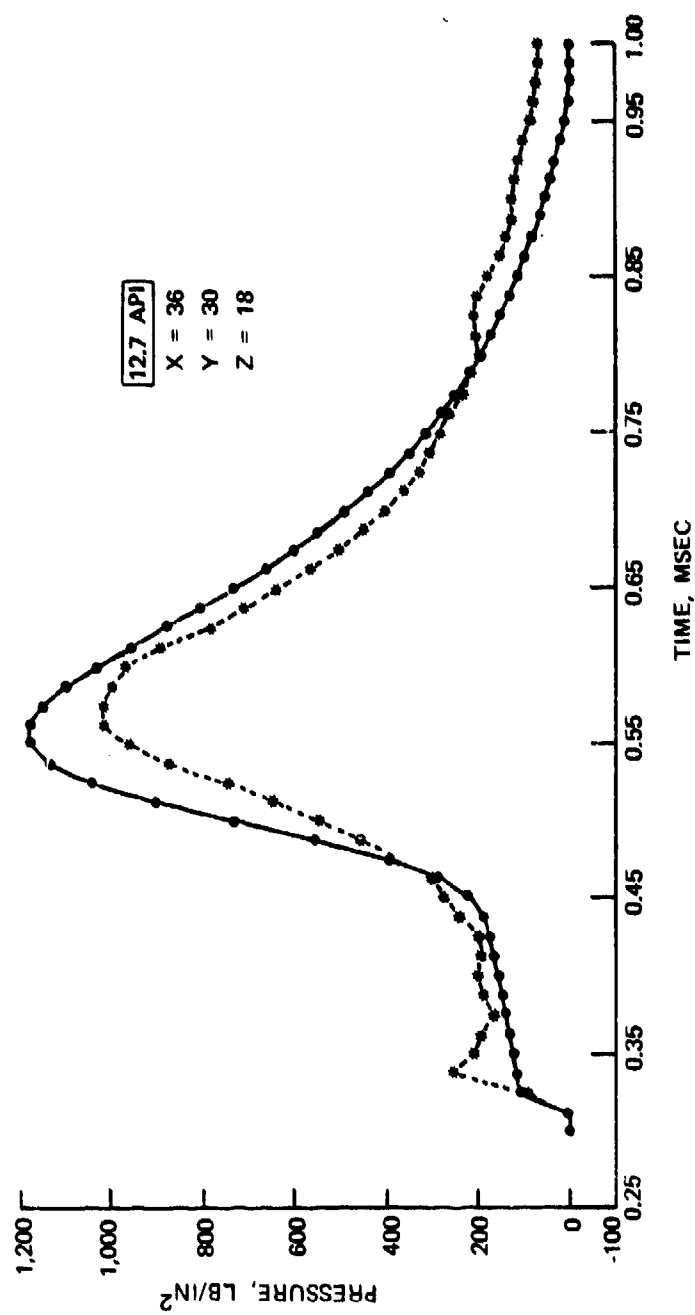


Figure 16. Pressure Versus Time Plot for Shot 2HR14 (Sheet 2 of 4).

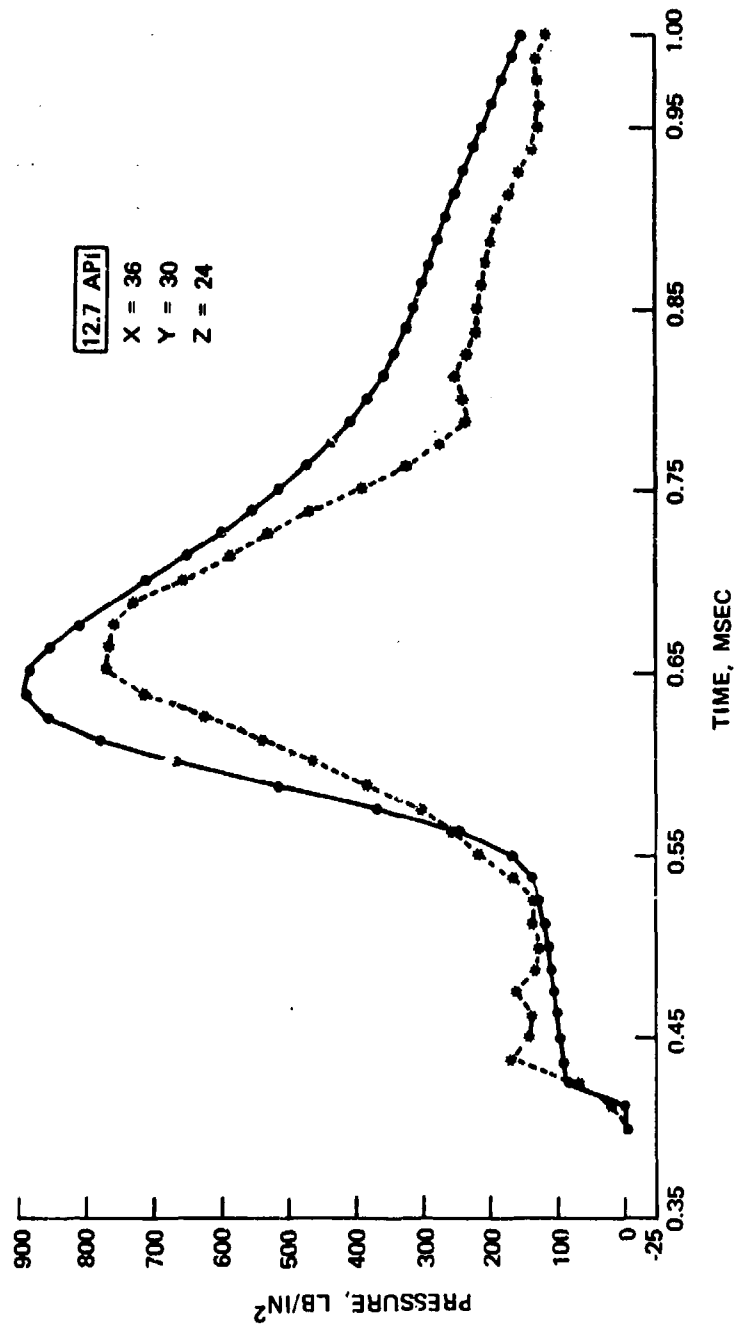


Figure 16. Pressure Versus Time Plot for Shot 2HR14 (Sheet 3 of 4).

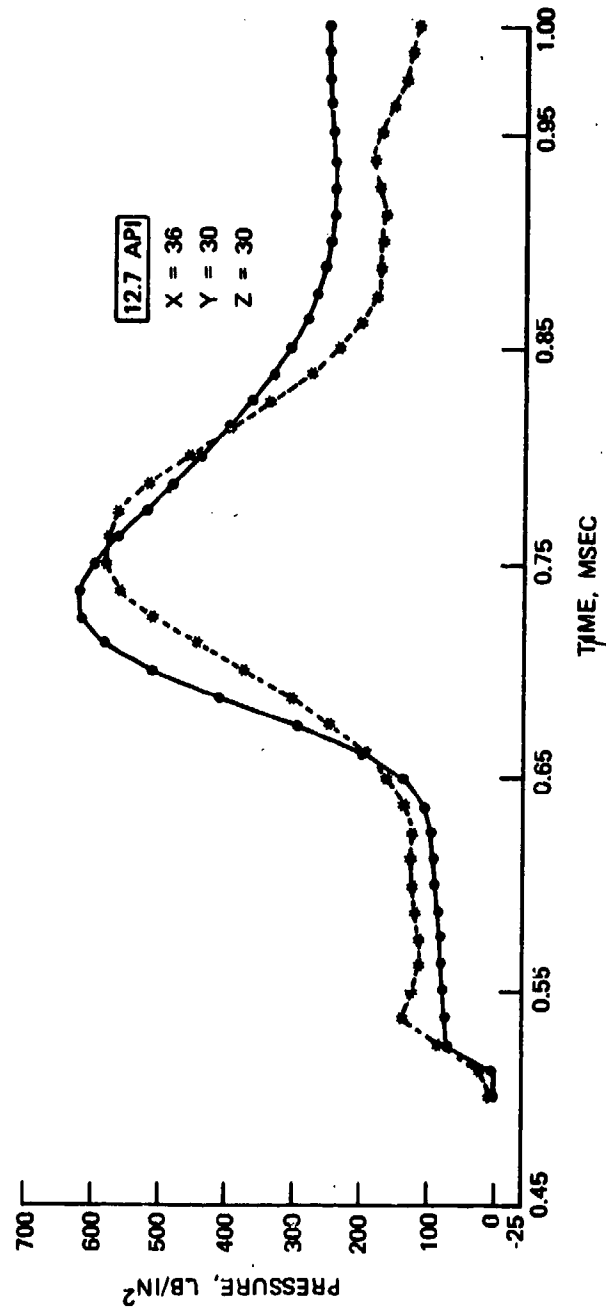


Figure 16. Pressure Versus Time Plot for Shot 2HR14 (Sheet 4 of 4).



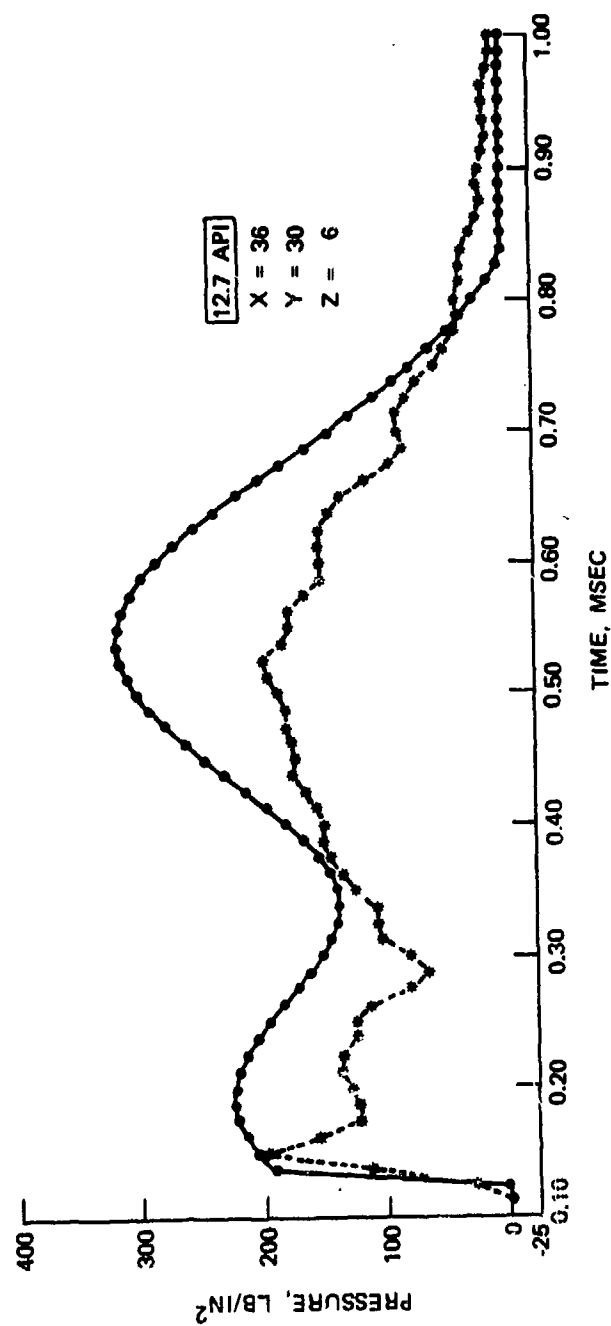


Figure 17. Pressure Versus Time Plot for Shot 2HR15 (Sheet 1 of 4).

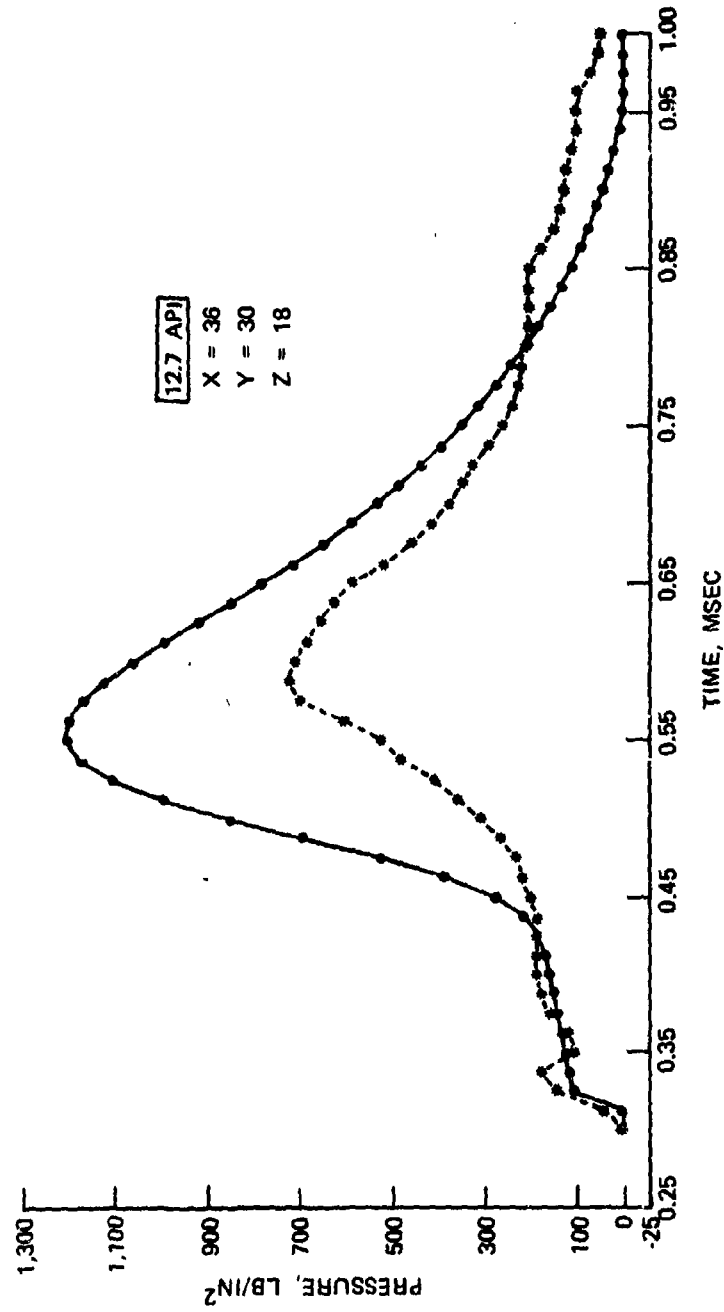


Figure 17. Pressure Versus Time Plot for Shot 2HR15 (Sheet 2 of 4).

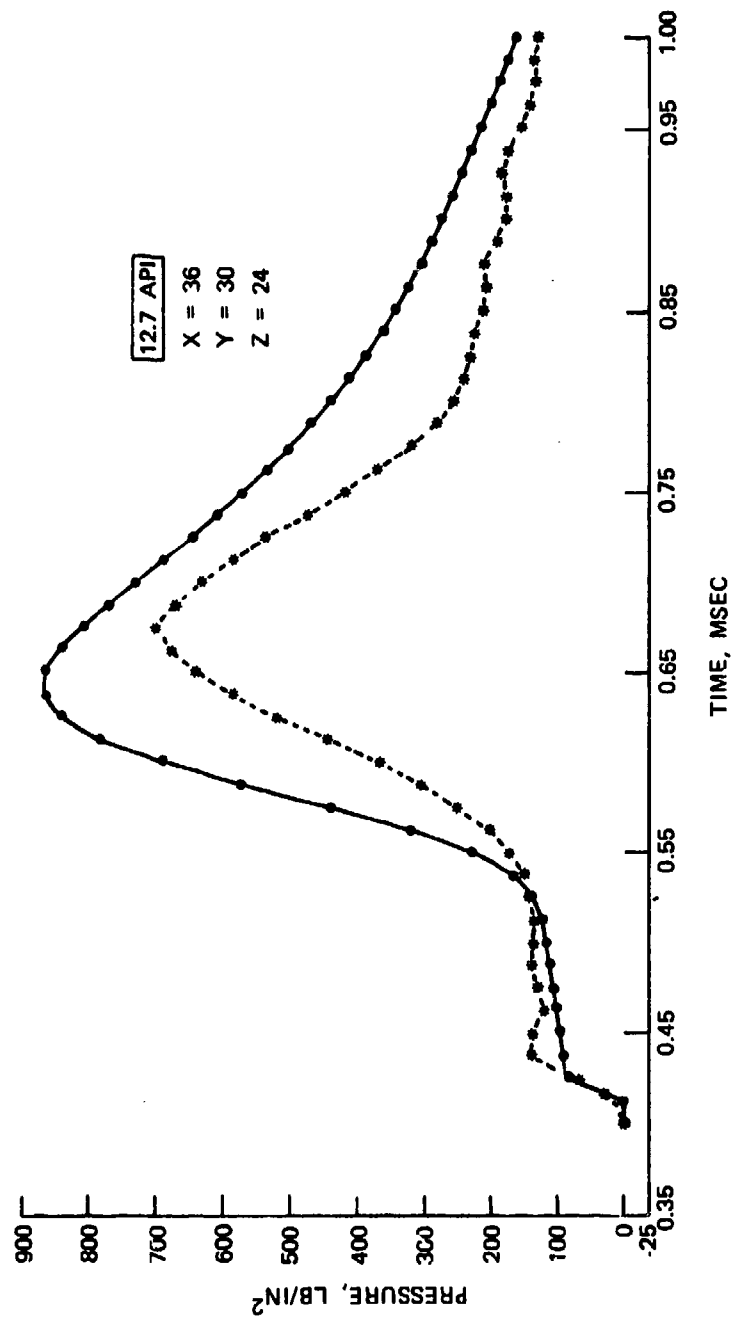


Figure 17. Pressure Versus Time Plot for Shot 2HR15 (Sheet 3 of 4).

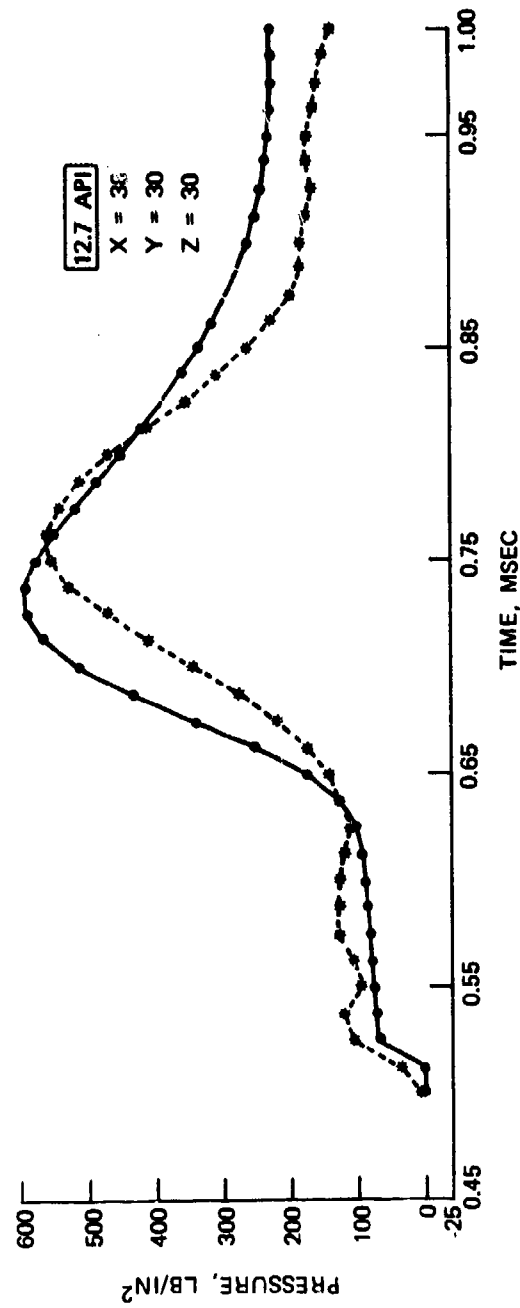


Figure 17. Pressure Versus Time Plot for Shot 2HR15 (Sheet 4 of 4).

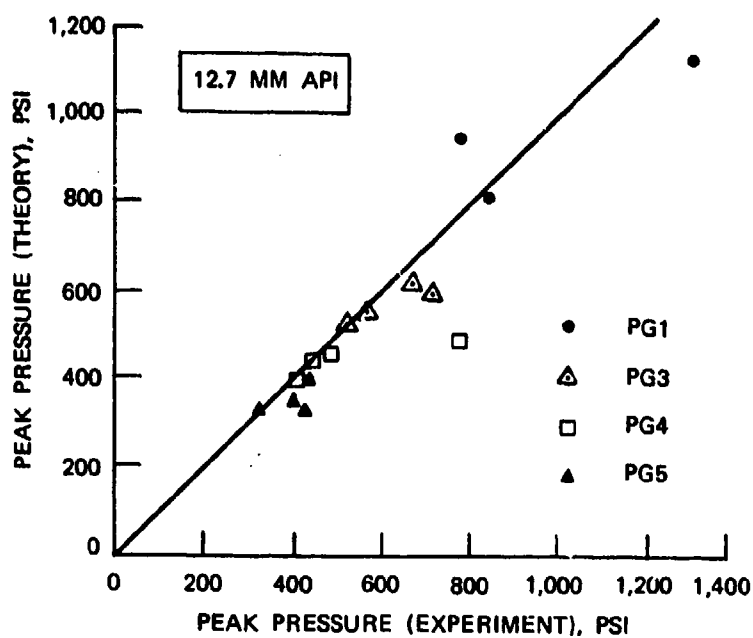


Figure 18. Peak Pressure—Theory Versus Experiment;  
0 Degree Obliquity, Tumbled.

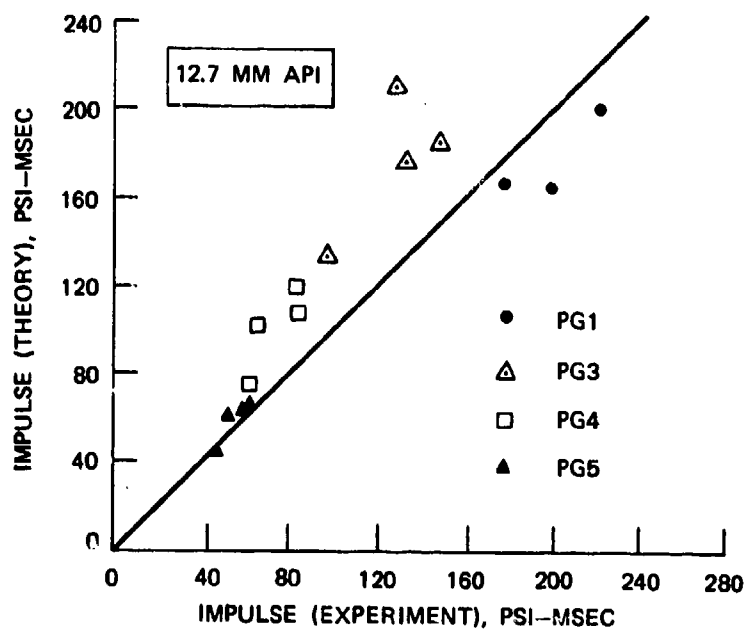


Figure 19. Impulse—Theory Versus Experiment;  
0 Degree Obliquity, Tumbled.

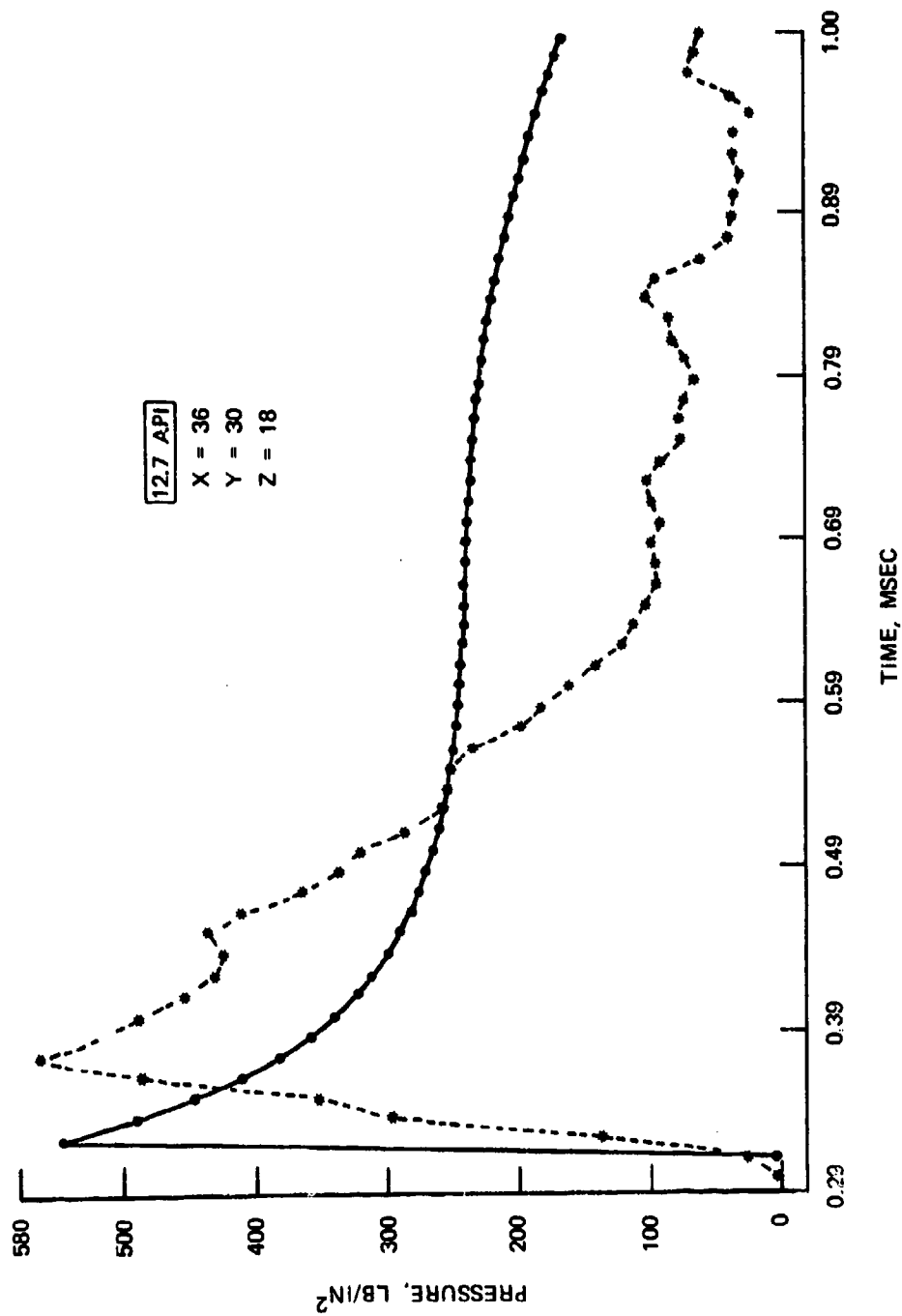


Figure 20. Pressure Versus Time Plot for Shot 2HR1 (Sheet 1 of 3).

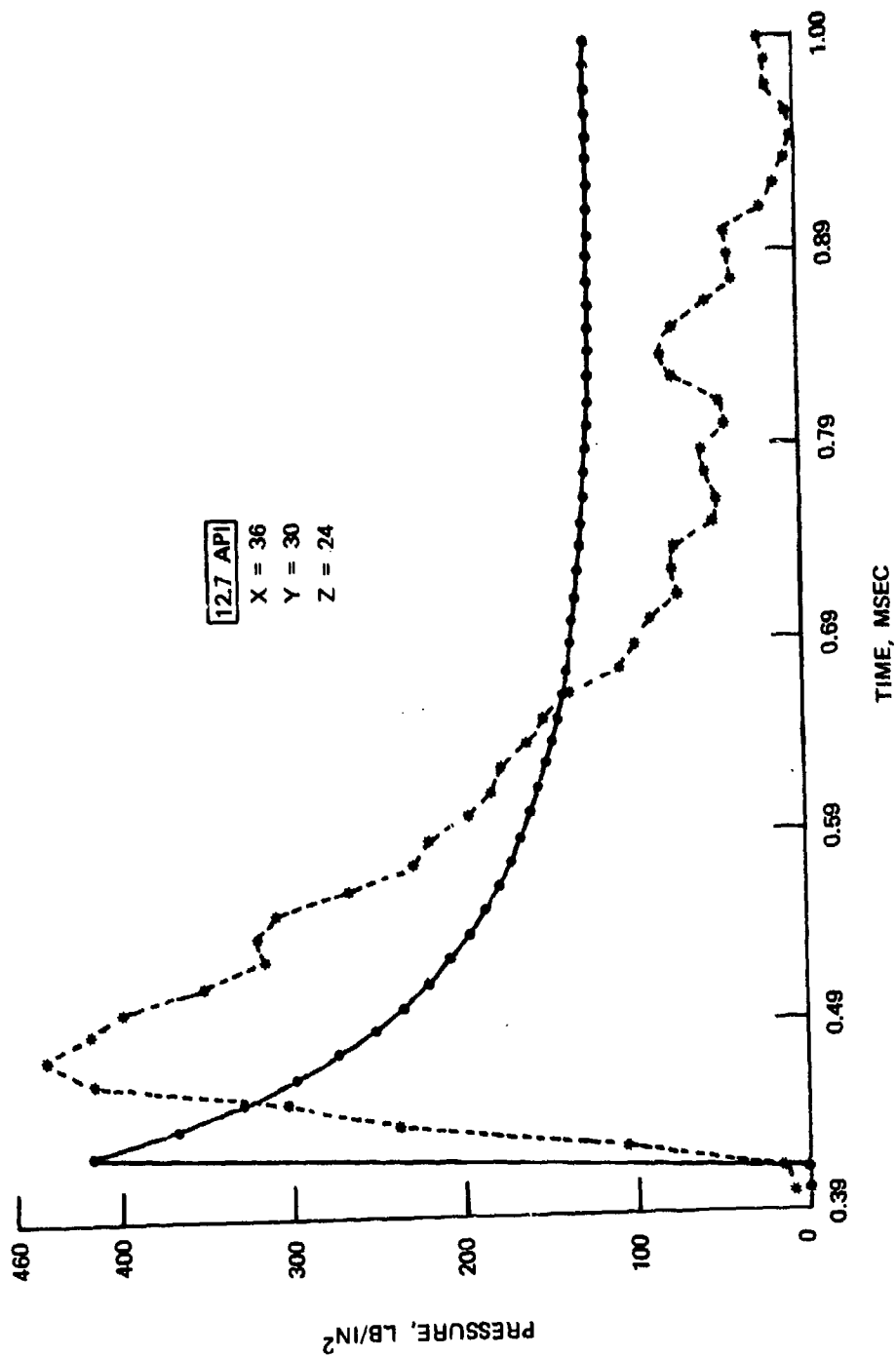


Figure 20. Pressure Versus Time Plot for Shot 2HR1 (Sheet 2 of 3).

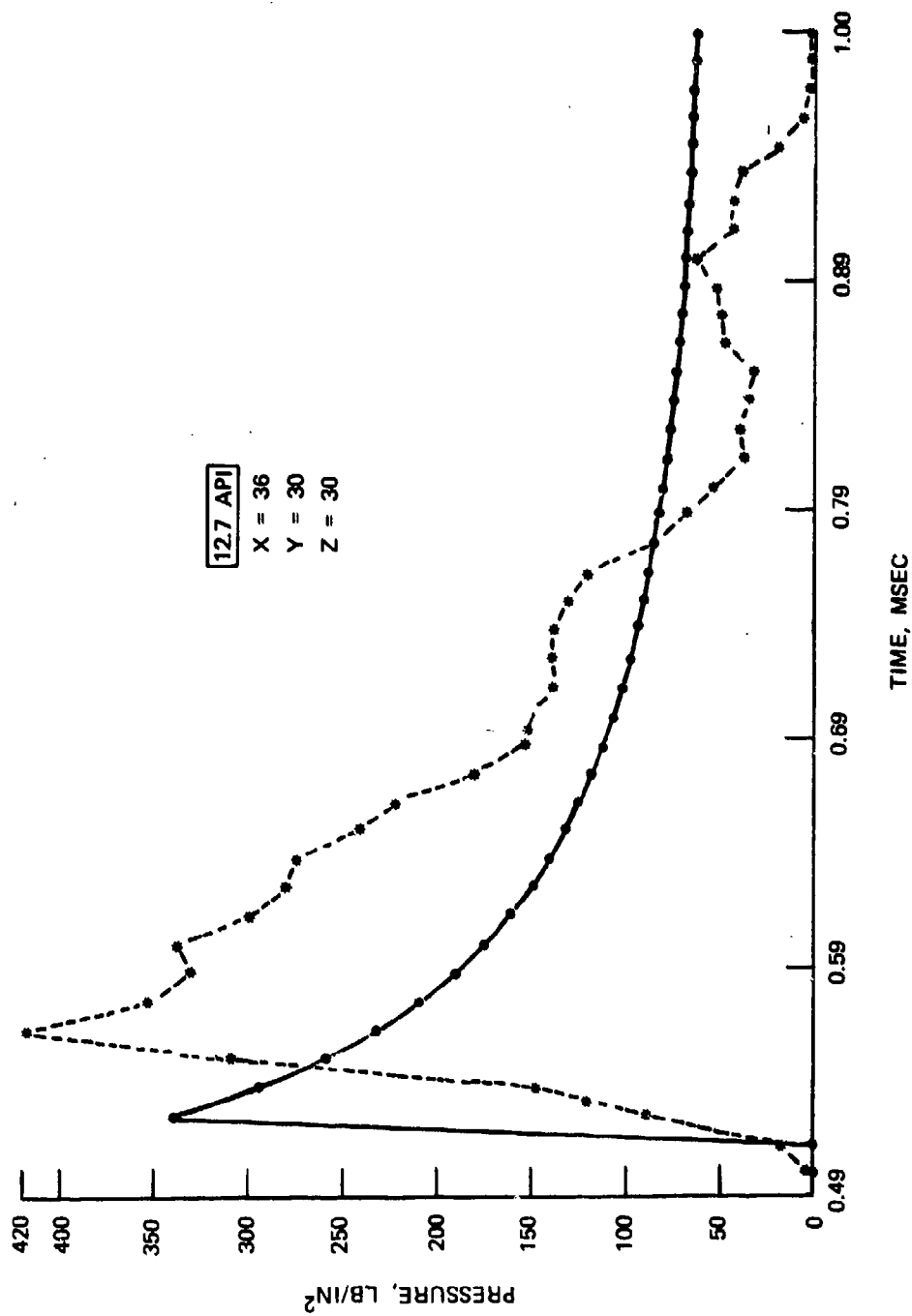


Figure 20. Pressure Versus Time Plot for Shot 2HR1 (Sheet 3 of 3).



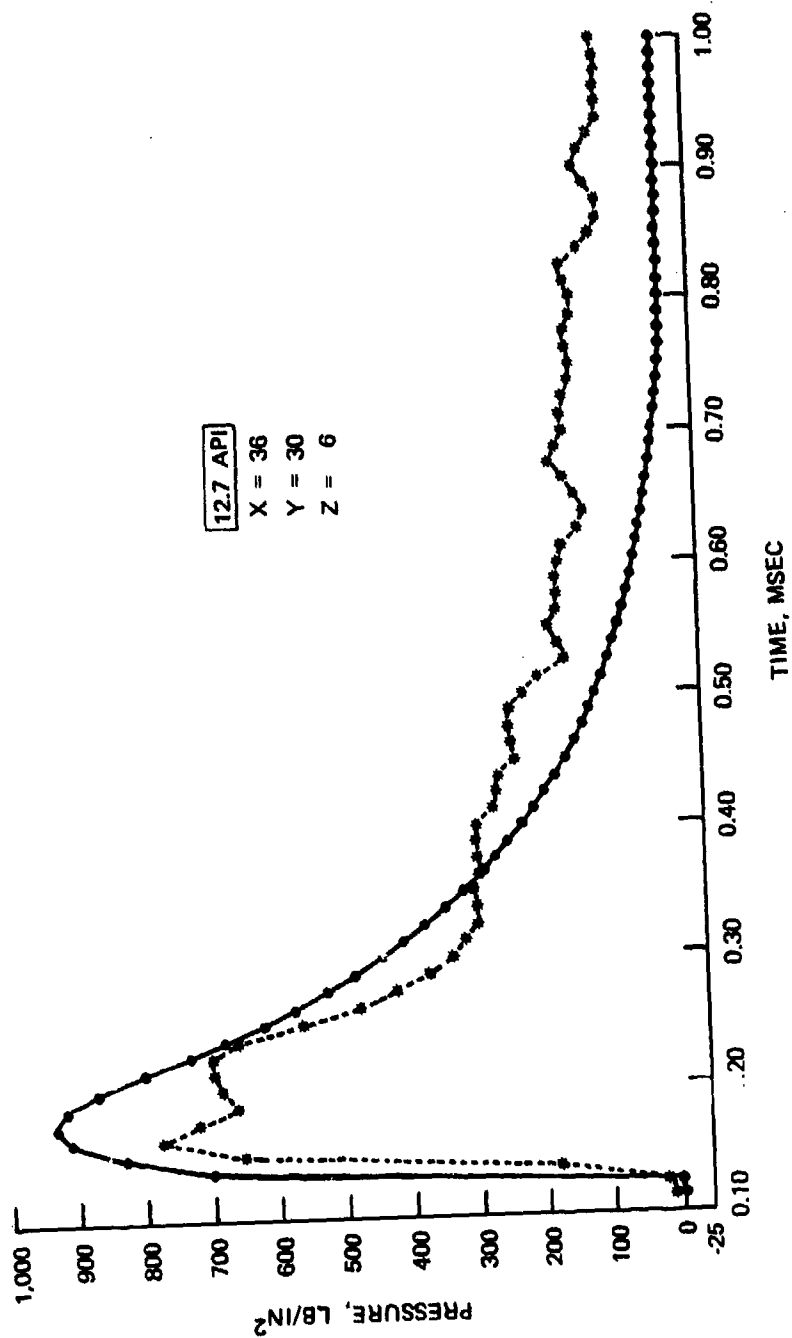


Figure 21. Pressure Versus Time Plot for Shot 2HR5 (Sheet 1 of 4).

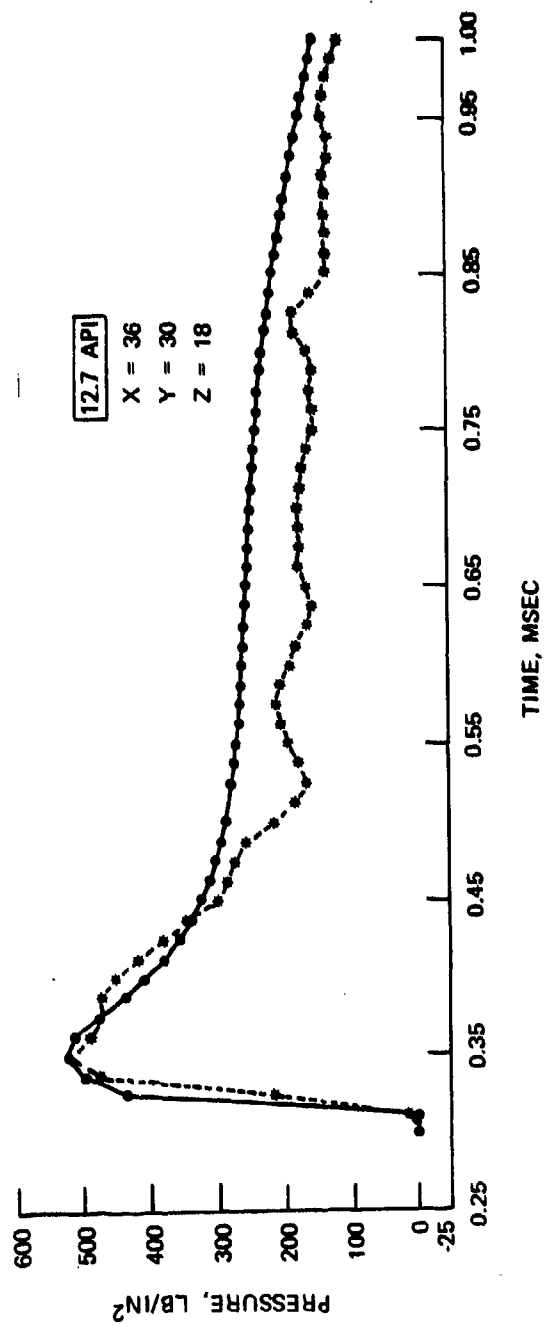


Figure 21. Pressure Versus Time Plot for Shot 2HR5 (Sheet 2 of 4).

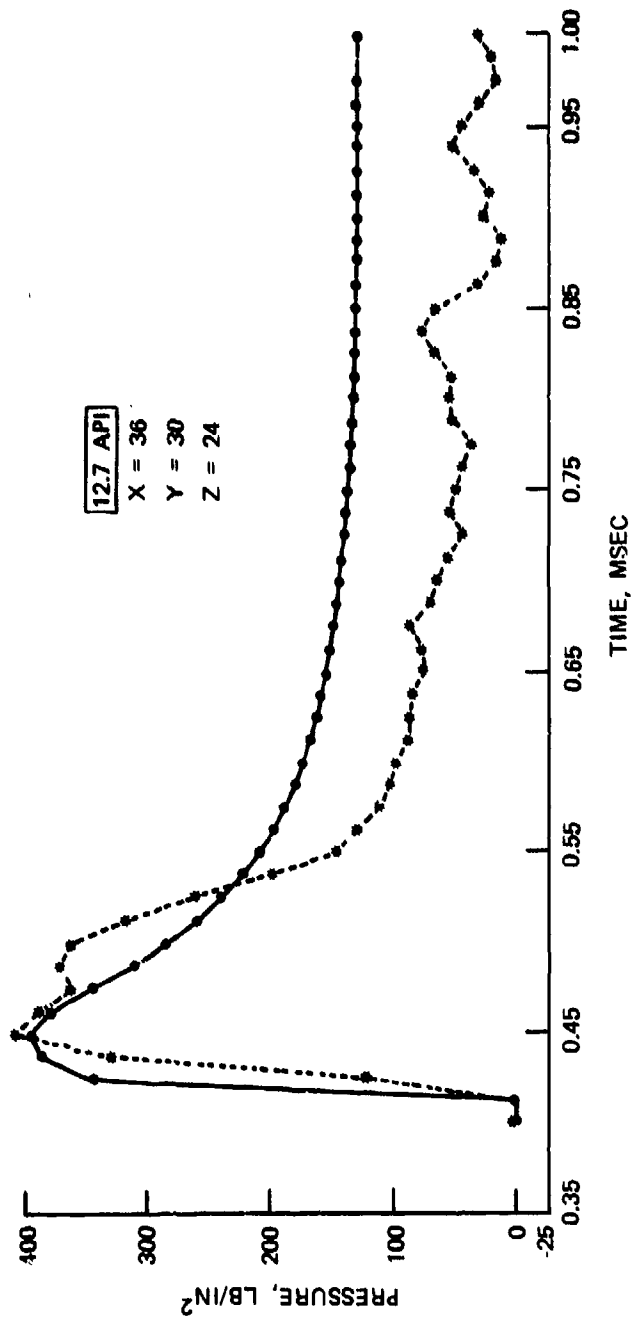


Figure 21. Pressure Versus Time Plot for Shot 2HR5 (Sheet 3 of 4).

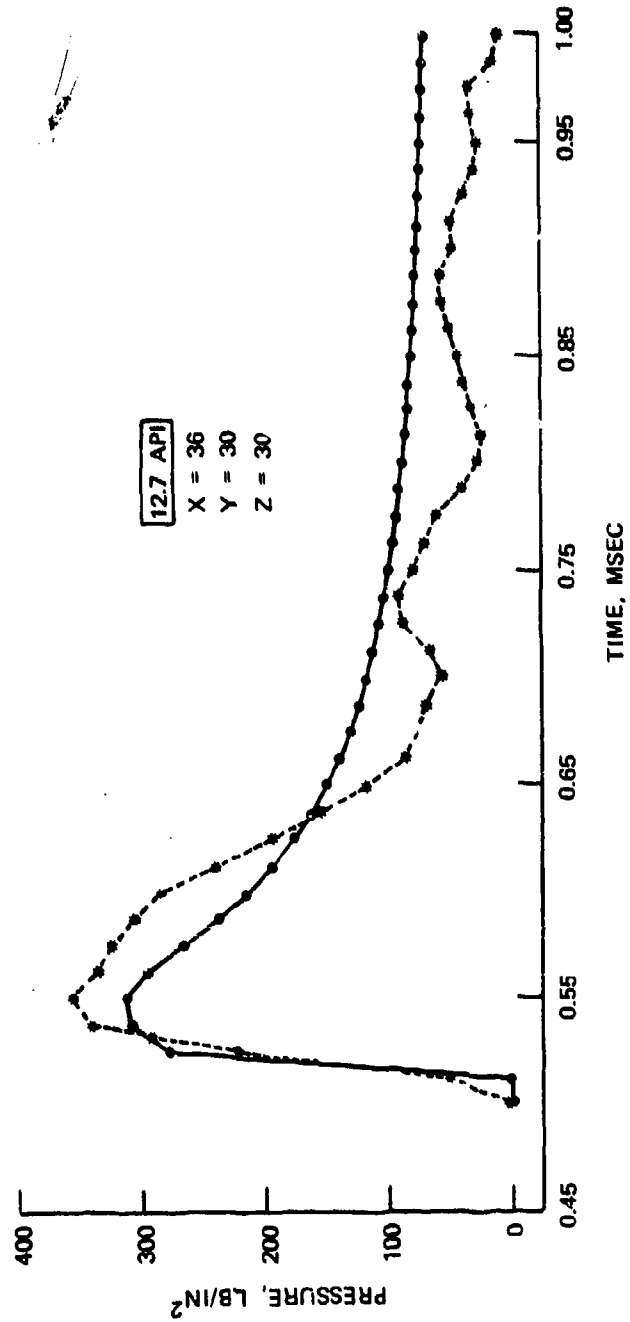


Figure 21. Pressure Versus Time Plot for Shot 2HR5 (Sheet 4 of 4).

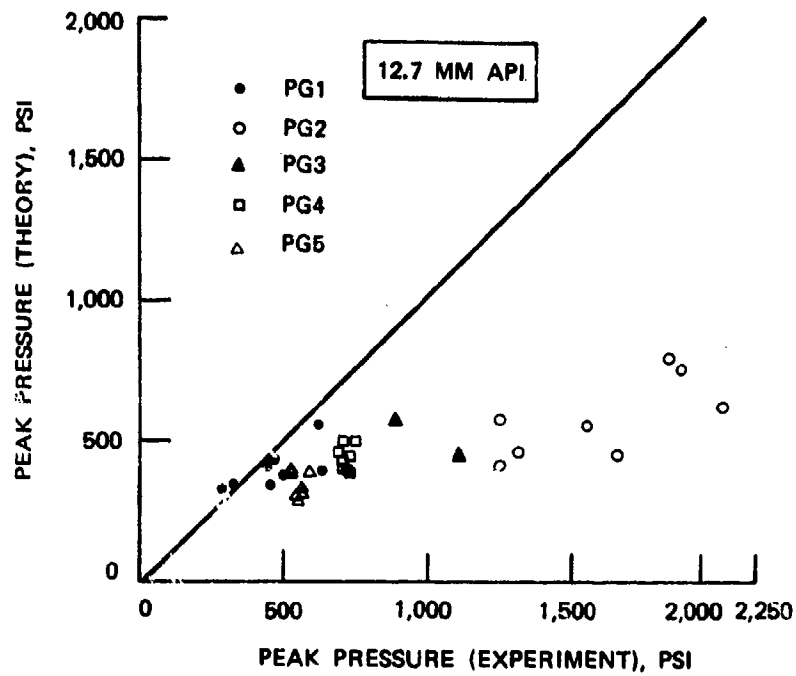


Figure 22. Peak Pressure—Theory Versus Experiment;  
30 to 45 Degrees Obliquity, 0 Degree Yaw.

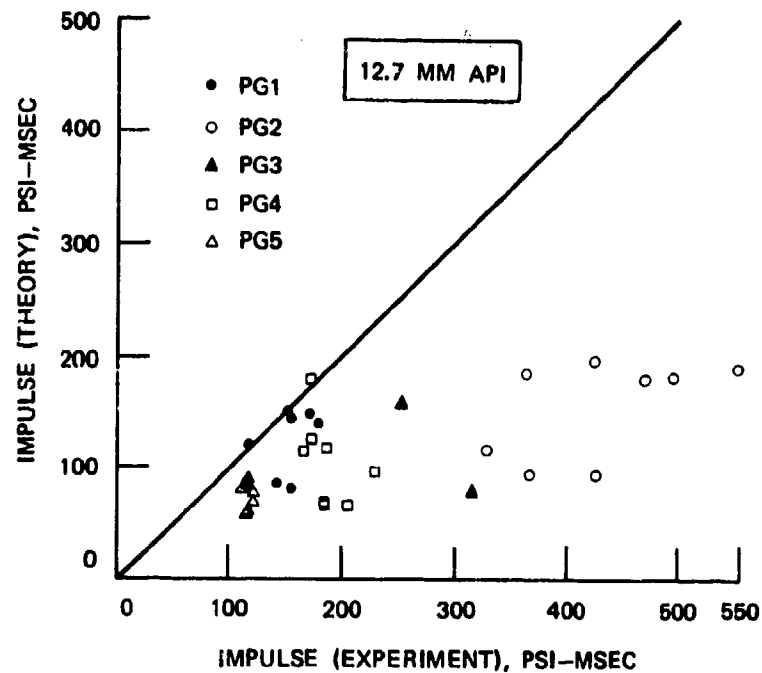


Figure 23. Impulse—Theory Versus Experiment;  
30 to 45 Degrees Obliquity, 0 Degree Yaw.

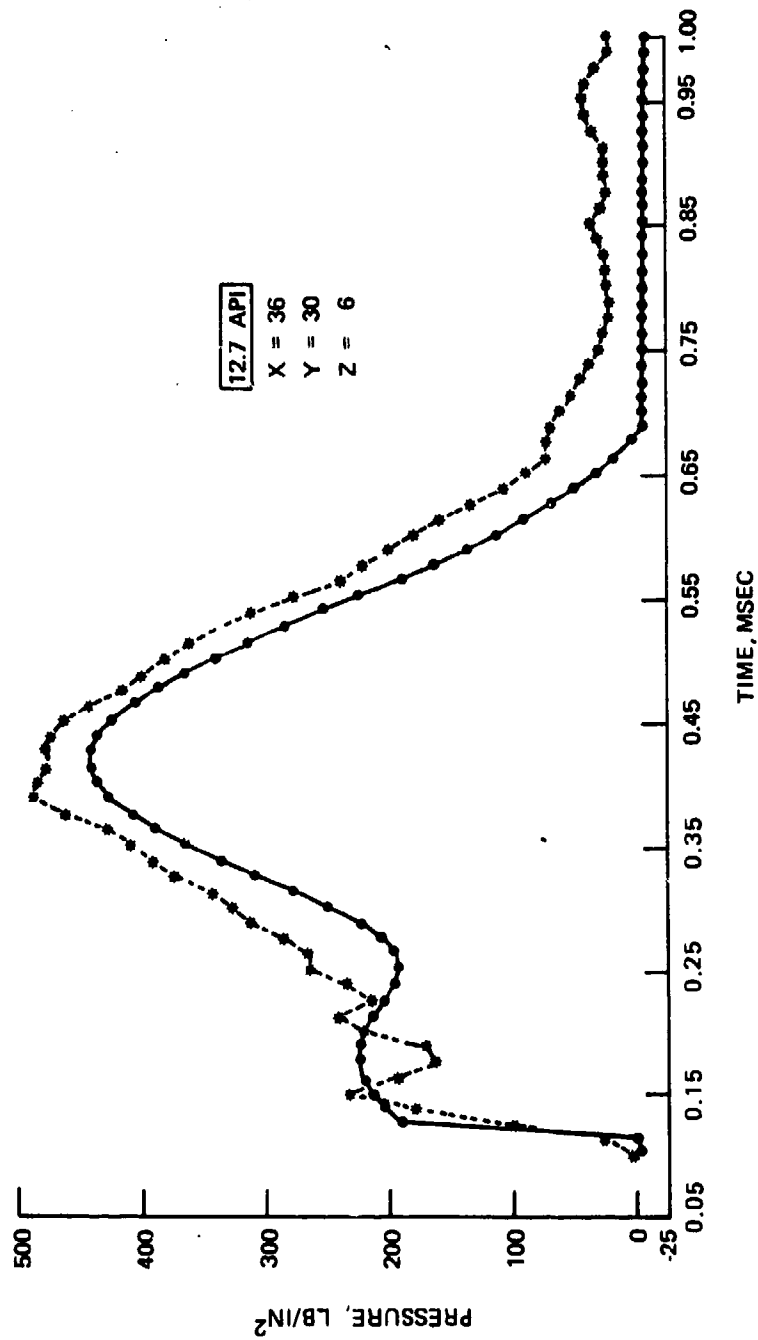


Figure 24. Pressure Versus Time Plot for Shot 3HR2 (Sheet 1 of 4).

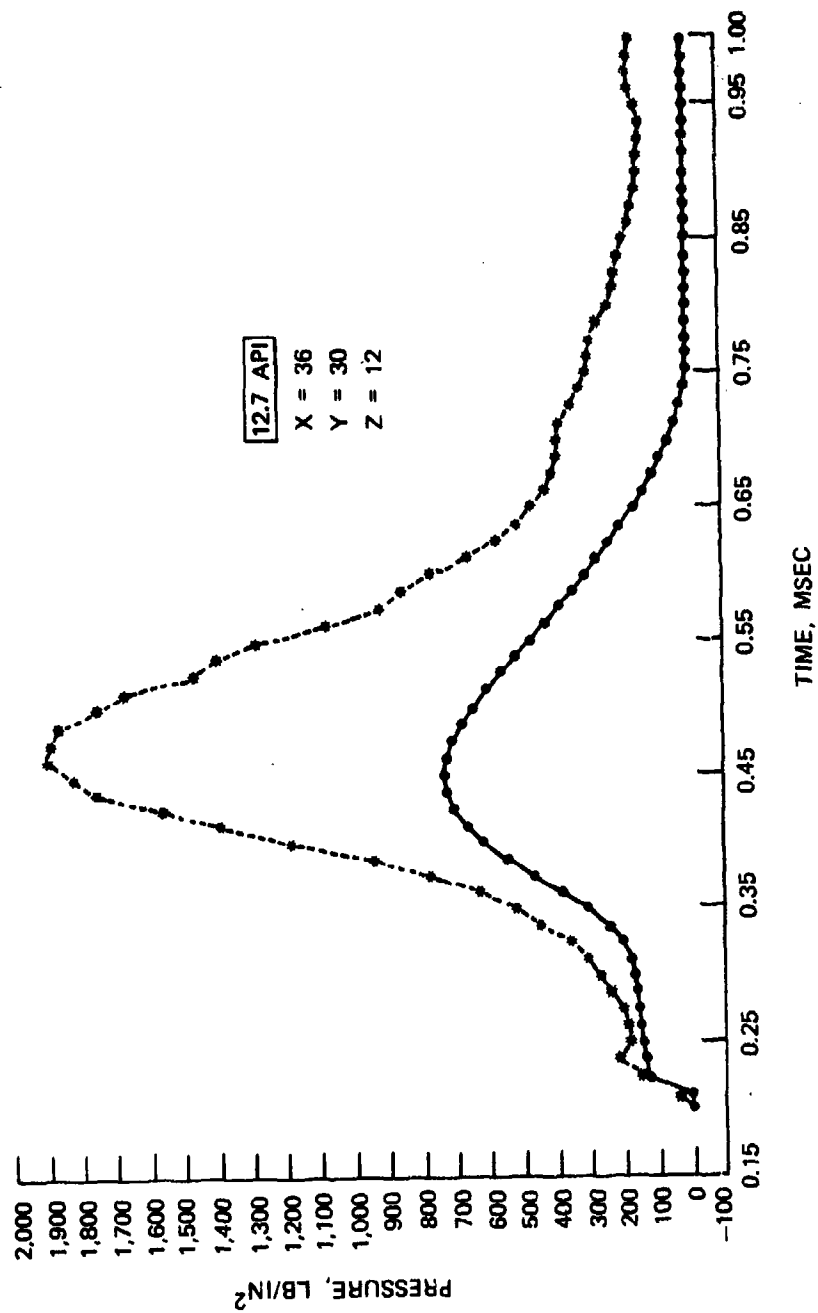


Figure 24. Pressure Versus Time Plot for Shot 3HR2 (Sheet 2 of 4).

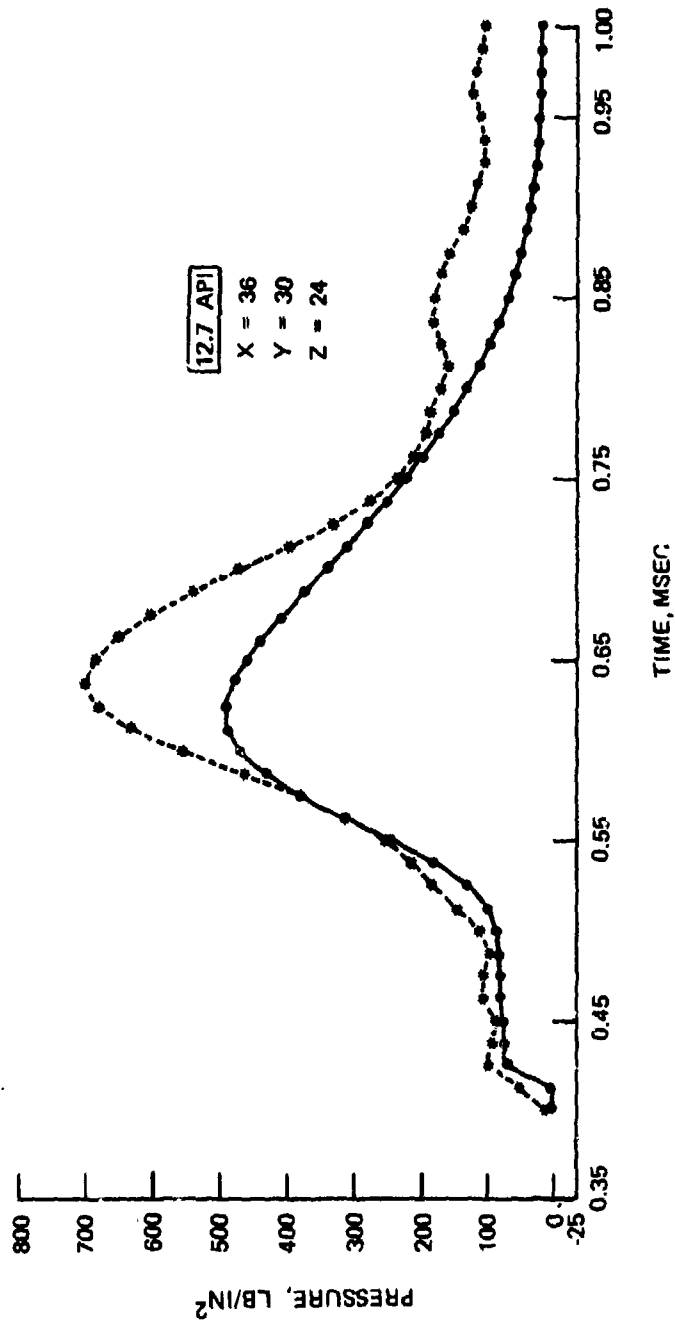


Figure 24. Pressure Versus Time Plot for Shot 3HR2 (Sheet 3 of 4).



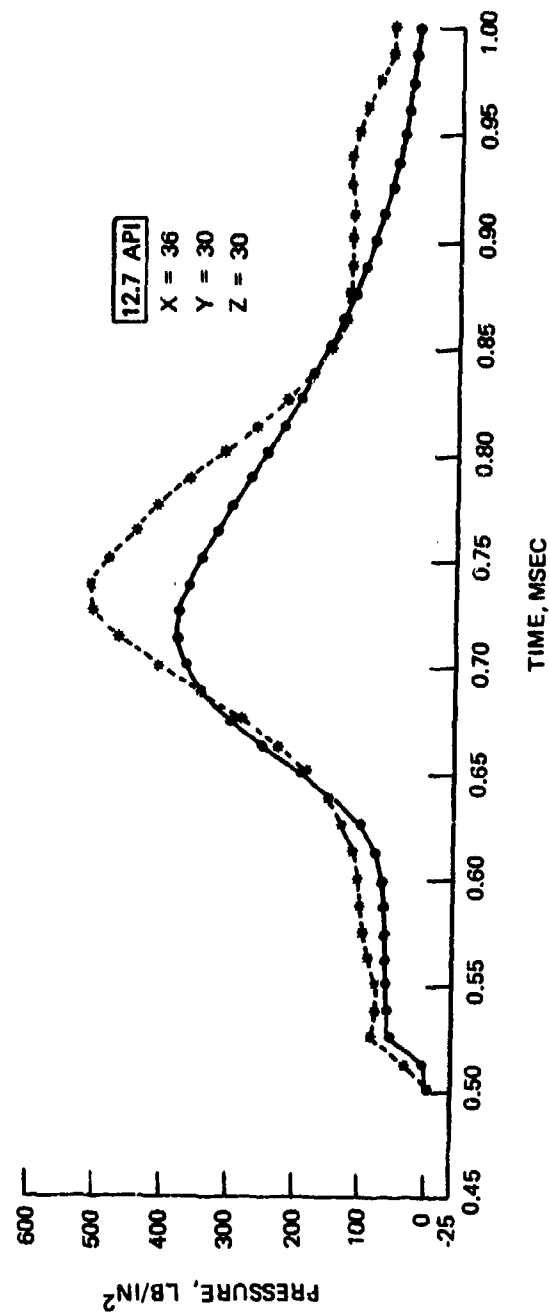


Figure 24. Pressure Versus Time Plot for Shot 3HR2 (Sheet 4 of 4).

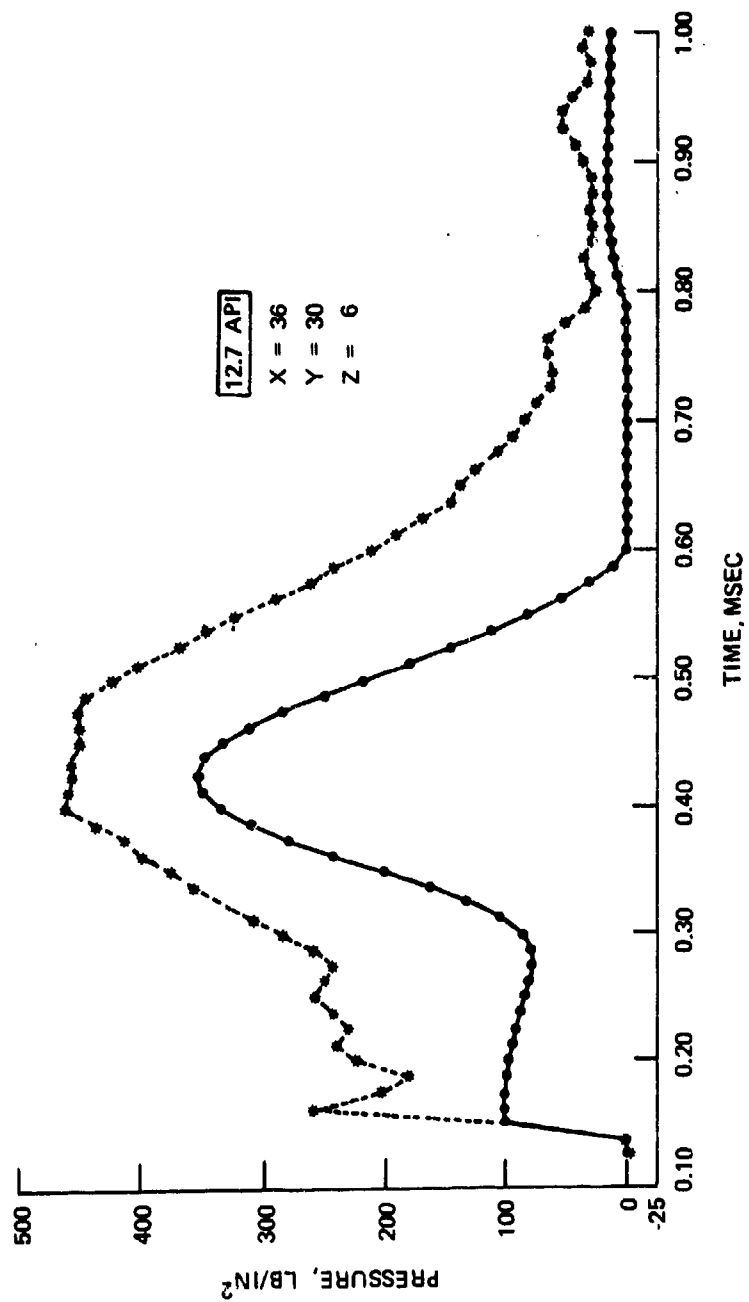


Figure 25. Pressure Versus Time Plot for Shot 3HR10 (Sheet 1 of 4).

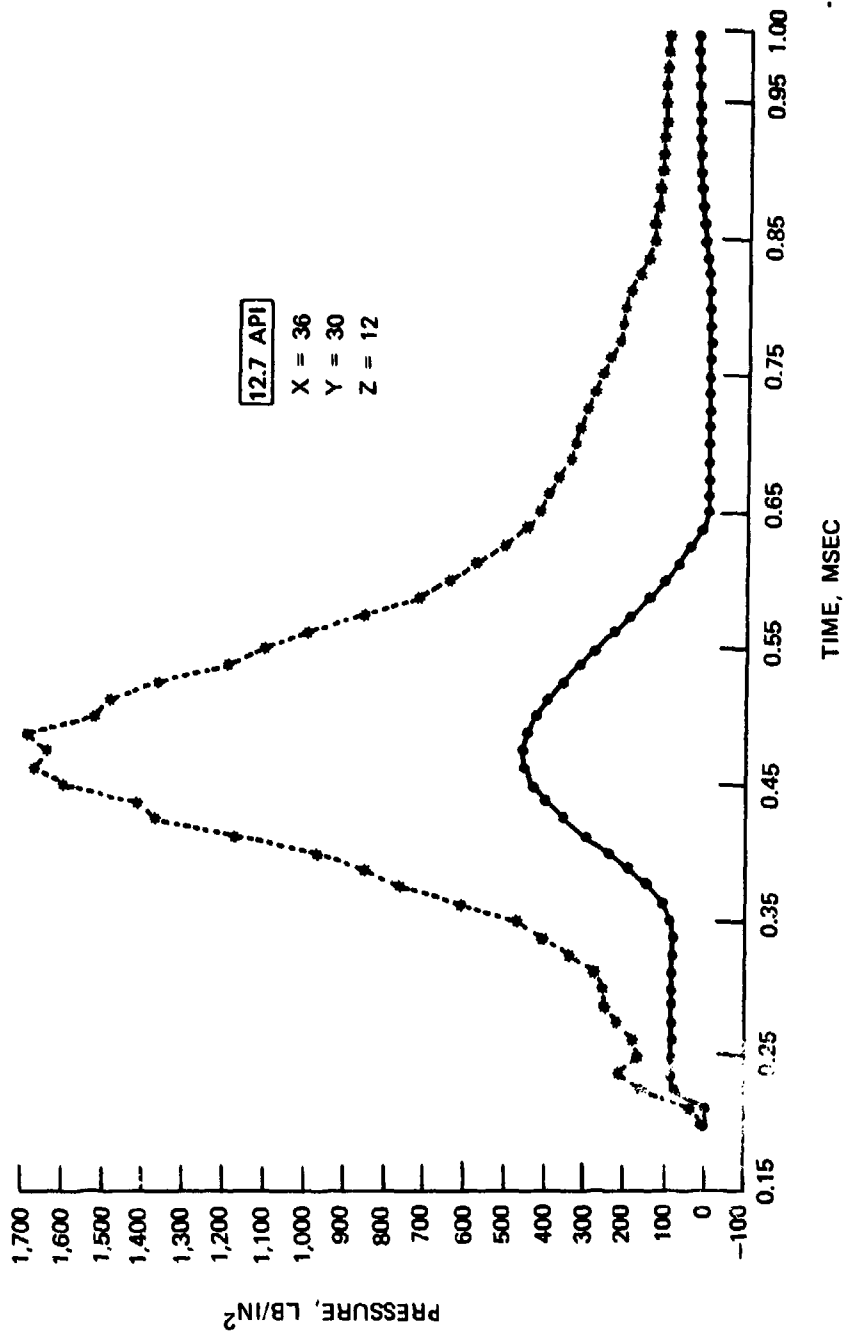


Figure 25. Pressure Versus Time Plot for Shot 3HR10 (Sheet 2 of 4).

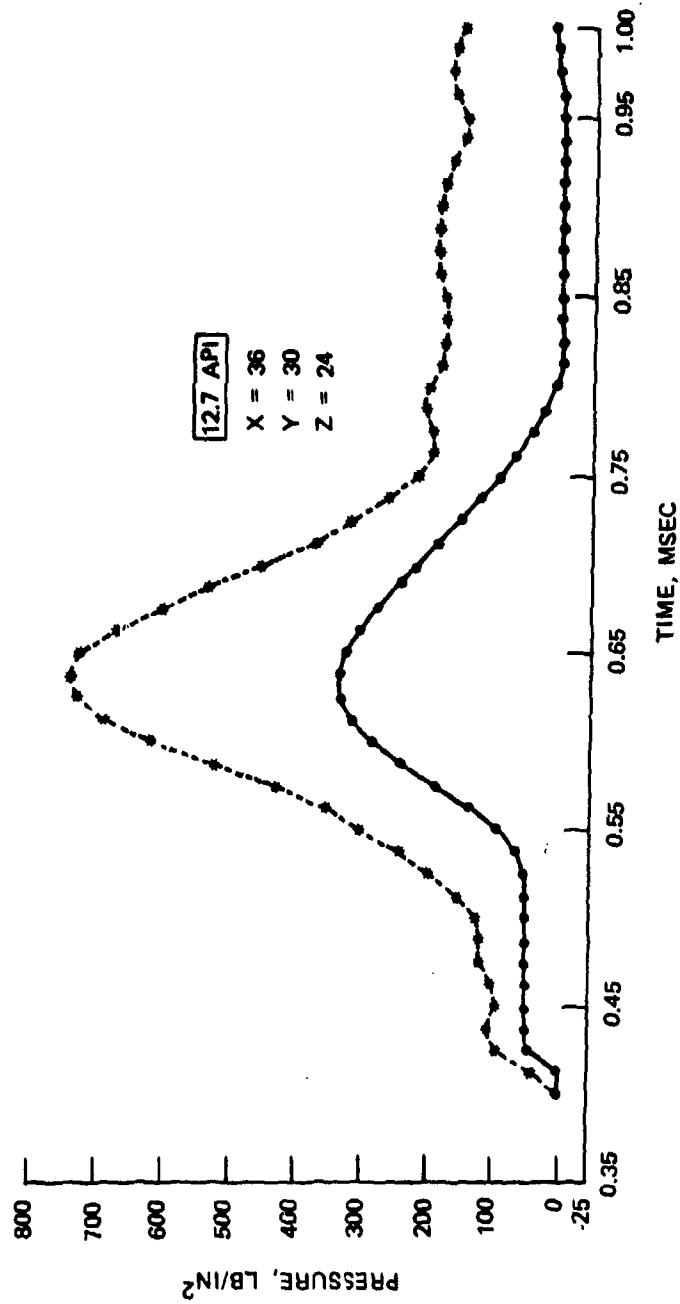


Figure 25. Pressure Versus Time Plot for Shot 3HR10 (Sheet 3 of 4).

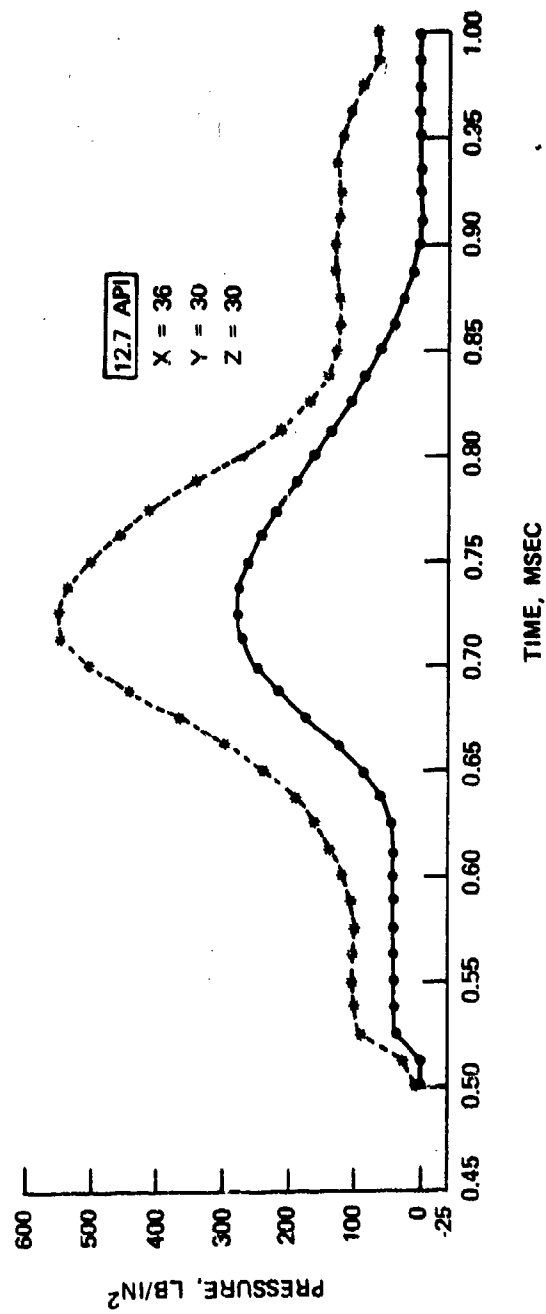


Figure 25. Pressure Versus Time Plot for Shot 3HR10 (Sheet 4 of 4).

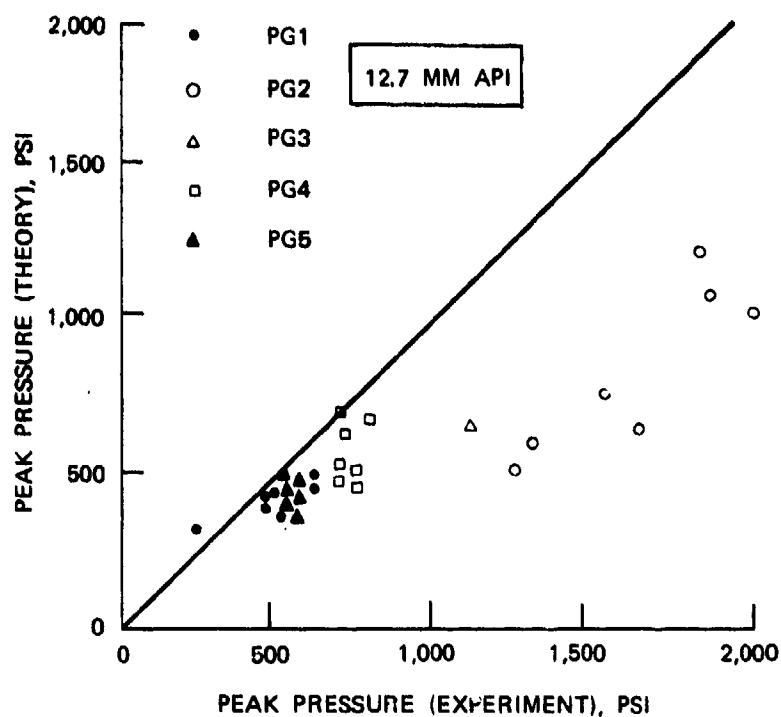


Figure 26. Peak Pressure—Theory Versus Experiment;  
15 to 25 Degrees Obliquity, 0 Degree Yaw.

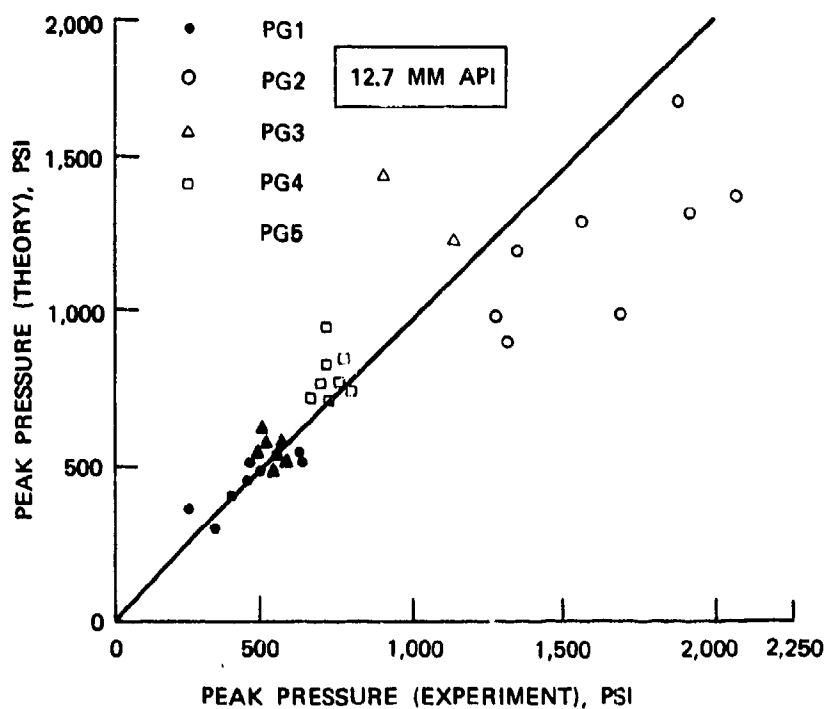


Figure 27. Peak Pressure—Theory Versus Experiment;  
0 to 0 Degree Obliquity, 0 Degree Yaw.

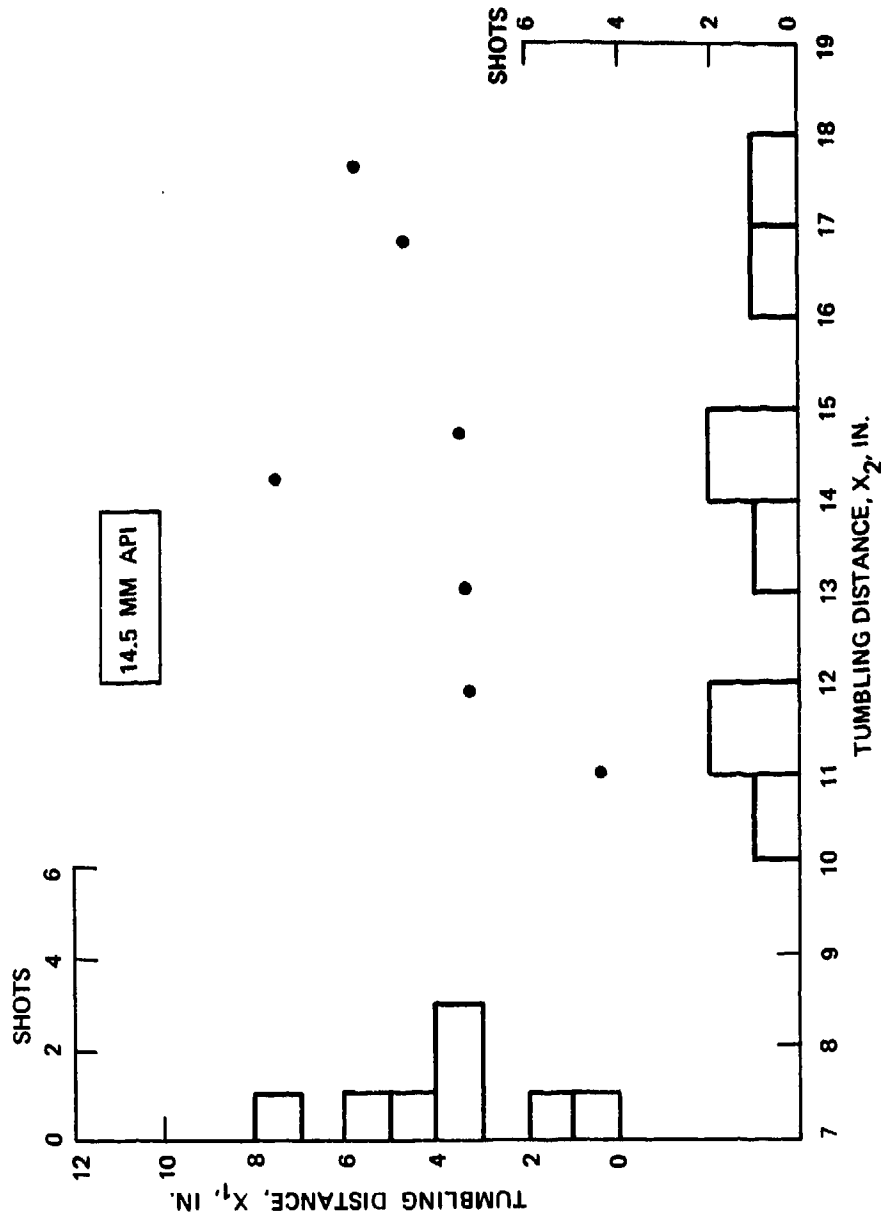


Figure 28. Tumbling Distance Distribution; 0 Degree Obliquity, 0 Degree Yaw.

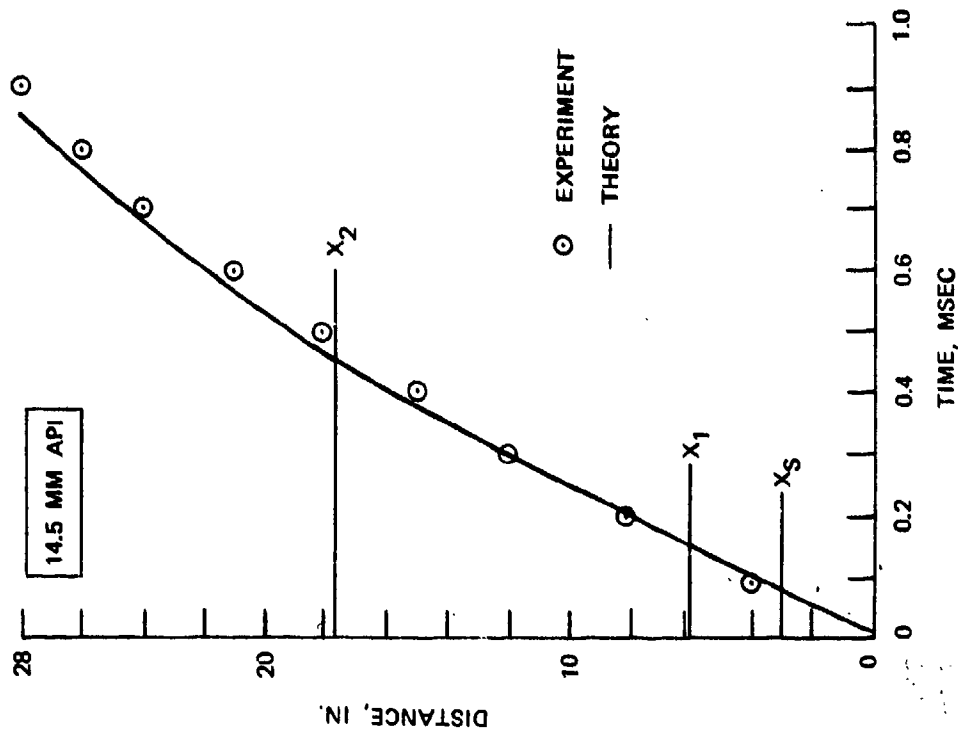


Figure 29. Experimental Trajectory for Shot 4HR6.

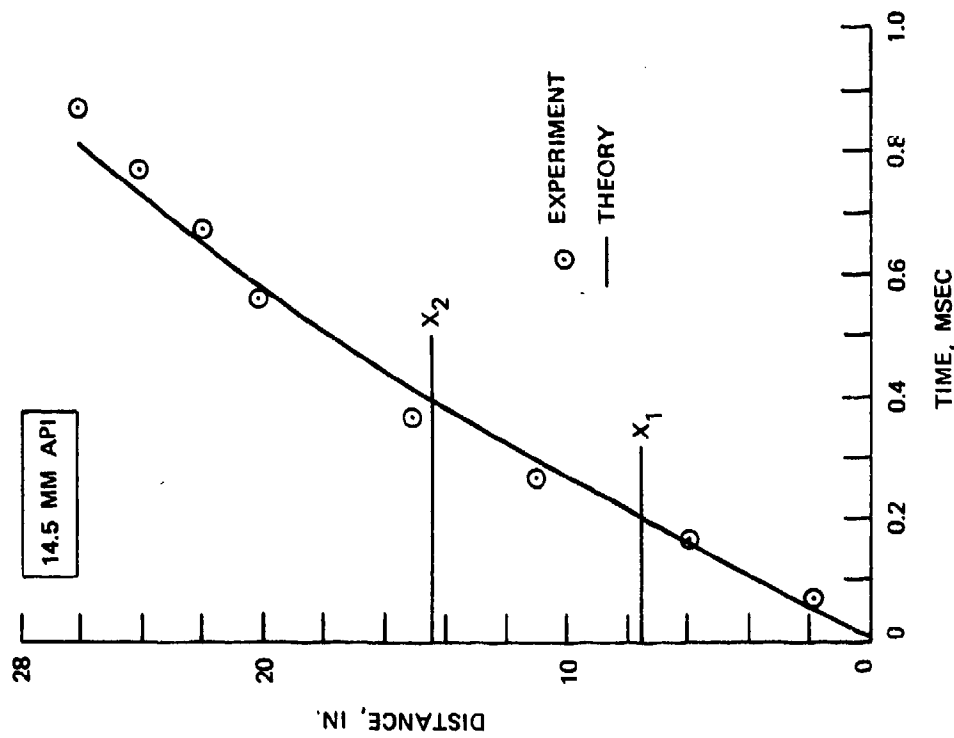


Figure 30. Experimental Trajectory for Shot 4HR7.



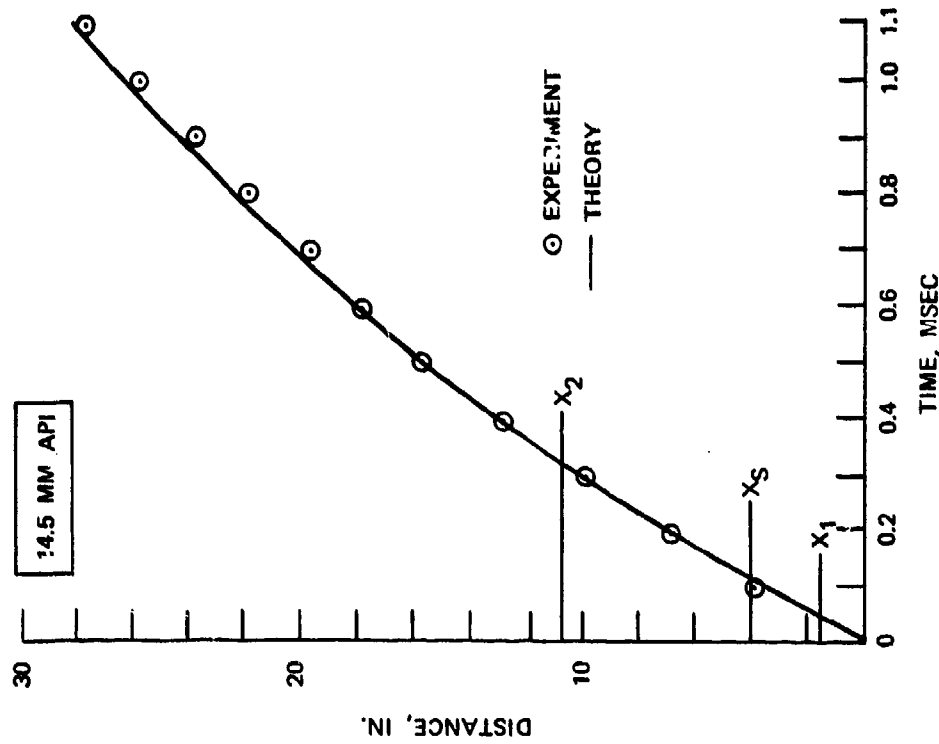


Figure 31. Experimental Trajectory for Shot 4HR8.

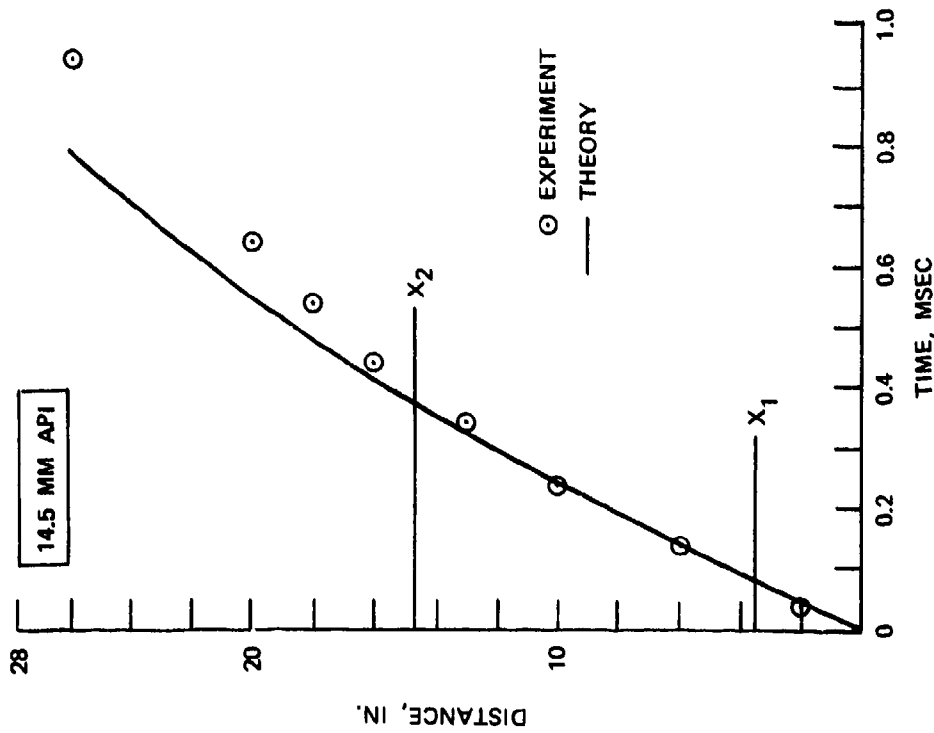


Figure 32. Experimental Trajectory for Shot 4HR9.

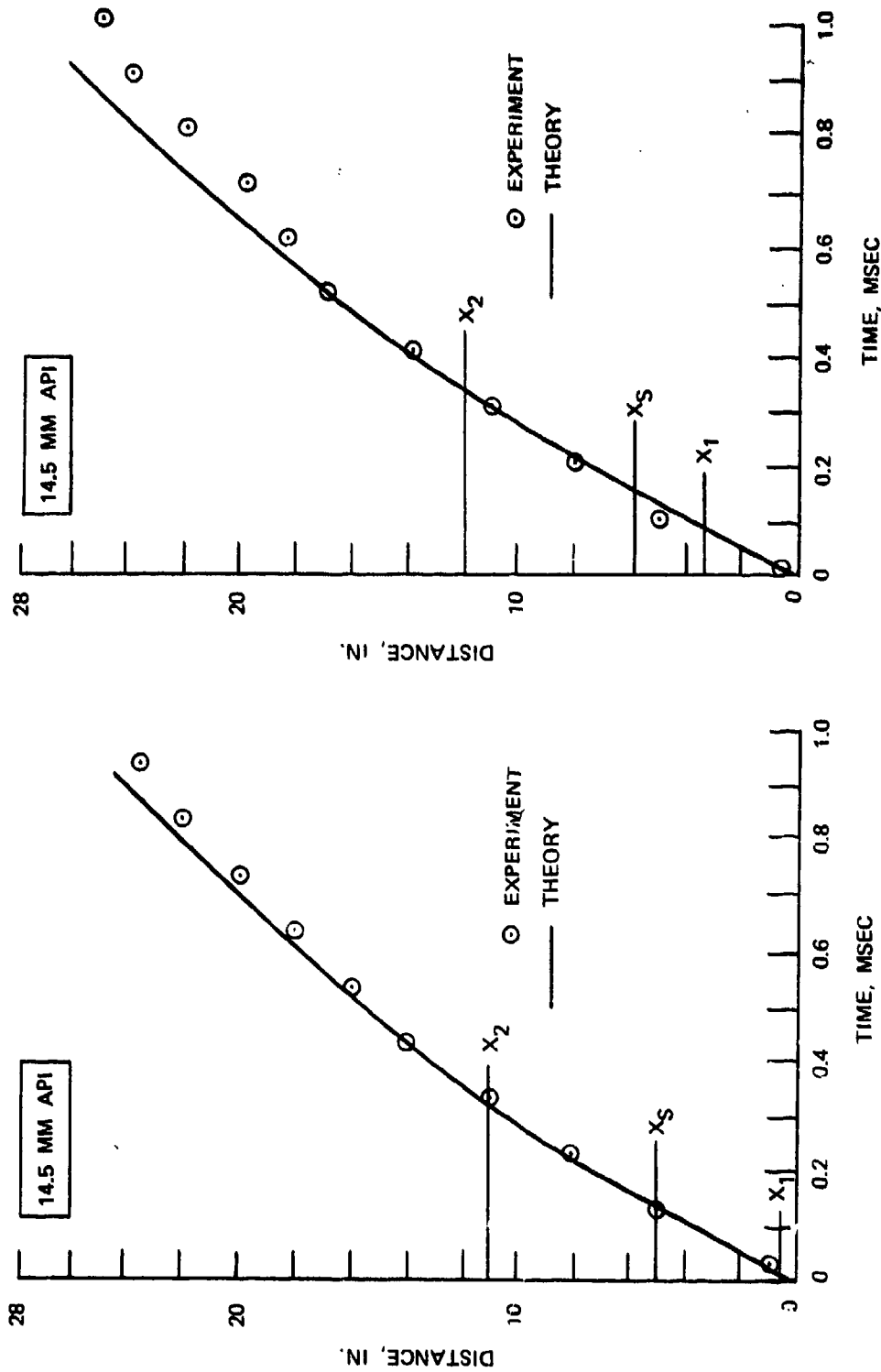


Figure 33. Experimental Trajectory for Shot 4HR10.

Figure 34. Experimental Trajectory for Shot 4HR11.

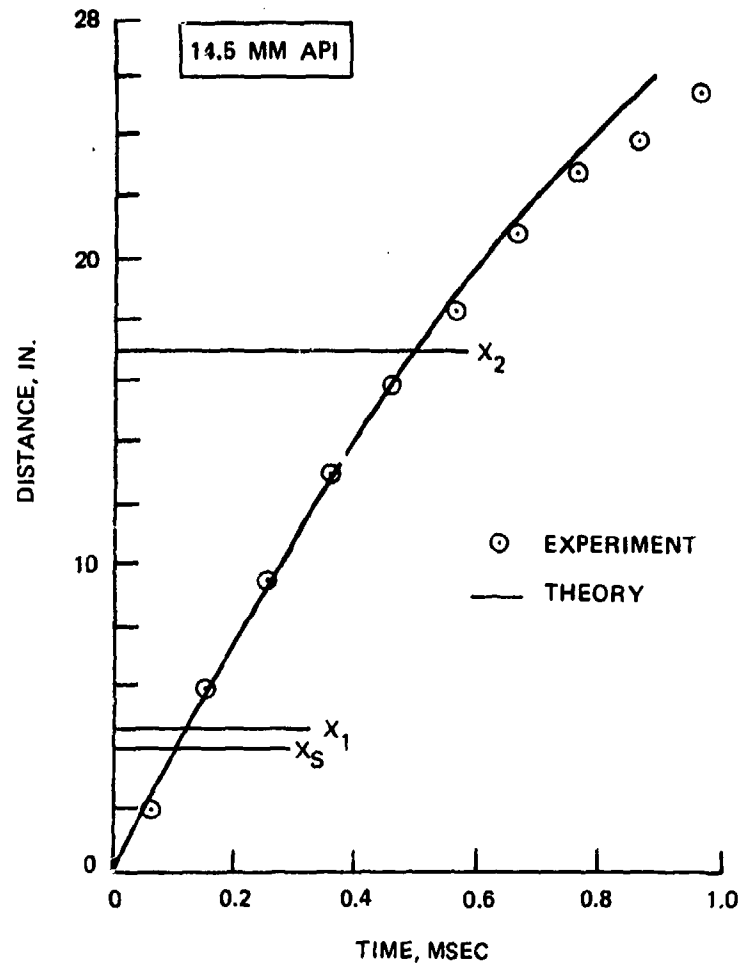


Figure 35. Experimental Trajectory for Shot 4HR12.

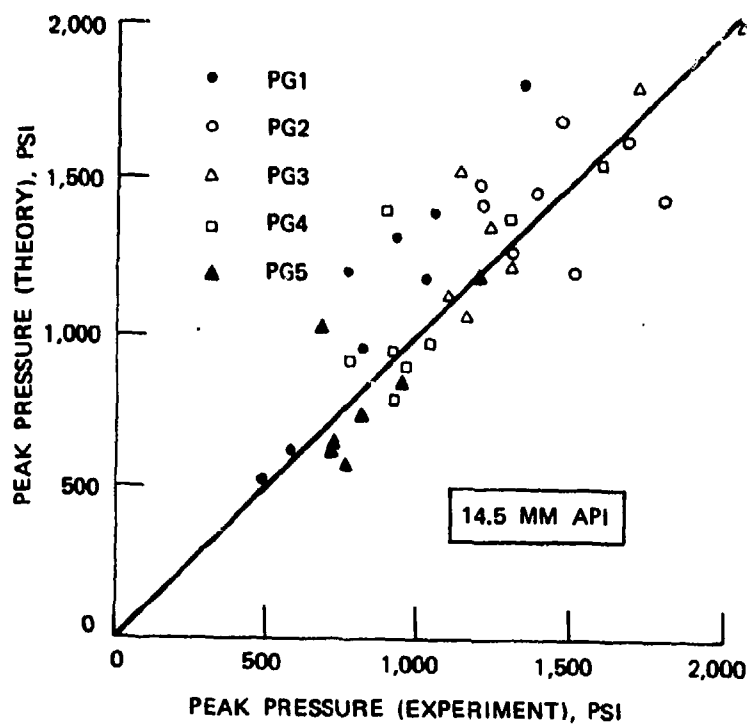


Figure 36. Peak Pressure—Theory Versus Experiment;  
0 Degree Obliquity, 0 Degree Yaw.

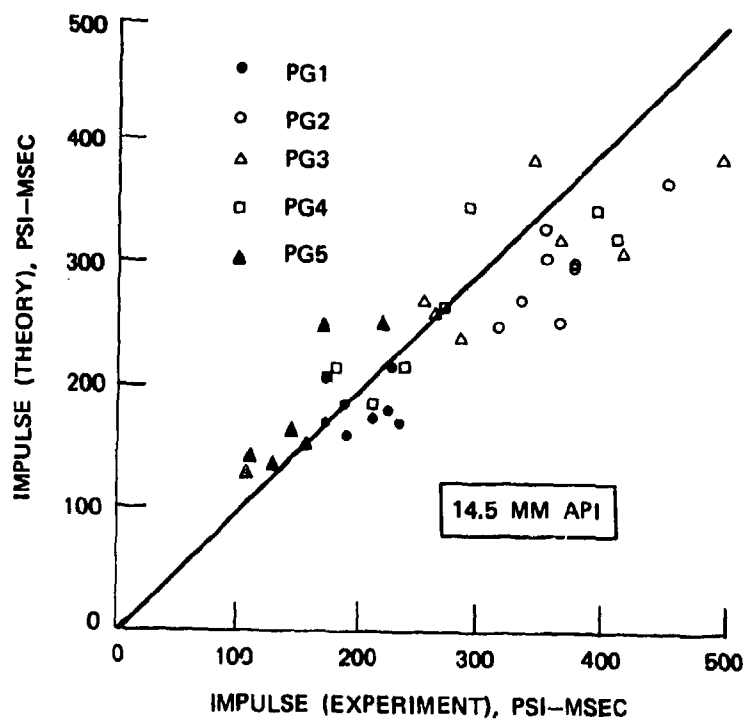


Figure 37. Impulse—Theory Versus Experiment;  
0 Degree Obliquity, 0 Degree Yaw.

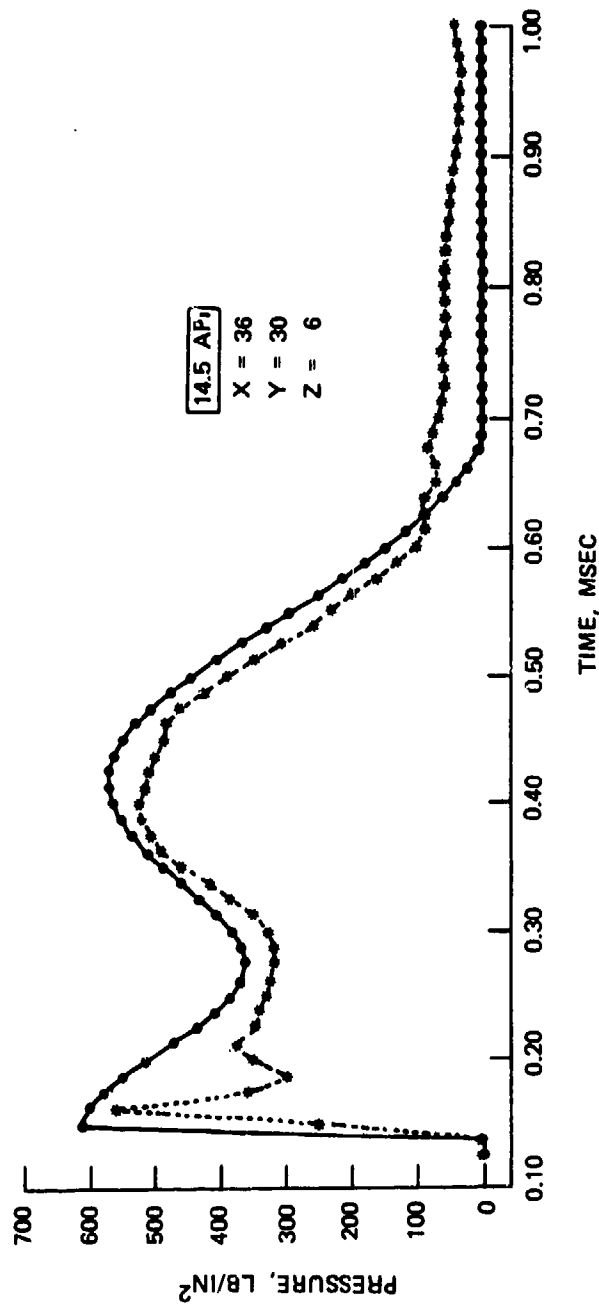


Figure 38. Pressure Versus Time Plot for Shot 4HR8 (Sheet 1 of 5).

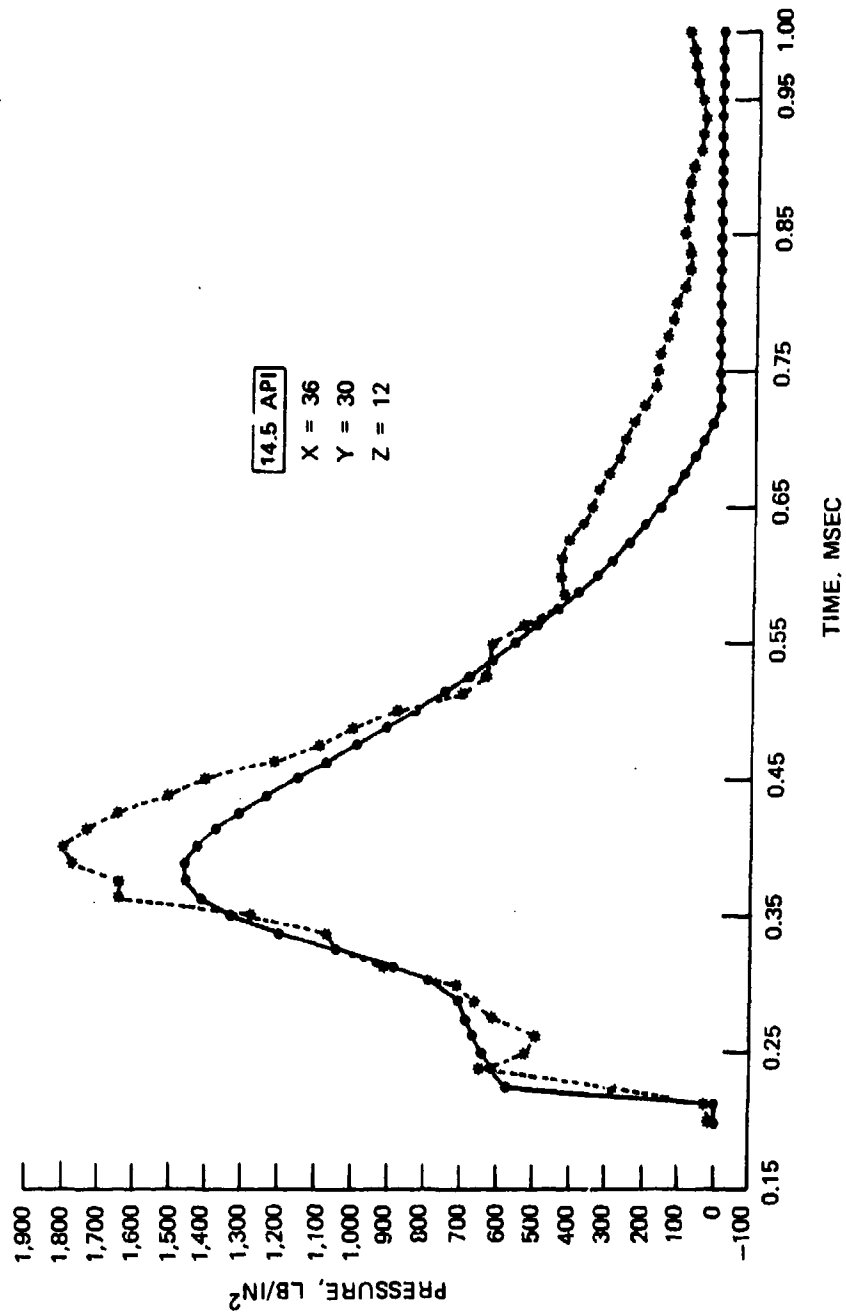


Figure 38. Pressure Versus Time Plot for Shot 4HR8 (Sheet 2 of 5).

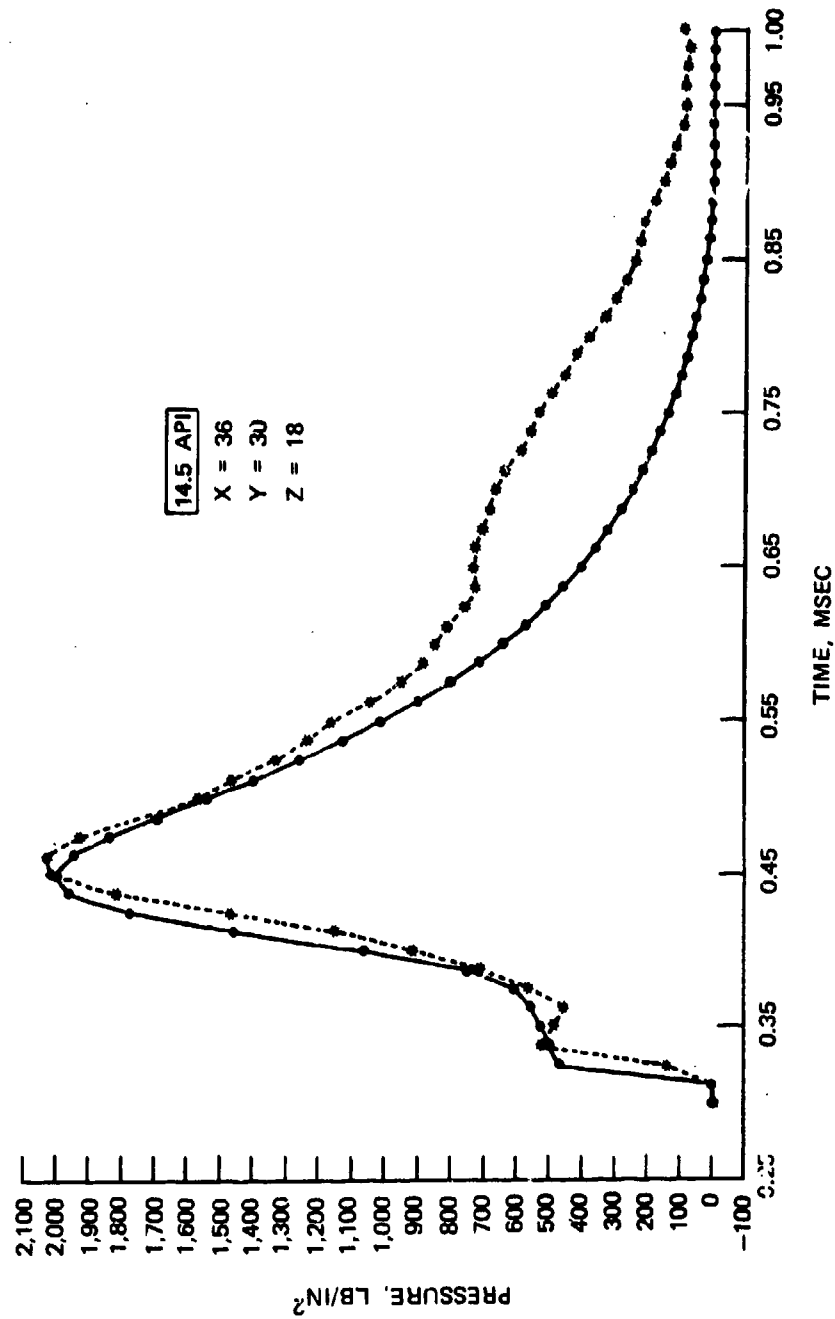


Figure 38. Pressure Versus Time Plot for Shot 4HR8 (Sheet 3 of 5).

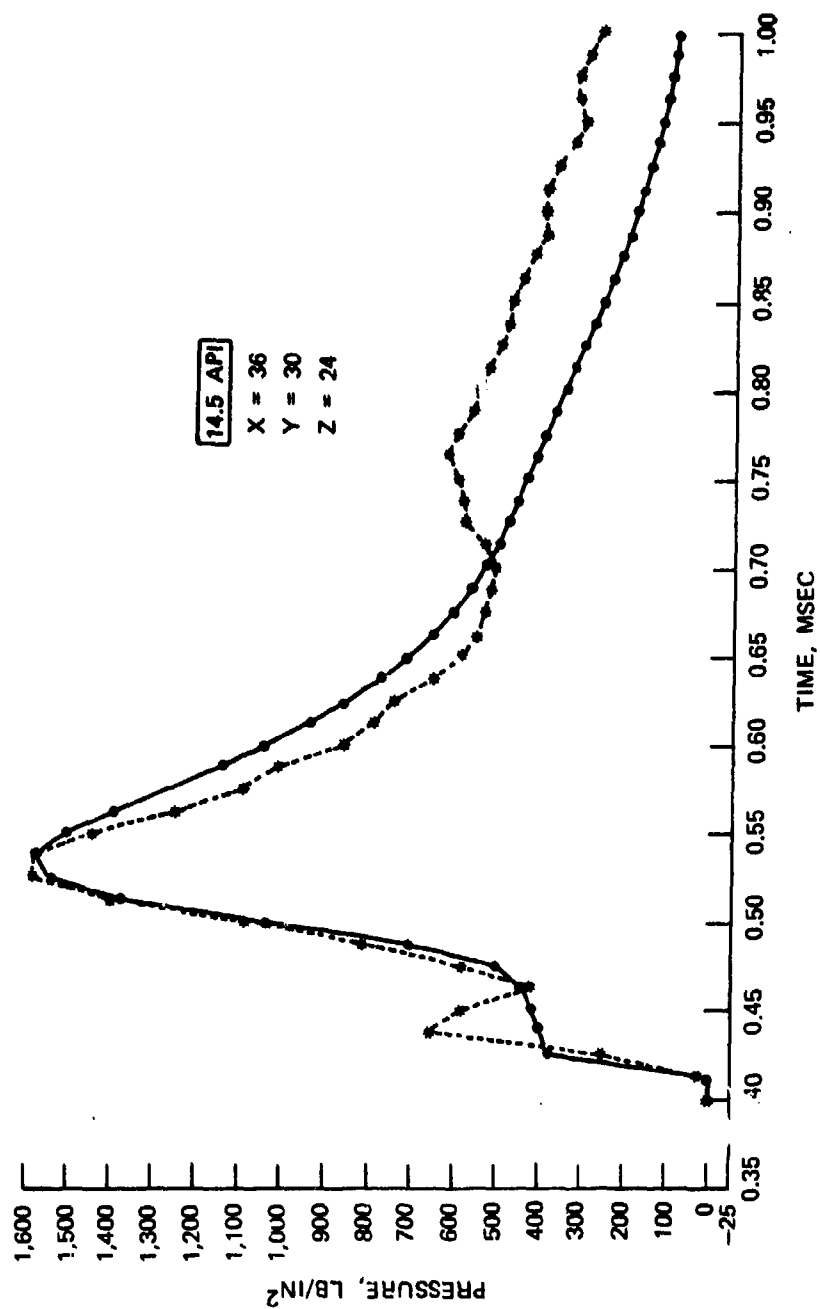


Figure 38. Pressure Versus Time Plot for Shot 4HR8 (Sheet 4 of 5).



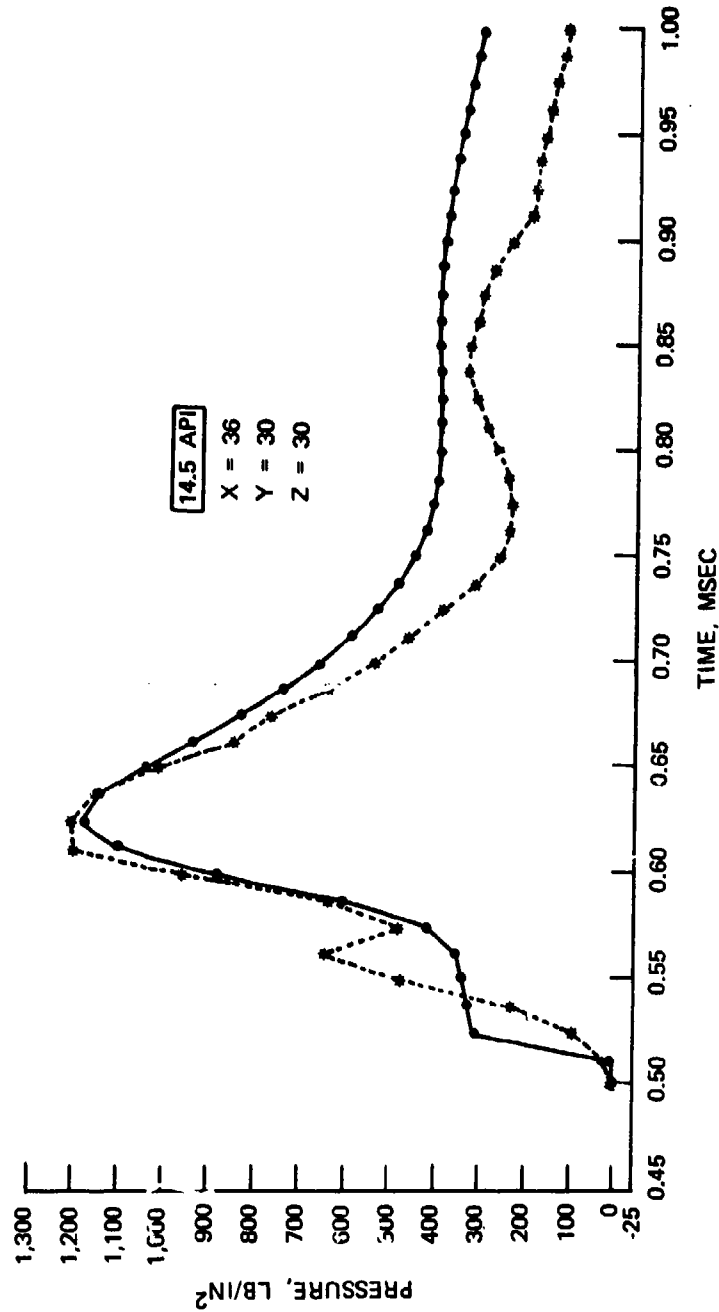


Figure 38. Pressure Versus Time Plot for Shot 4HR8 (Sheet 5 of 5).

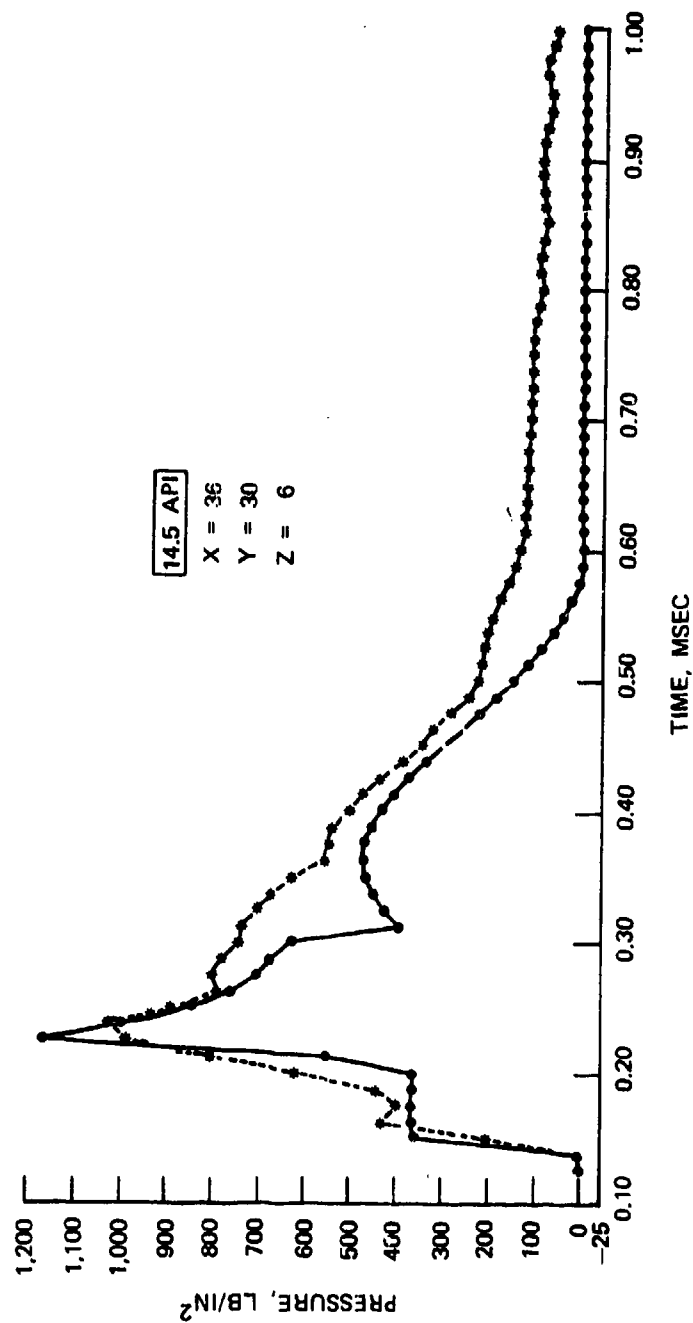


Figure 39. Pressure Versus Time Plot for Shot 4HR9 (Sheet 1 of 5).

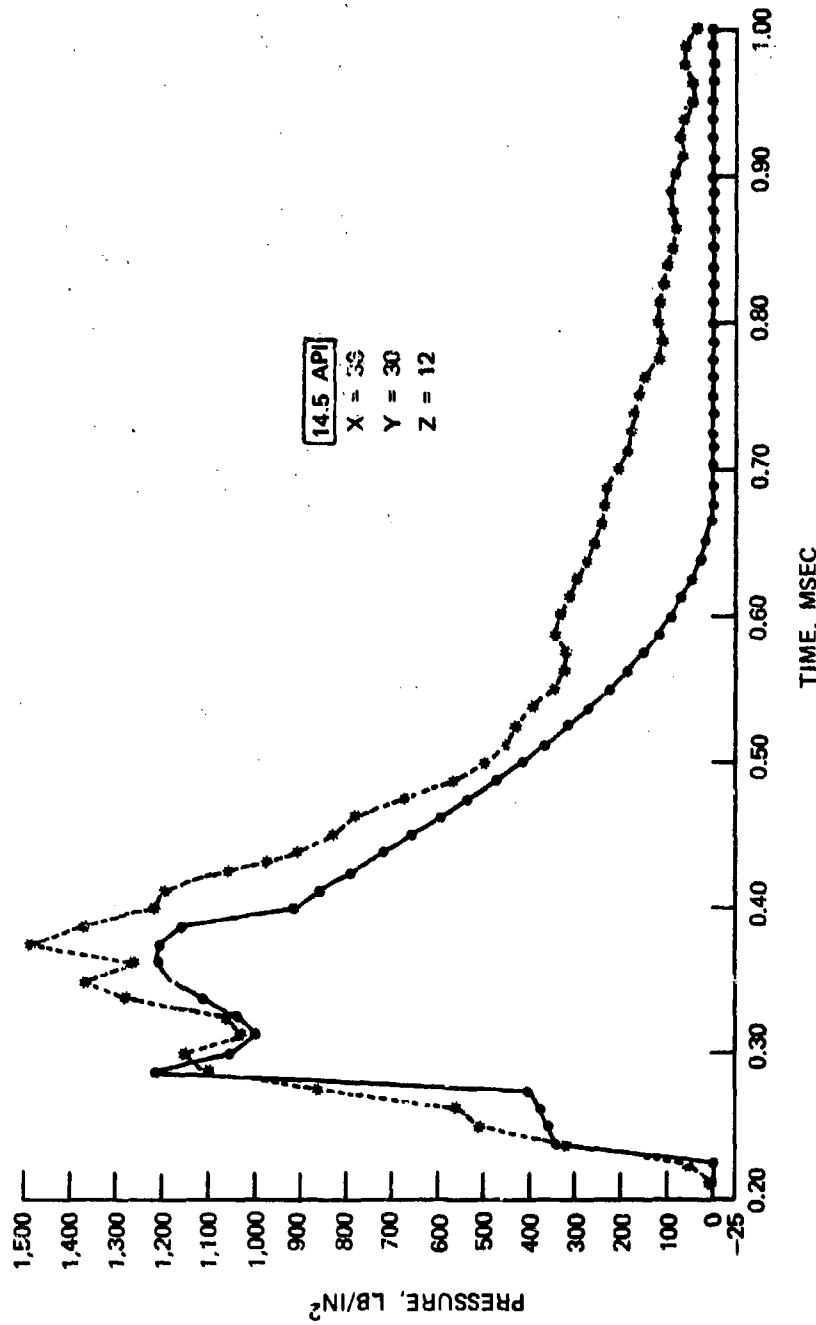


Figure 39. Pressure Versus Time Plot for Shot 4HR9 (Sheet 2 of 5).

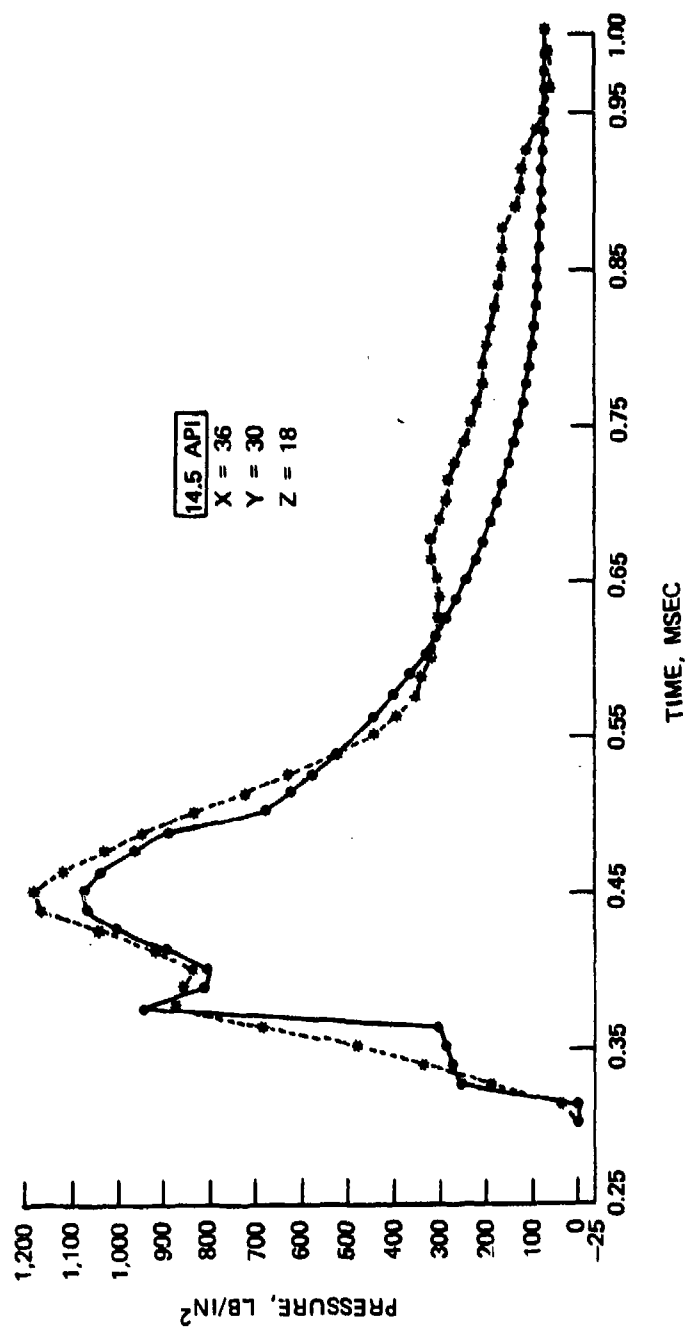


Figure 39. Pressure Versus Time Plot for Shot 4HR9 (Sheet 3 of 5).

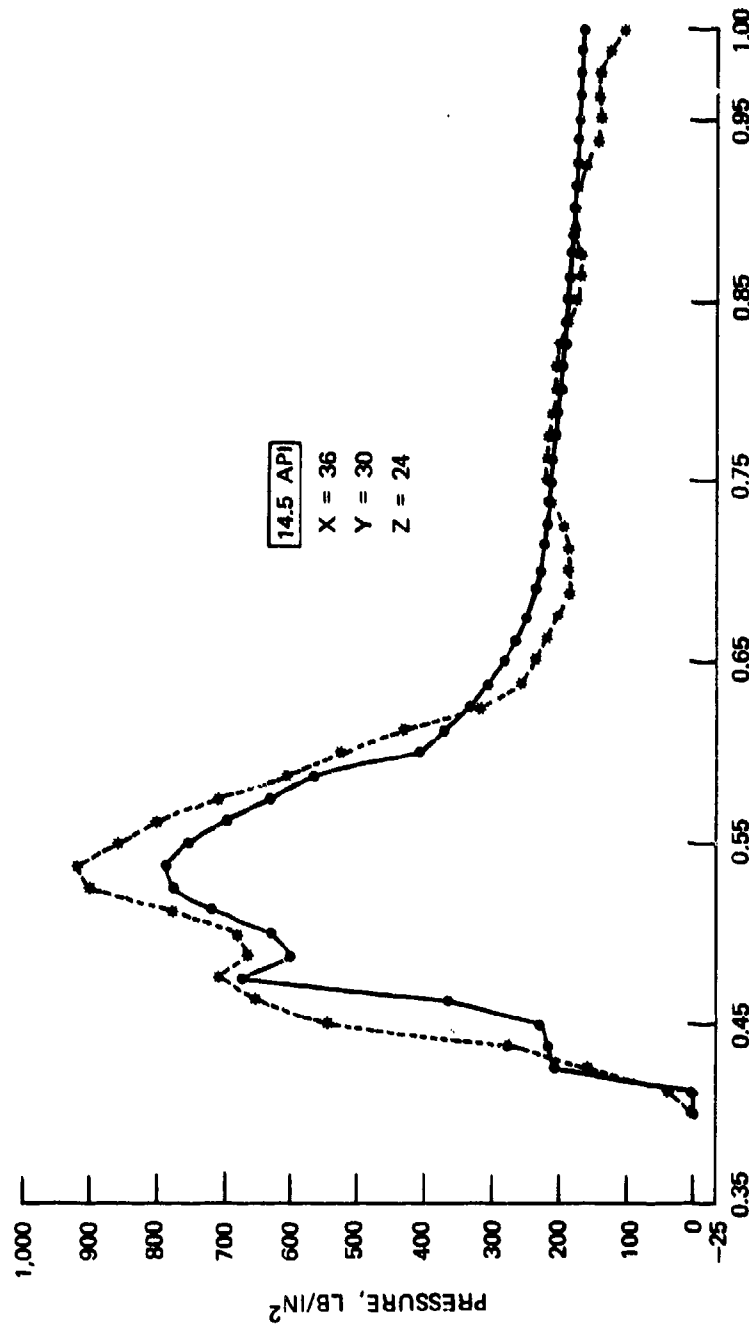


Figure 39. Pressure Versus Time Plot for Shot 4HR9 (Sheet 4 of 5).

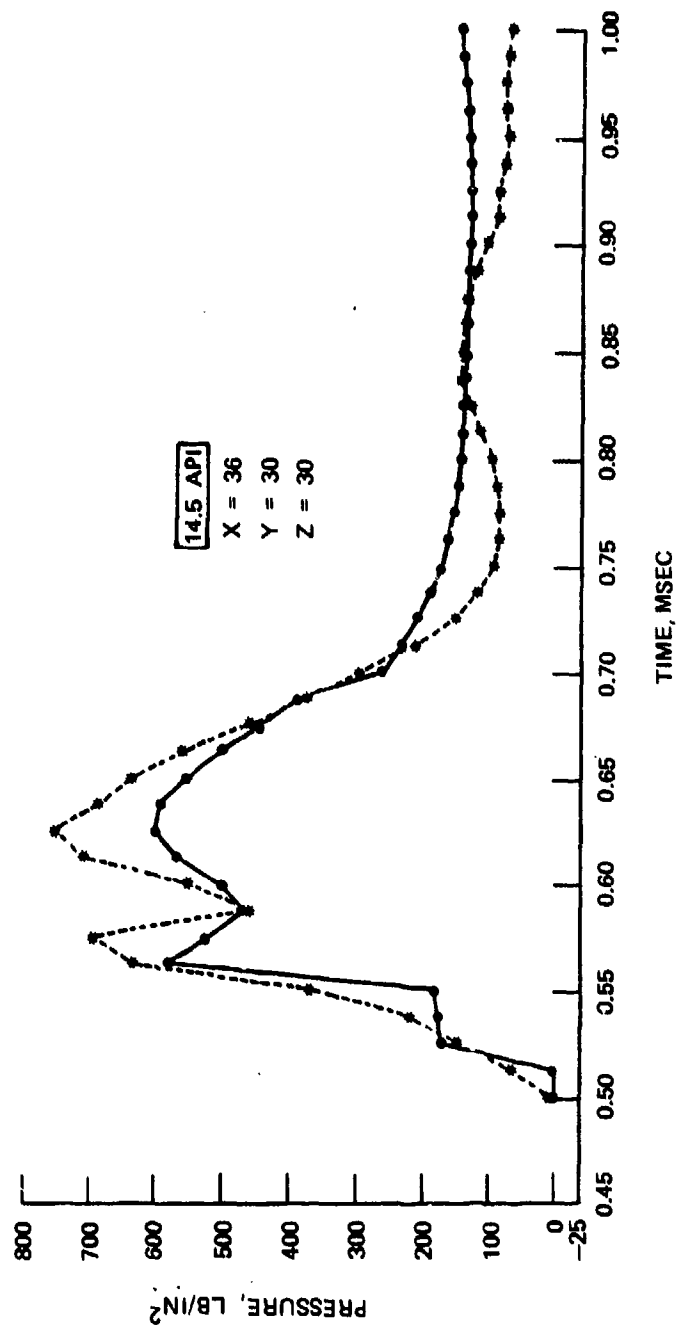


Figure 39. Pressure Versus Time Plot for Shot 4HR9 (Sheet 5 of 5).

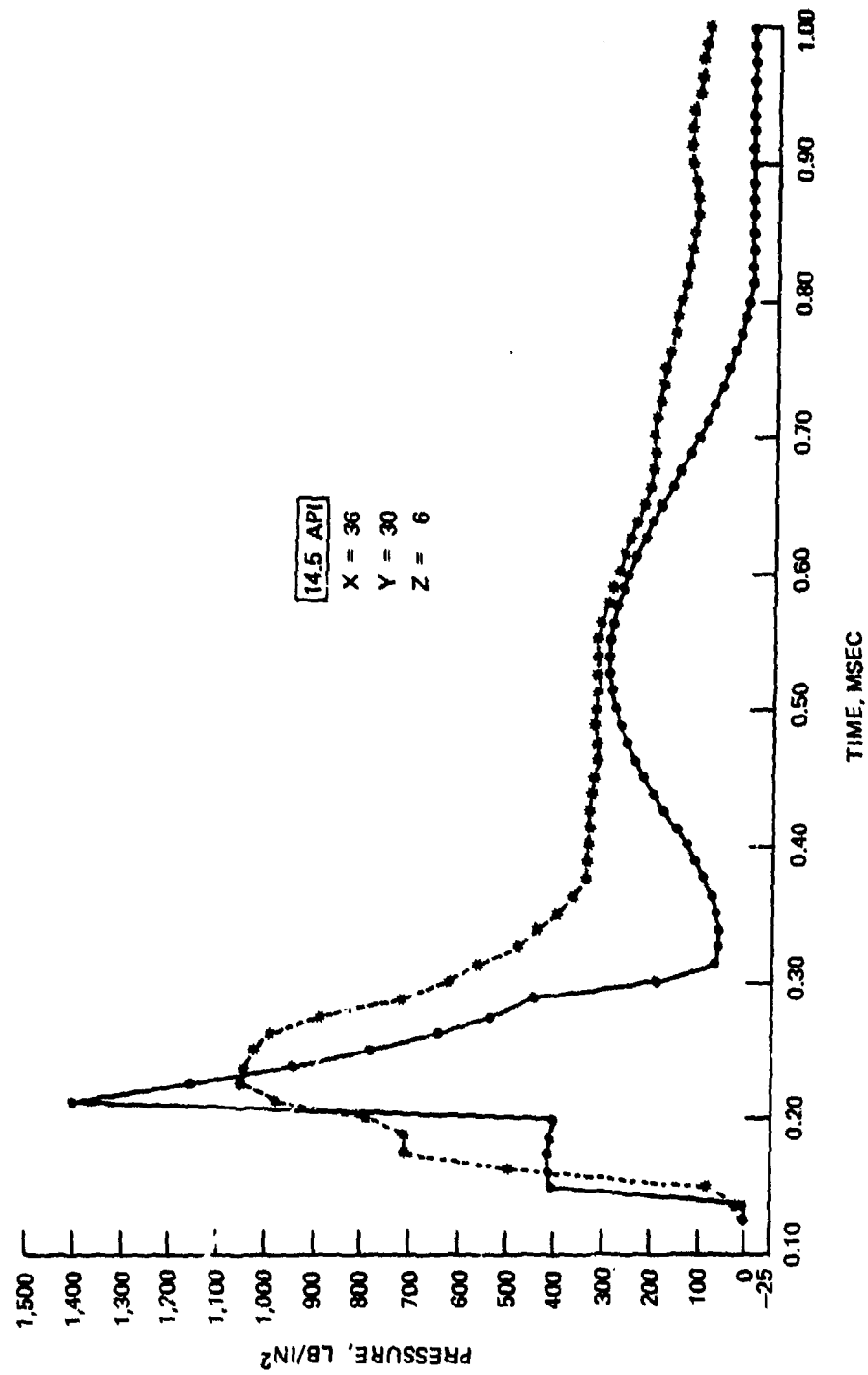


Figure 40. Pressure Versus Time Plot for Shot 4HR12 (Sheet 1 of 5).

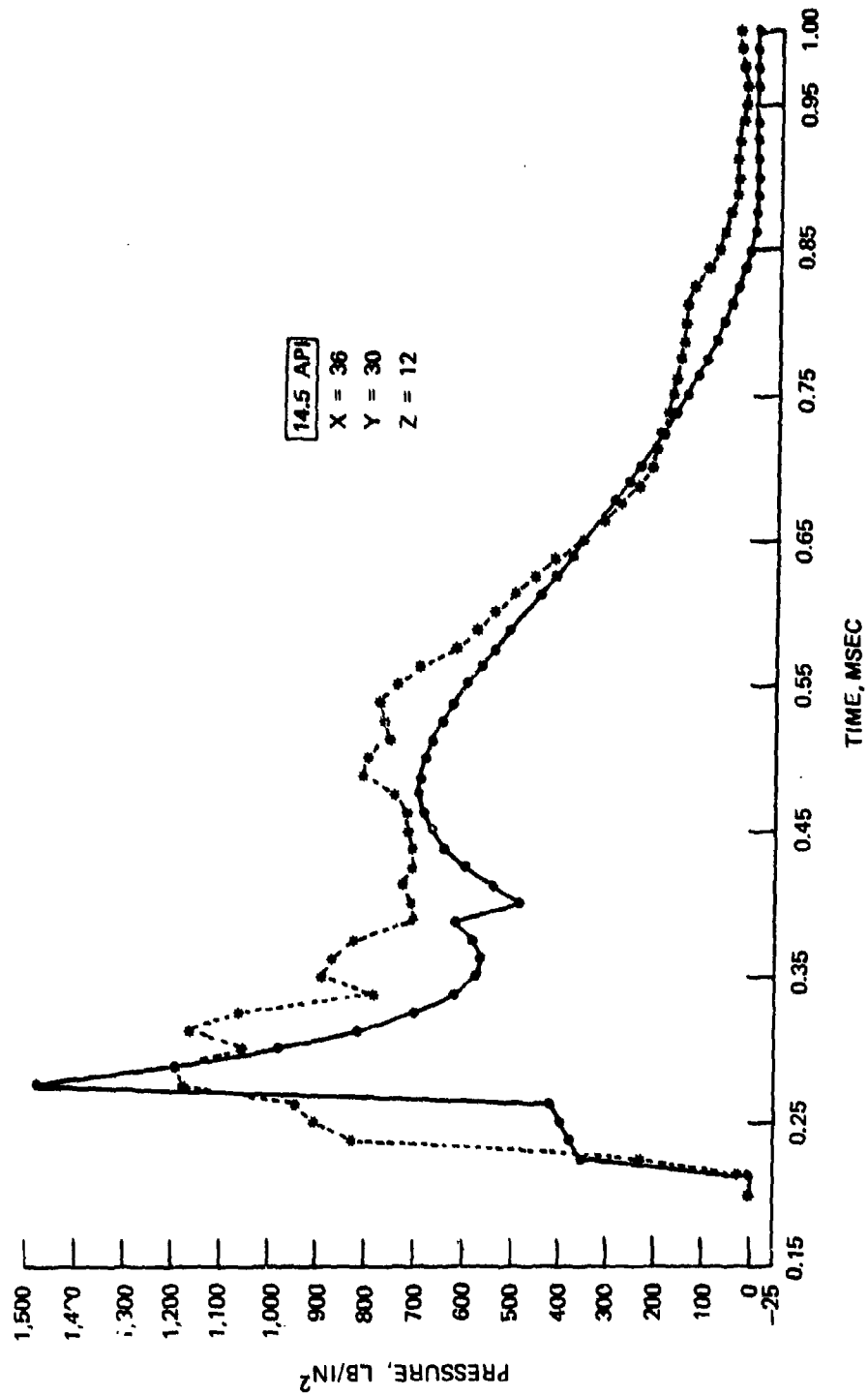


Figure 40. Pressure Versus Time Plot for Shot 4HR12 (Sheet 2 of 5).



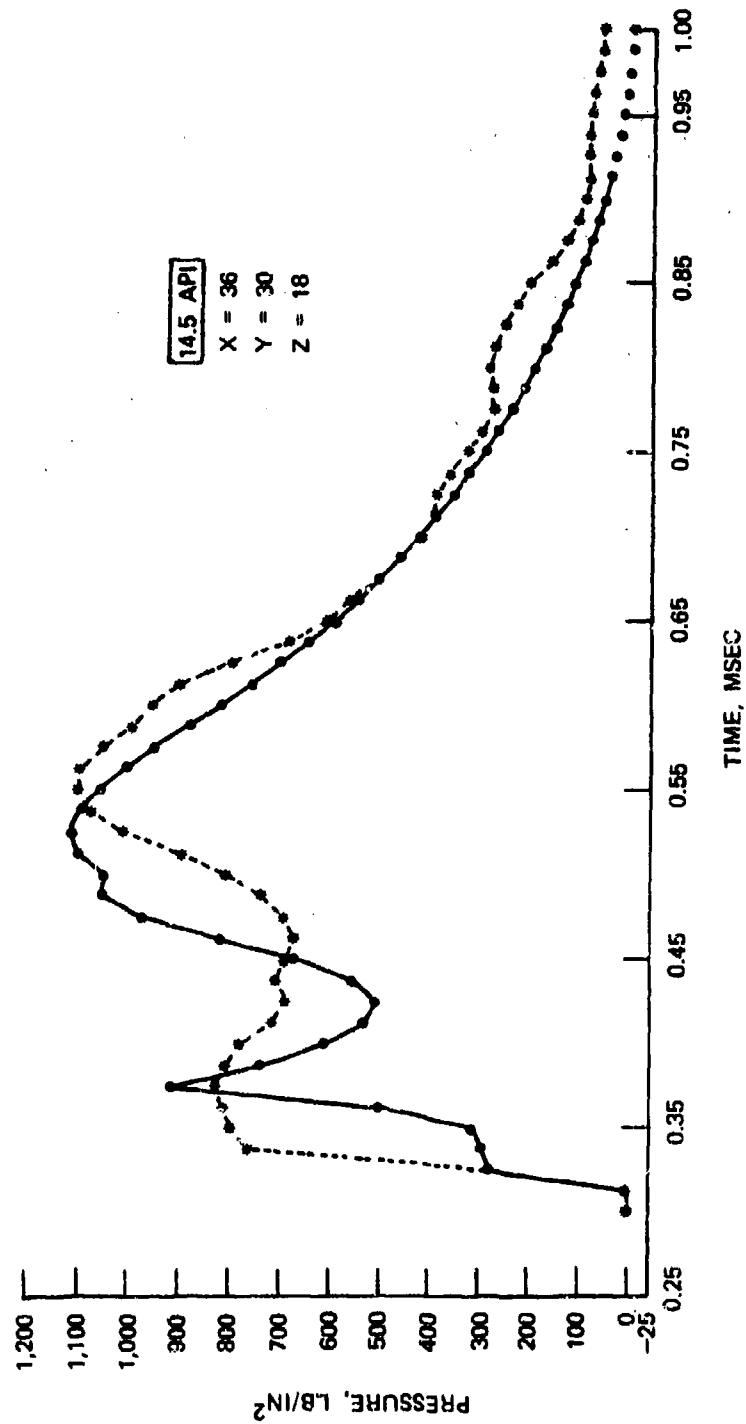


Figure 40. Pressure Versus Time Plot for Shot 4HR12 (Sheet 3 of 5).

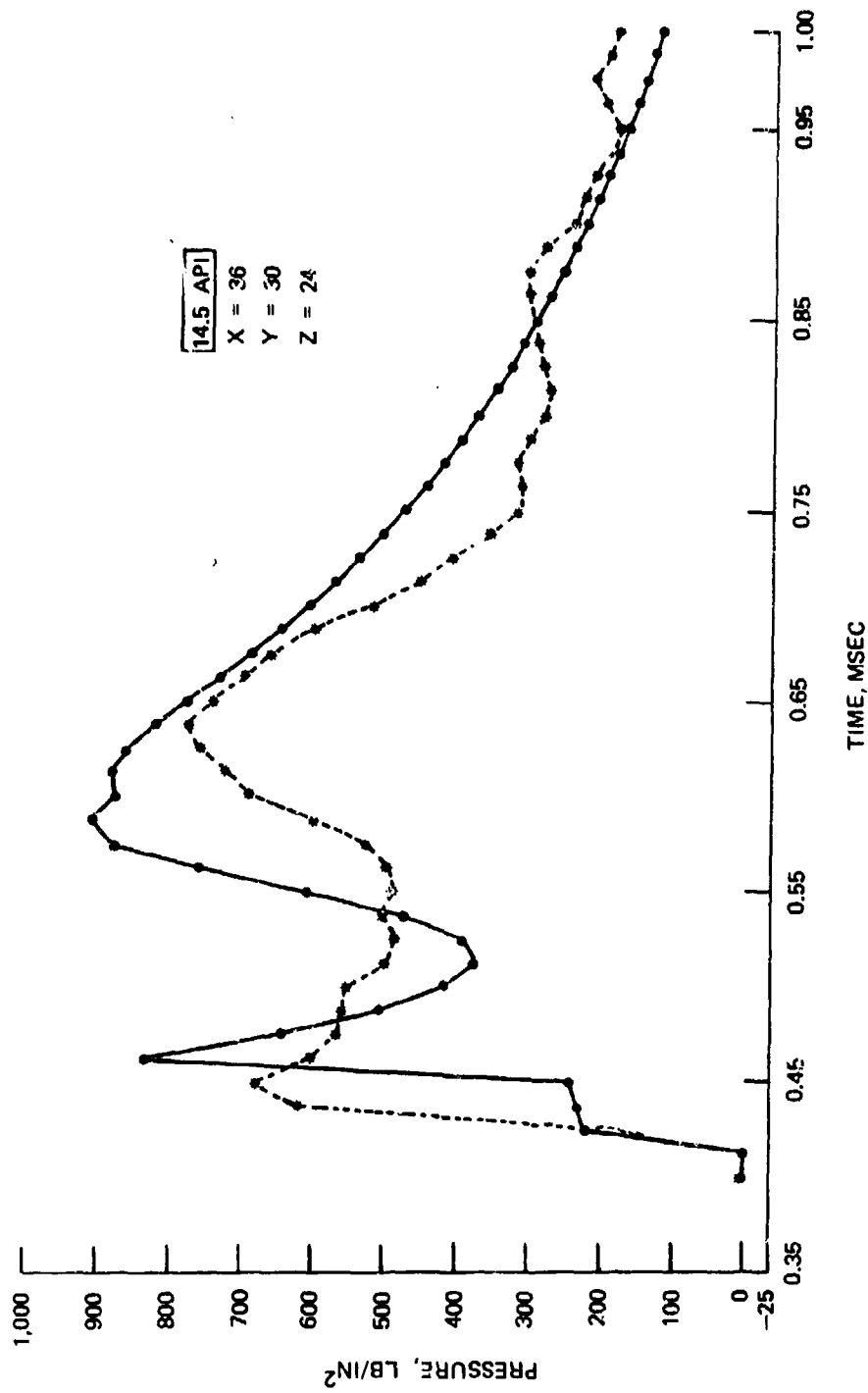


Figure 40. Pressure Versus Time Plot for Shot 4HR12 (Sheet 4 of 5).

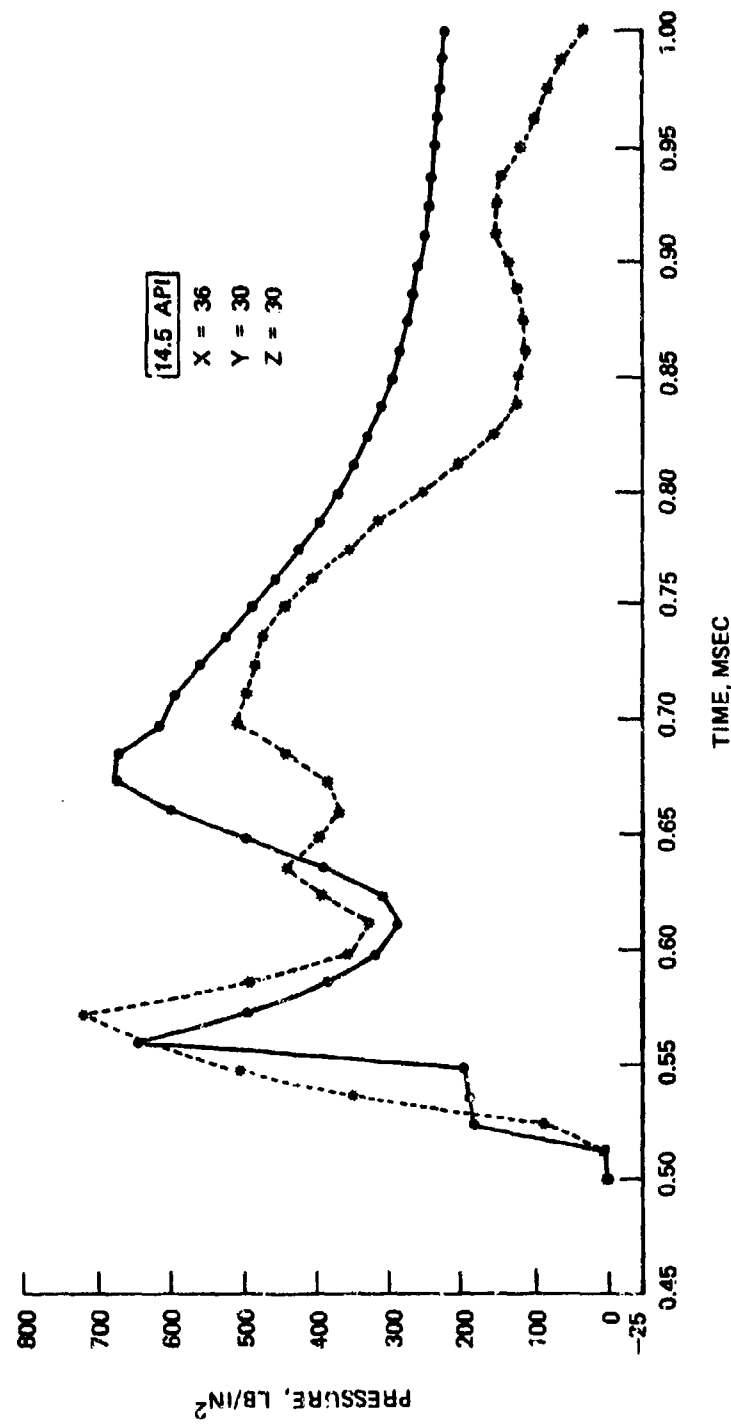


Figure 40. Pressure Versus Time Plot for Shot 4HR12 (Sheet 5 of 5).

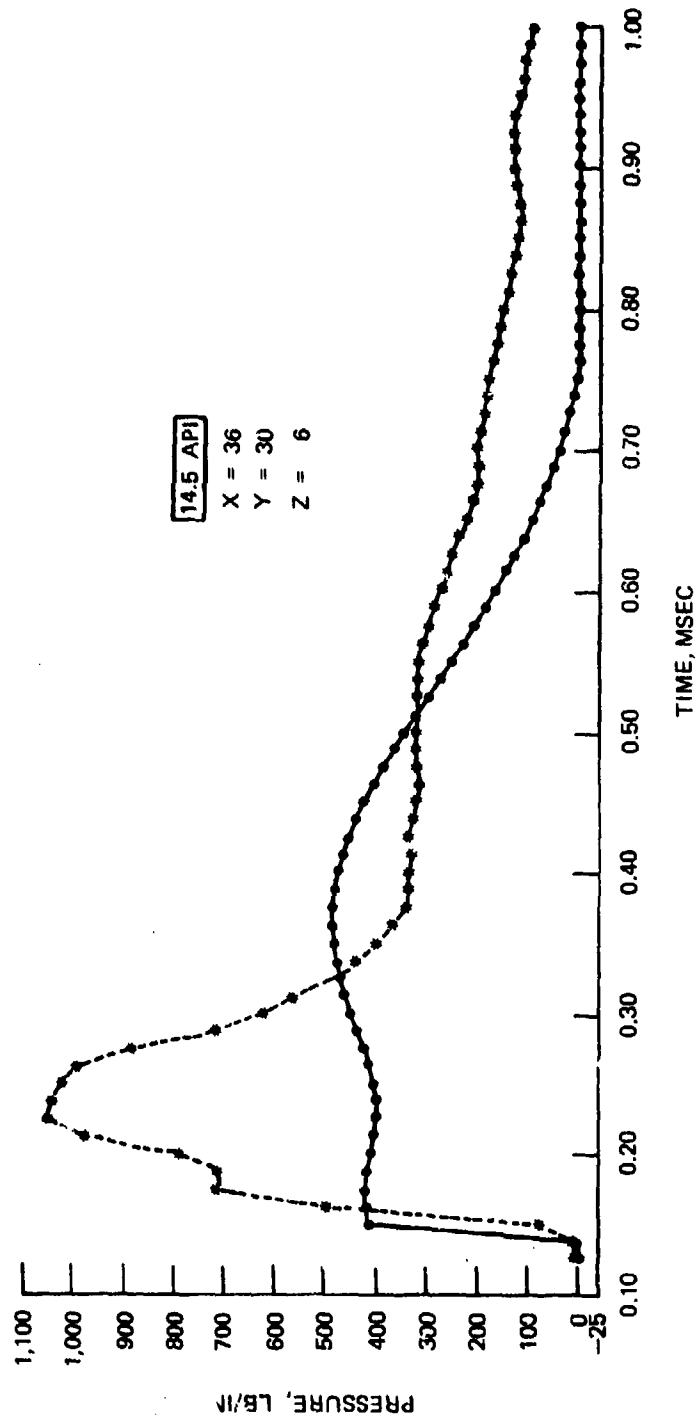


Figure 41. Pressure Versus Time Plot for Shot 4HR12 (Sheet 1 of 5).

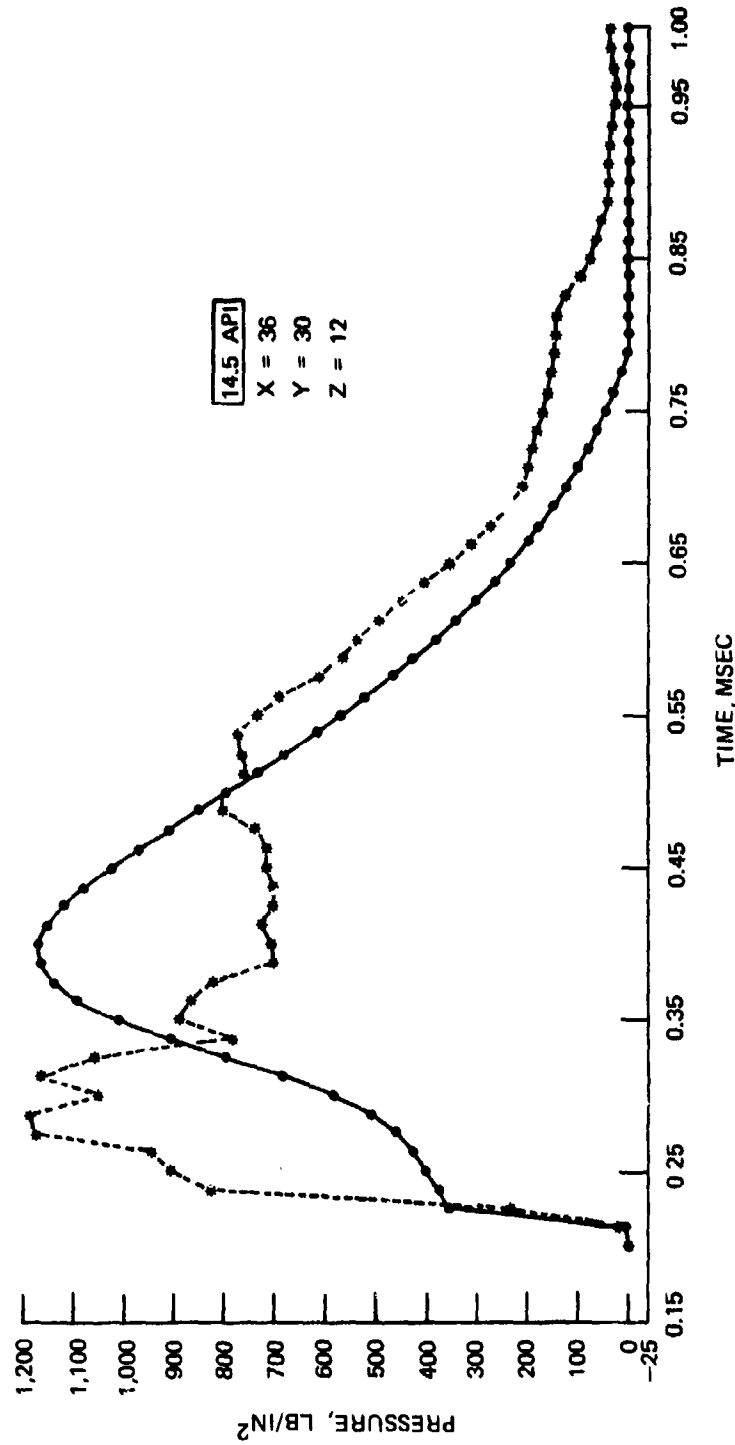


Figure 41. Pressure Versus Time Plot for Shot 4HR12 (Sheet 2 of 5).

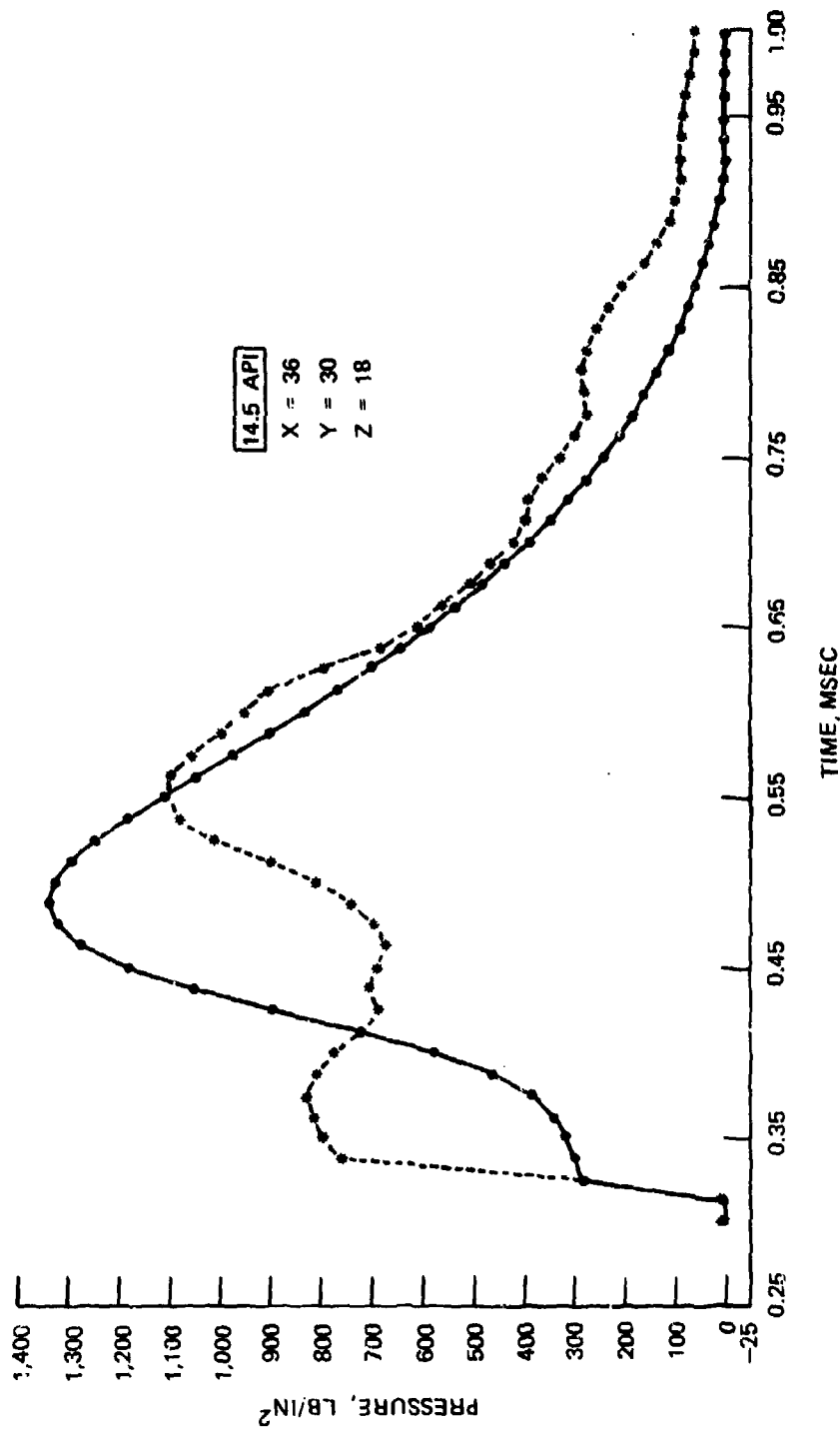


Figure 41. Pressure Versus Time Plot for Shot 4HR12 (Sheet 3 of 5).

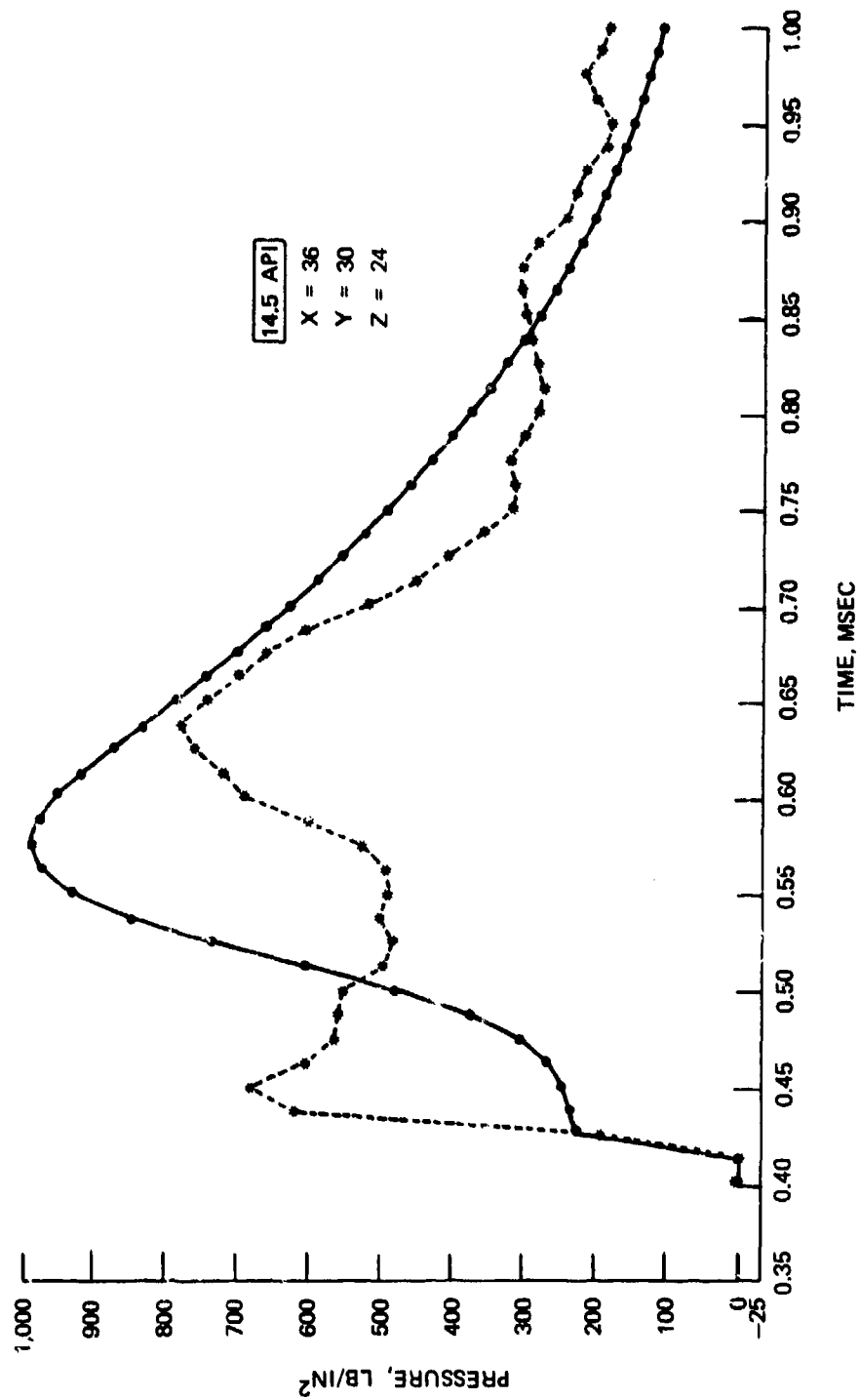


Figure 41. Pressure Versus Time Plot for Shot 4HR12 (Sheet 4 of 5).

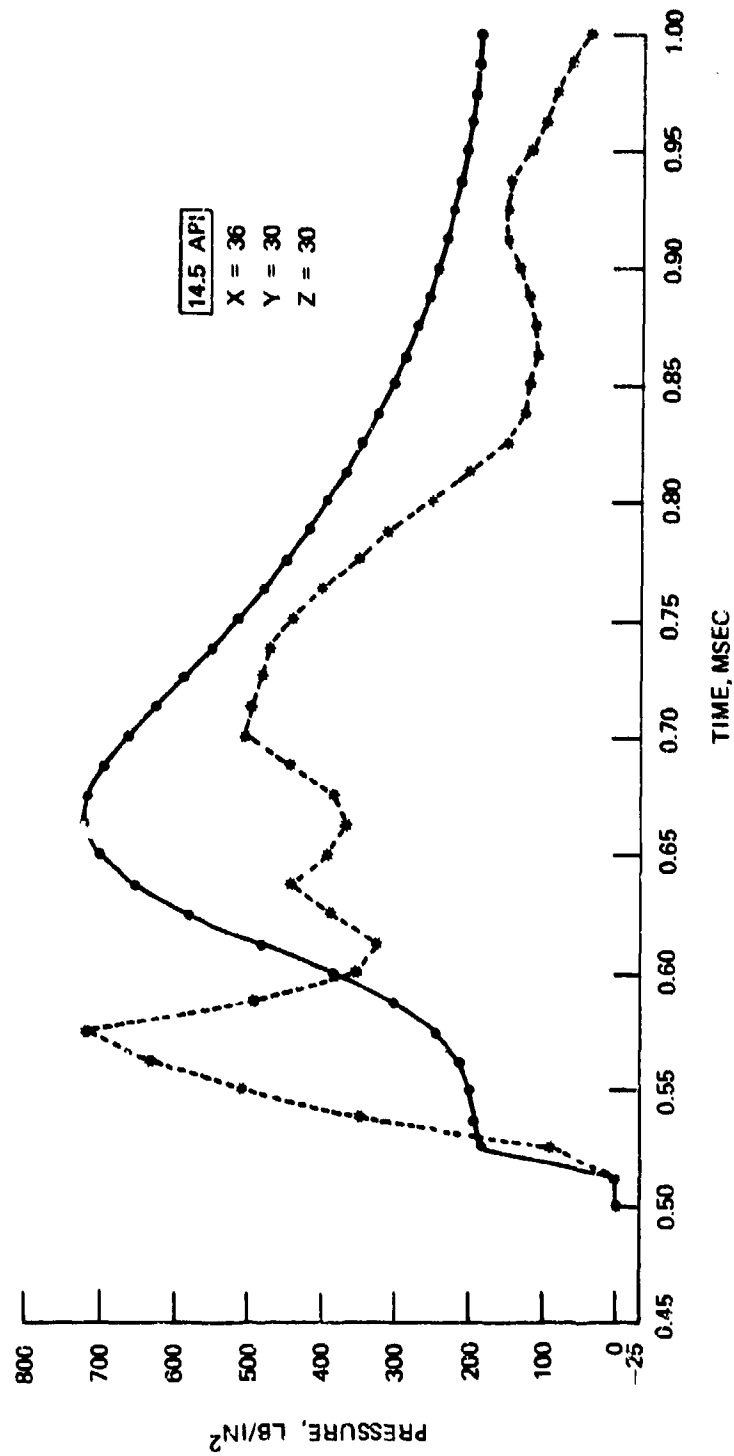


Figure 41. Pressure Versus Time Plot for Shot 4HR12 (Sheet 5 of 5).



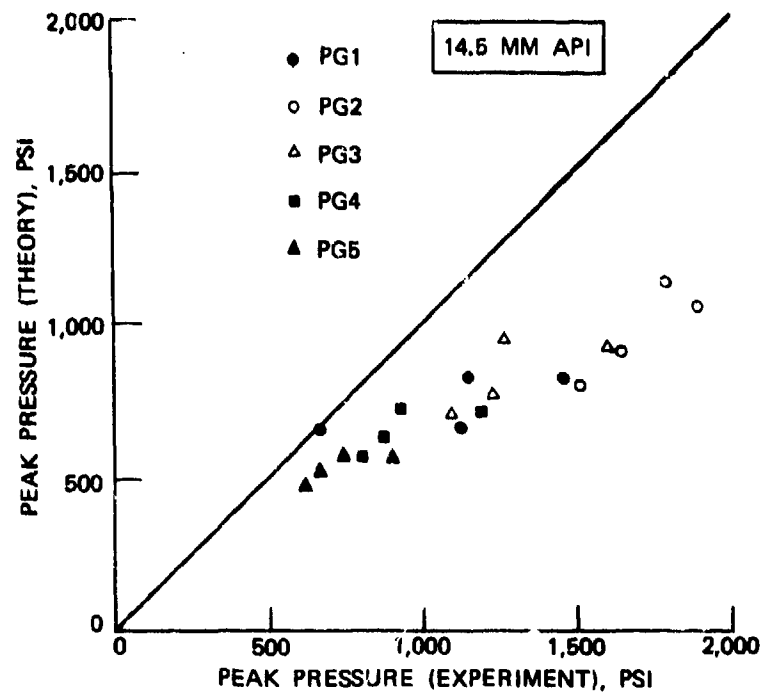


Figure 42. Peak Pressure—Theory Versus Experiment;  
30 to 45 Degrees Obliquity, 0 Degree Yaw.

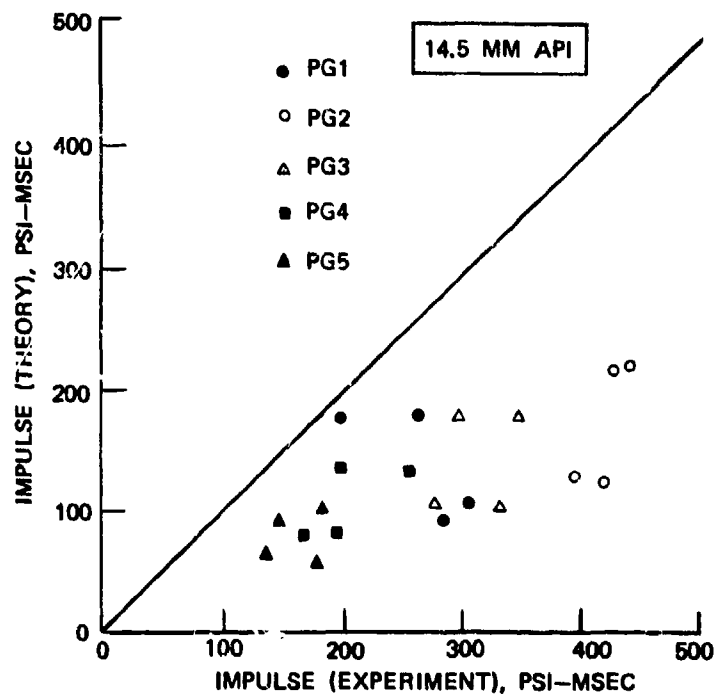


Figure 43. Impulse—Theory Versus Experiment;  
30 to 45 Degrees Obliquity, 0 Degree Yaw.

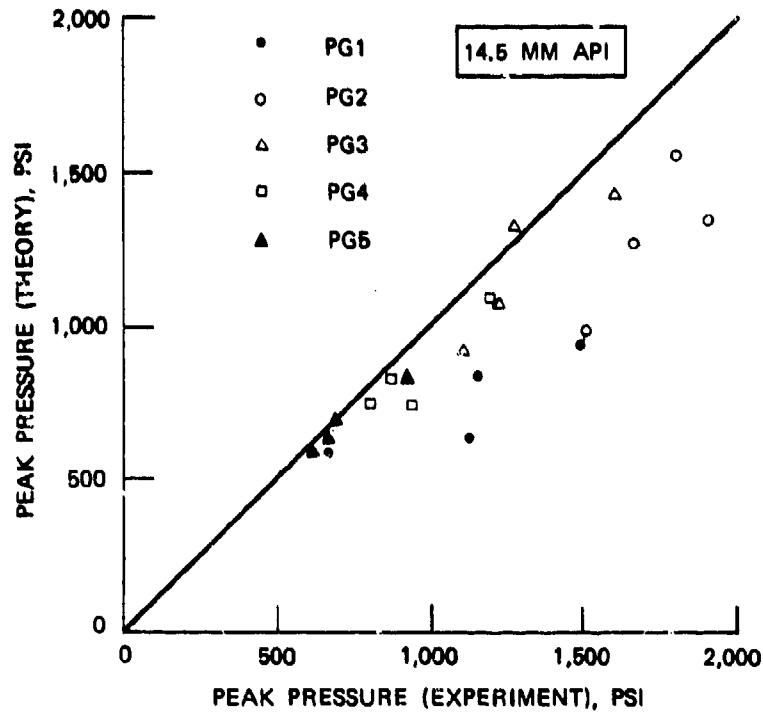


Figure 44. Peak Pressure—Theory Versus Experiment; 15 to 25 Degrees Obliquity, 0 Degree Yaw.

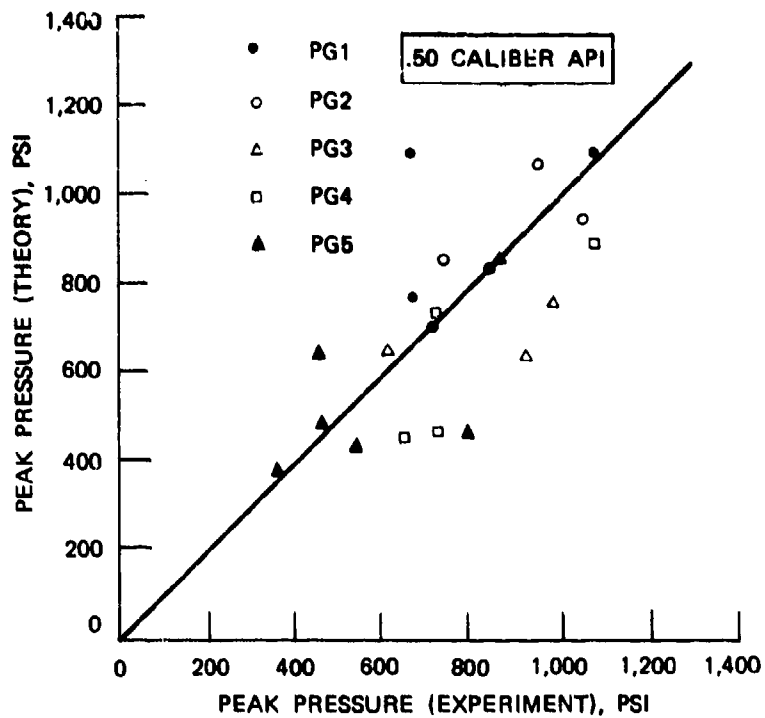
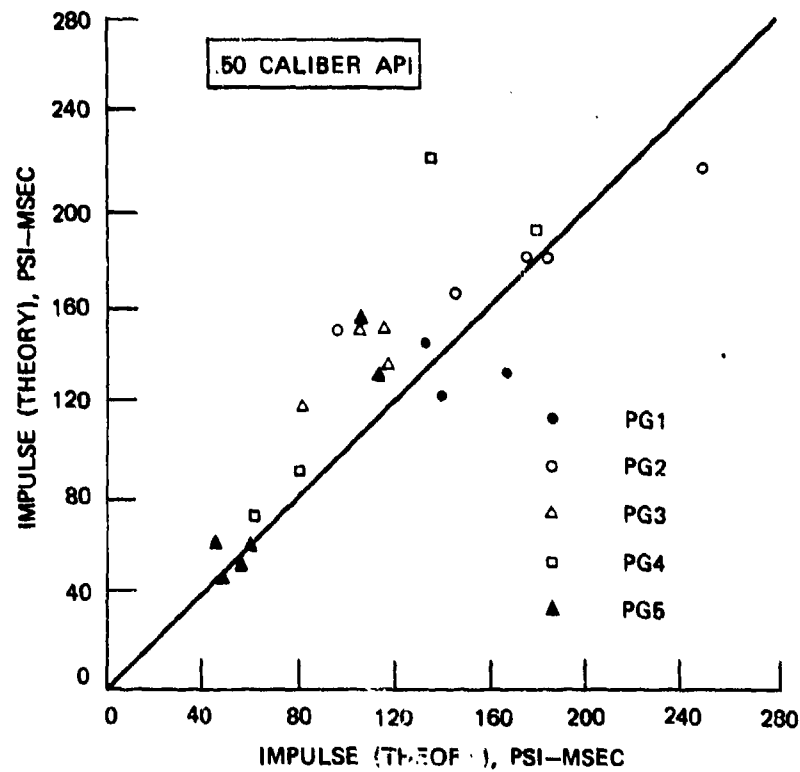


Figure 45. Peak Pressure—Theory Versus Experiment.



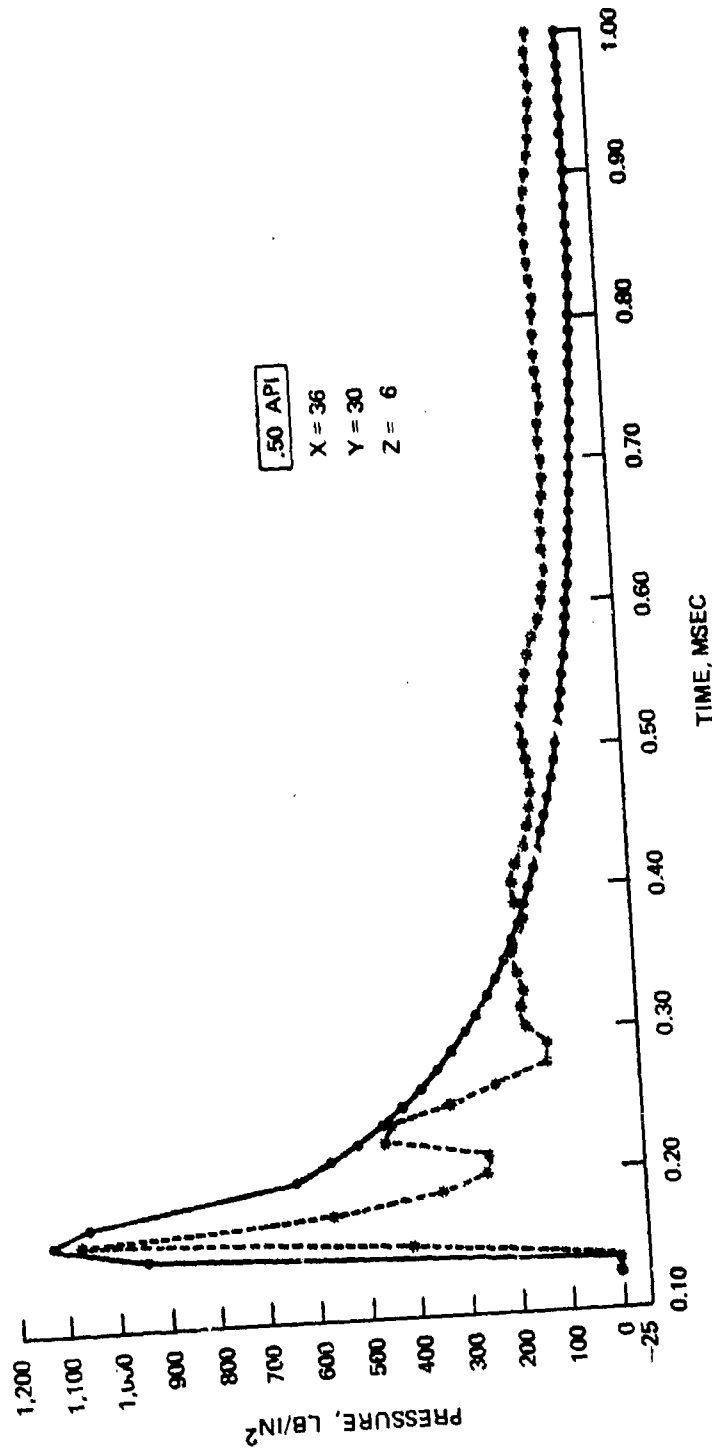


Figure 47. Pressure Versus Time Plot for Shot IHR3 (Sheet 1 of 4).

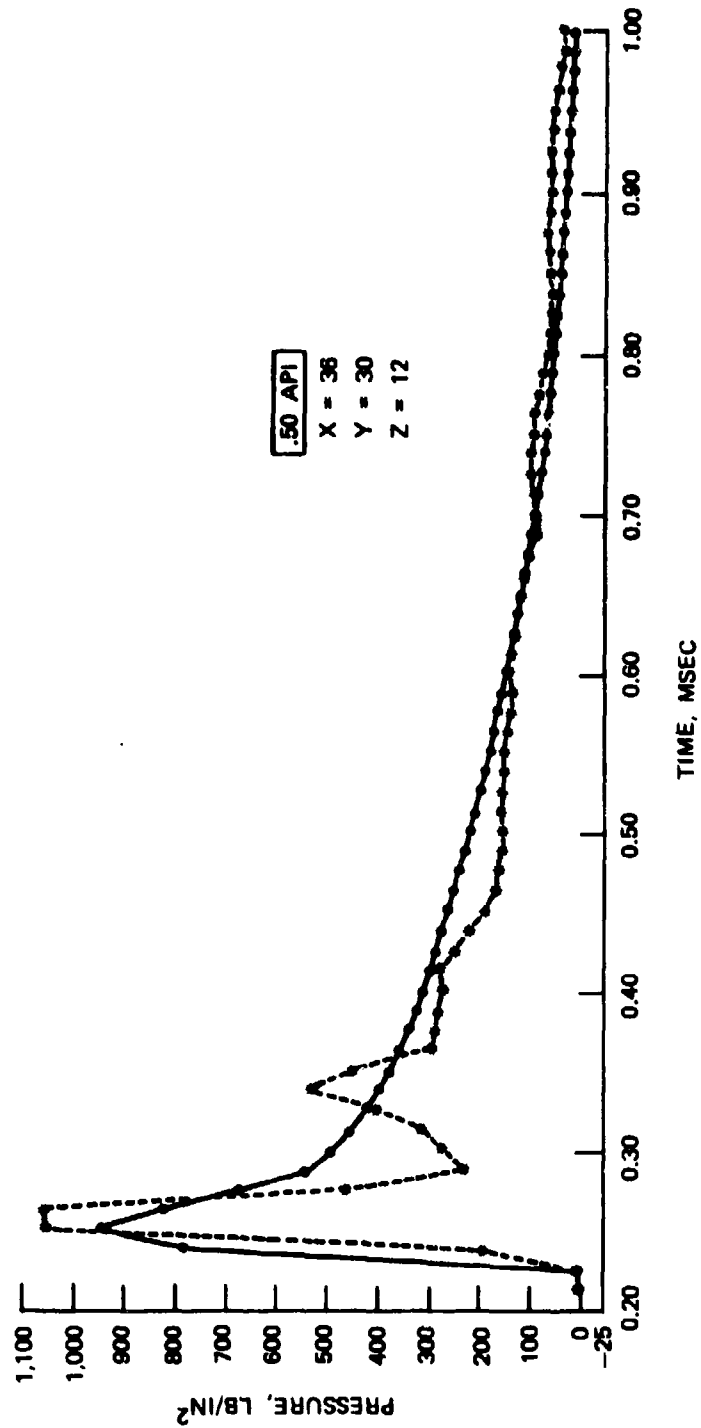


Figure 47. Pressure Versus Time Plot for Shot 1HR3 (Sheet 2 of 4).

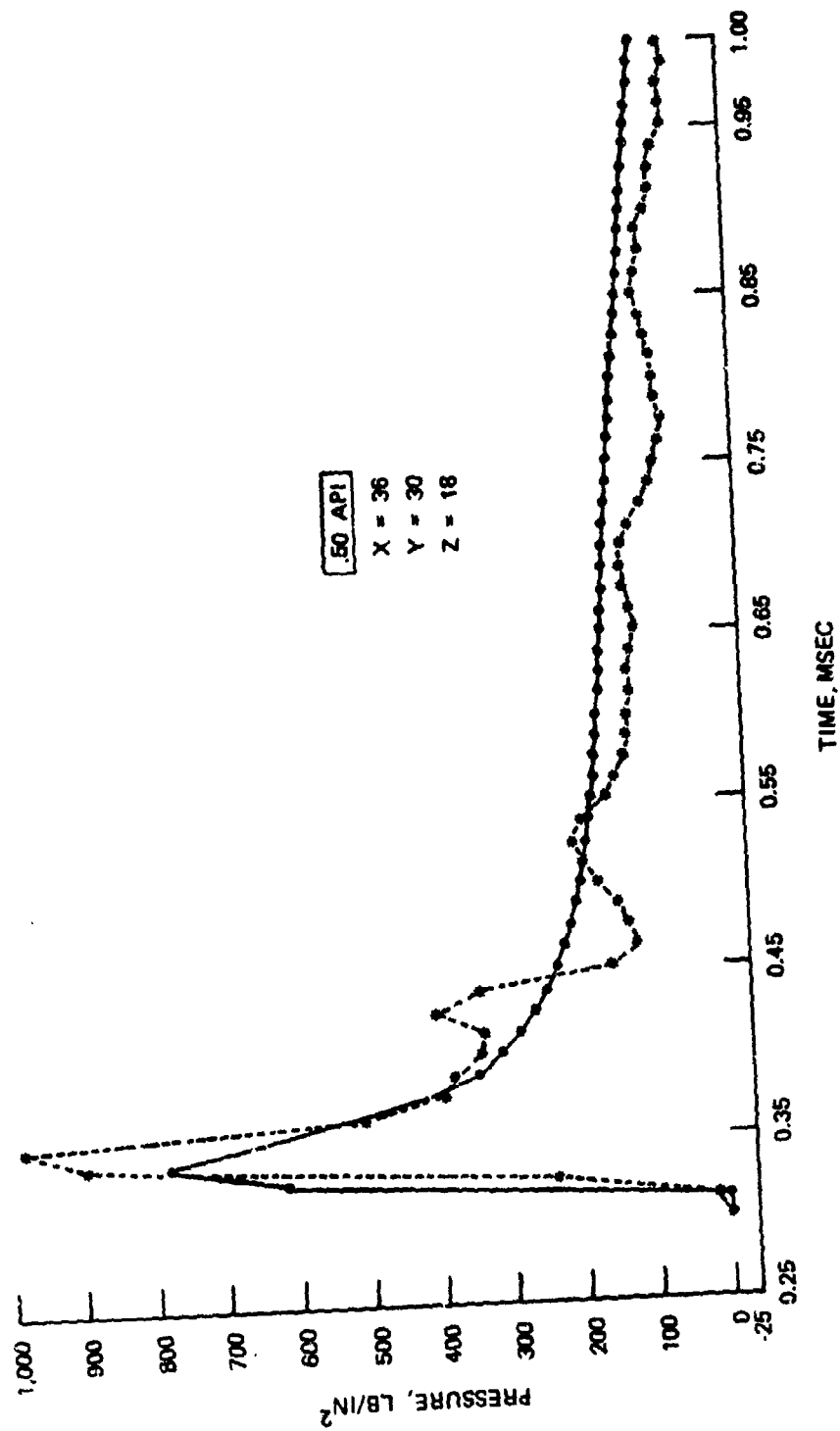


Figure 47. Pressure Versus Time Plot for Shot 1HR3 (Sheet 3 of 4).

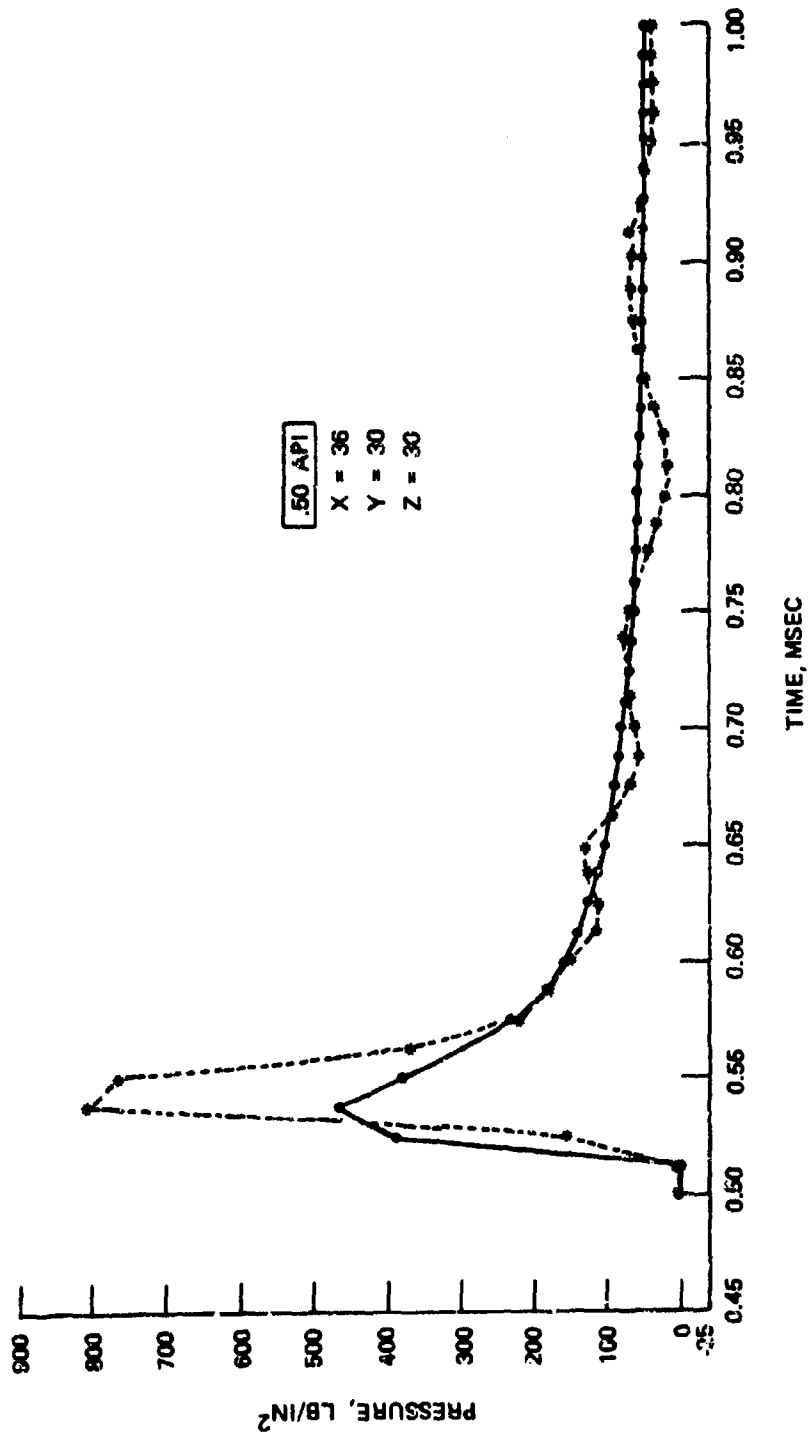


Figure 47. Pressure Versus Time Plot for Shot 1HR3 (Sheet 4 of 4).

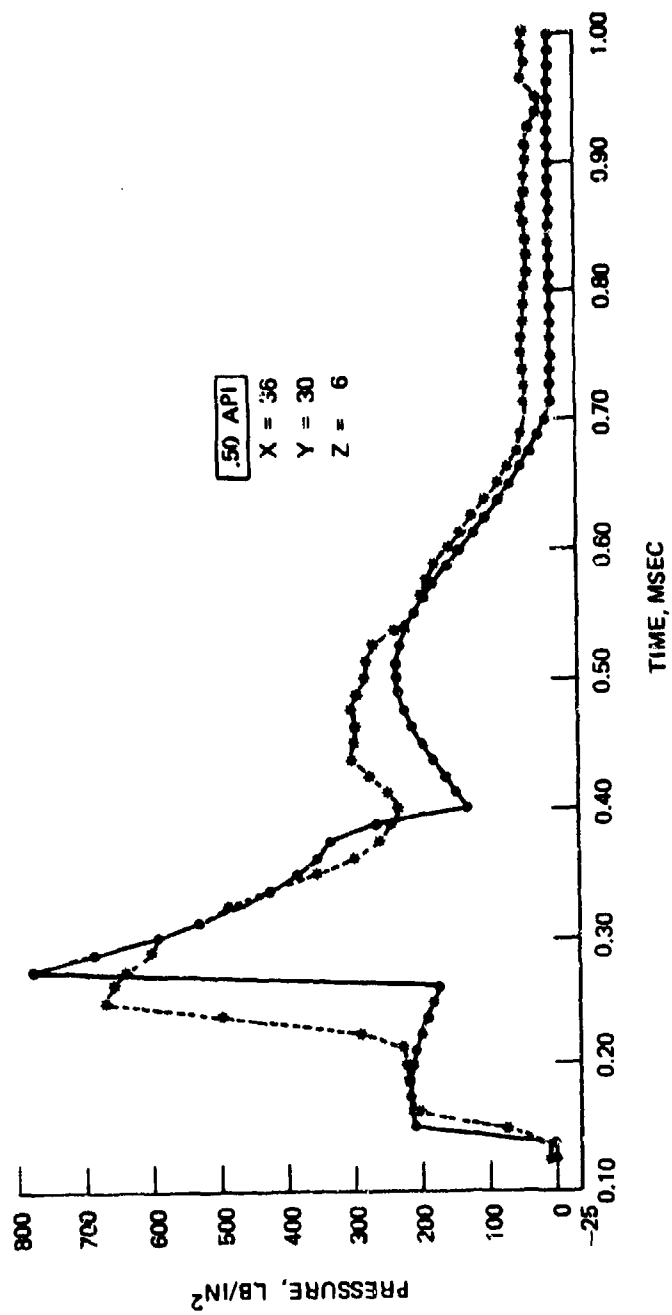


Figure 48. Pressure Versus Time Plot for Shot 1HR13 (Sheet 1 of 4).



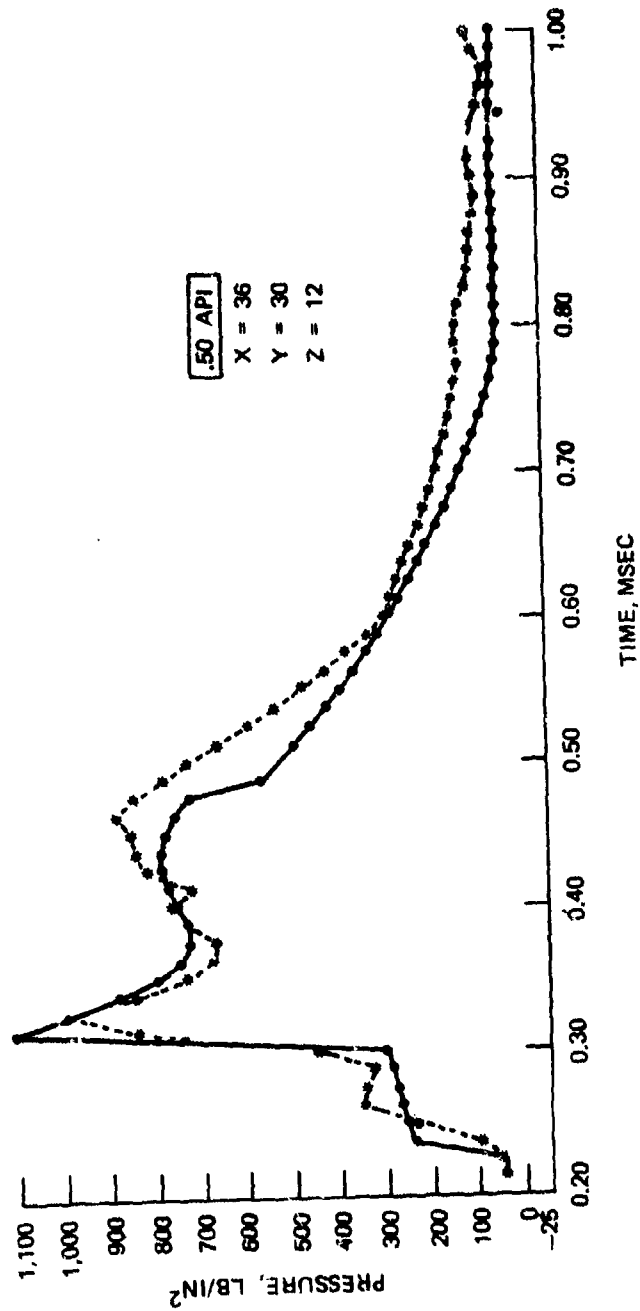


Figure 48. Pressure Versus Time Plot for Shot 1HR13 (Sheet 2 of 4).

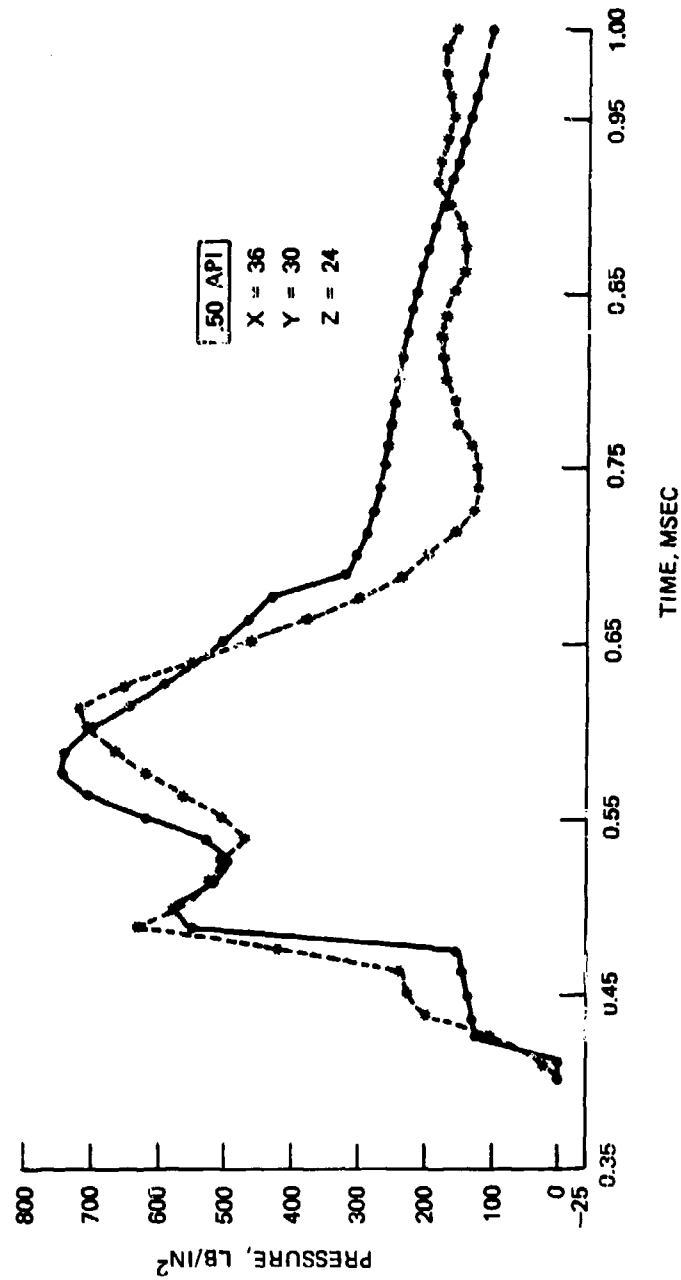


Figure 48. Pressure Versus Time Plot for Shot 1HR13 (Sheet 3 of 4).

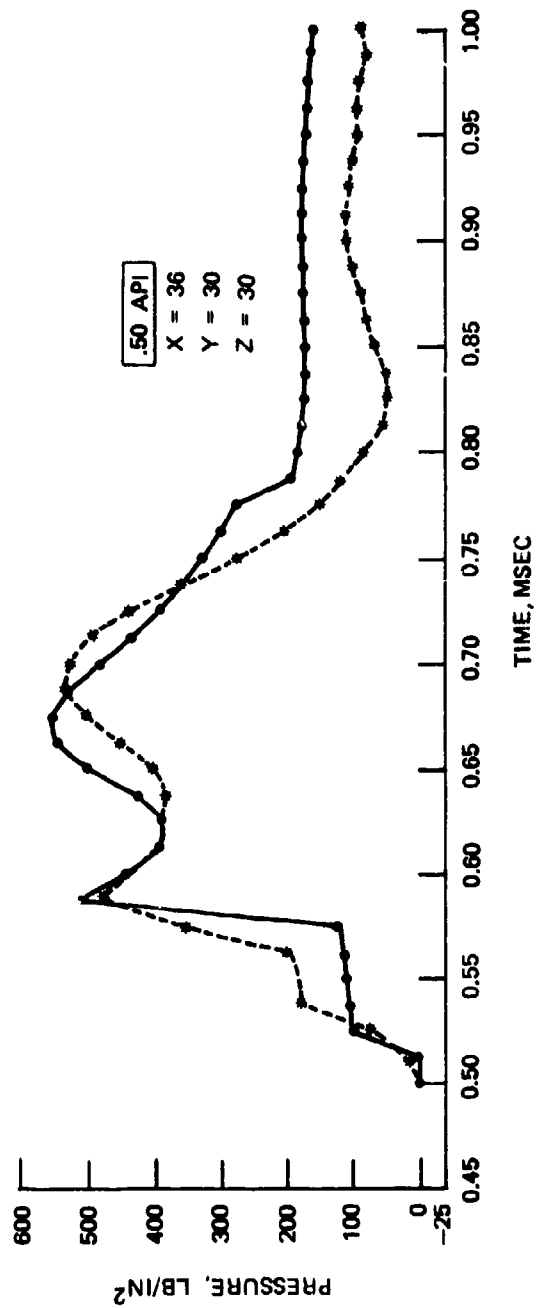


Figure 48. Pressure Versus Time Plot for Shot 1HR13 (Sheet 4 of 4).

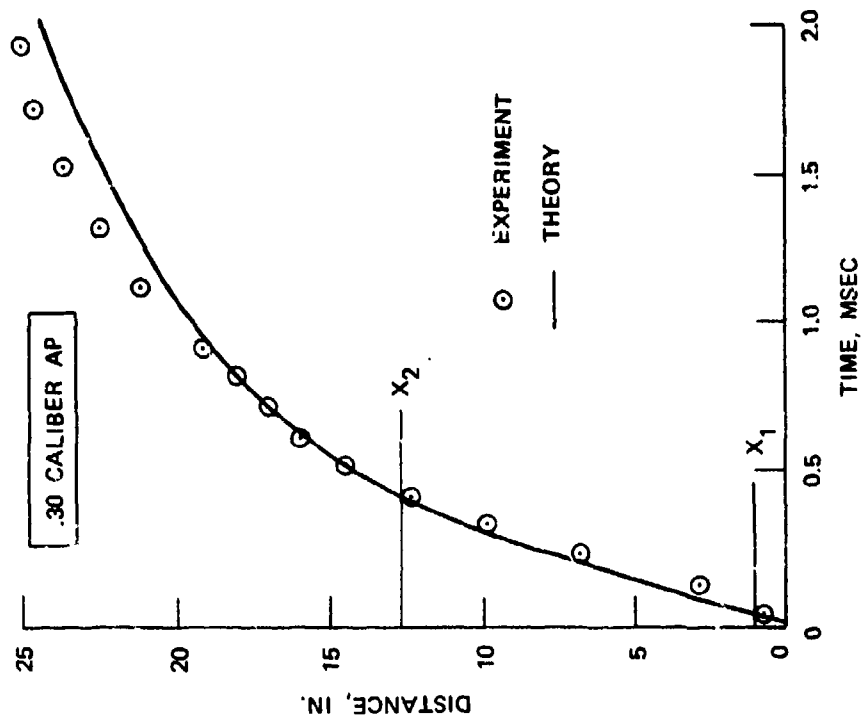


Figure 50. Experimental Trajectory for Shot 4HR3.

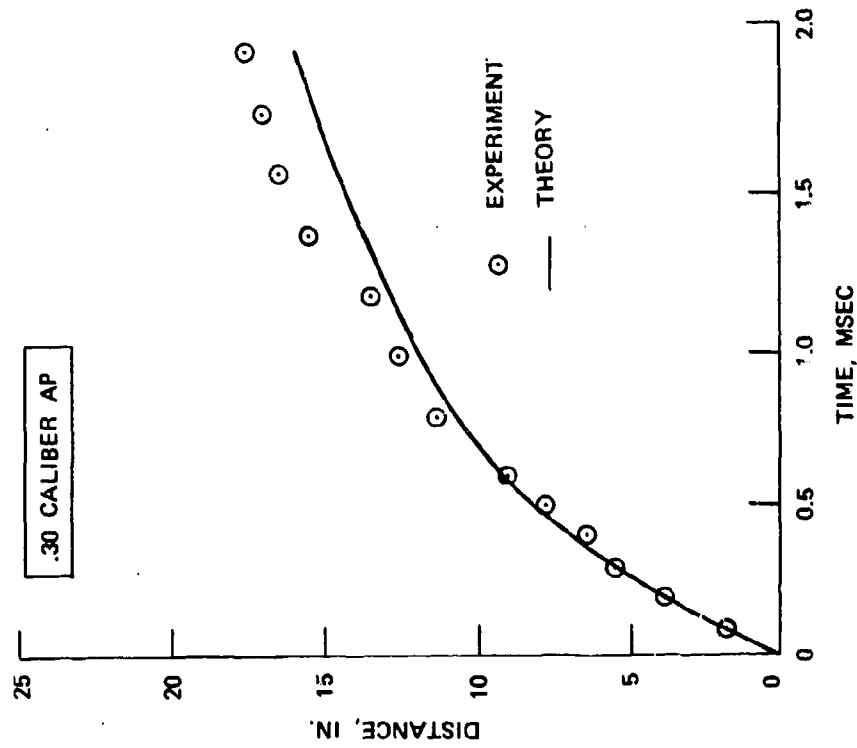


Figure 49. Experimental Trajectory for Shot 4HR2.

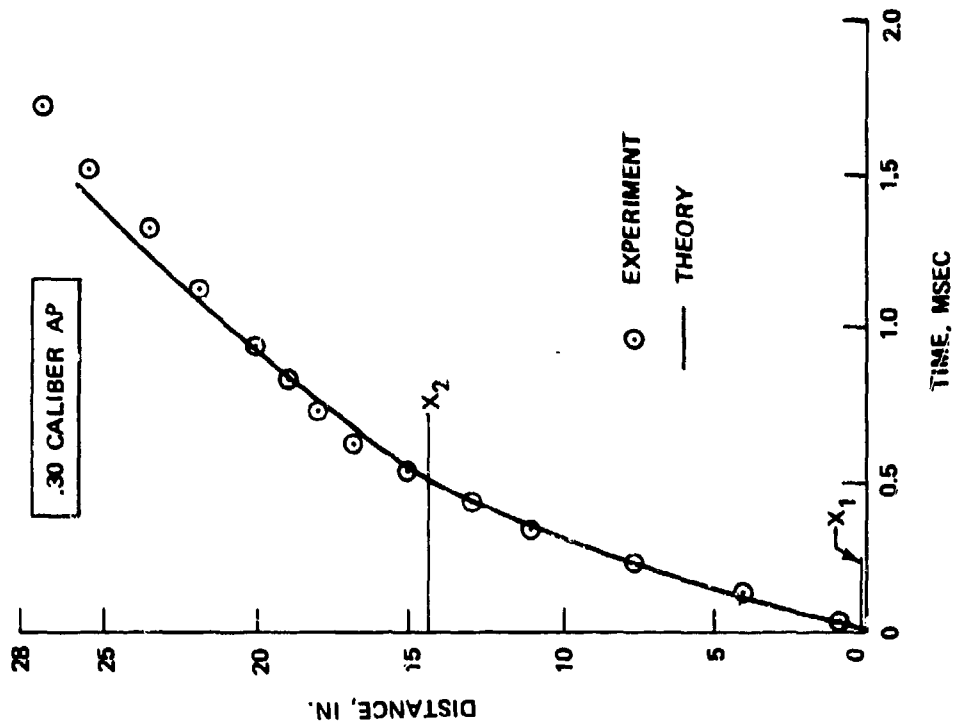


Figure 51. Experimental Trajectory for Shot 4HR4.

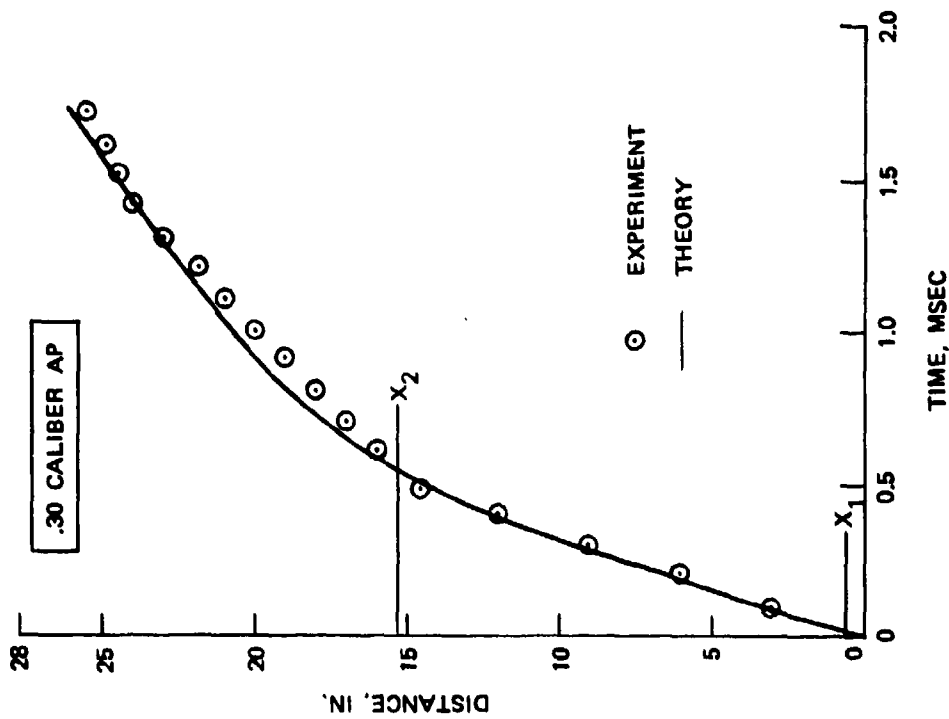


Figure 52. Experimental Trajectory for Shot 4HR5.

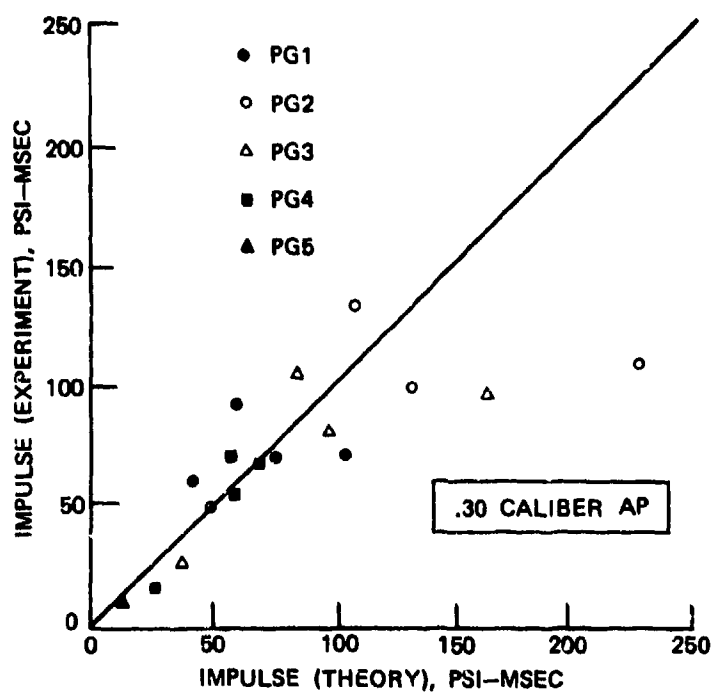


Figure 53. Peak Pressure—Theory Versus Experiment.

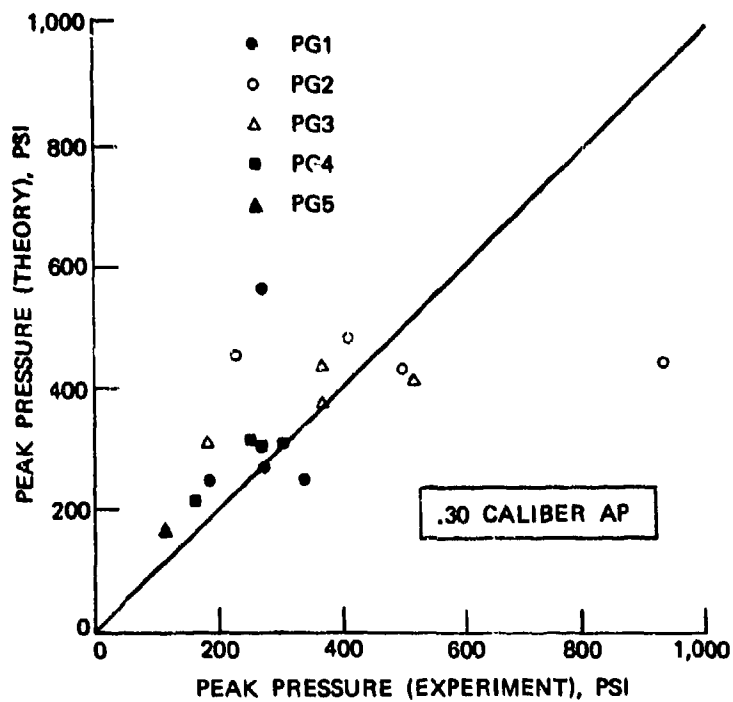


Figure 54. Impulse—Theory Versus Experiment.

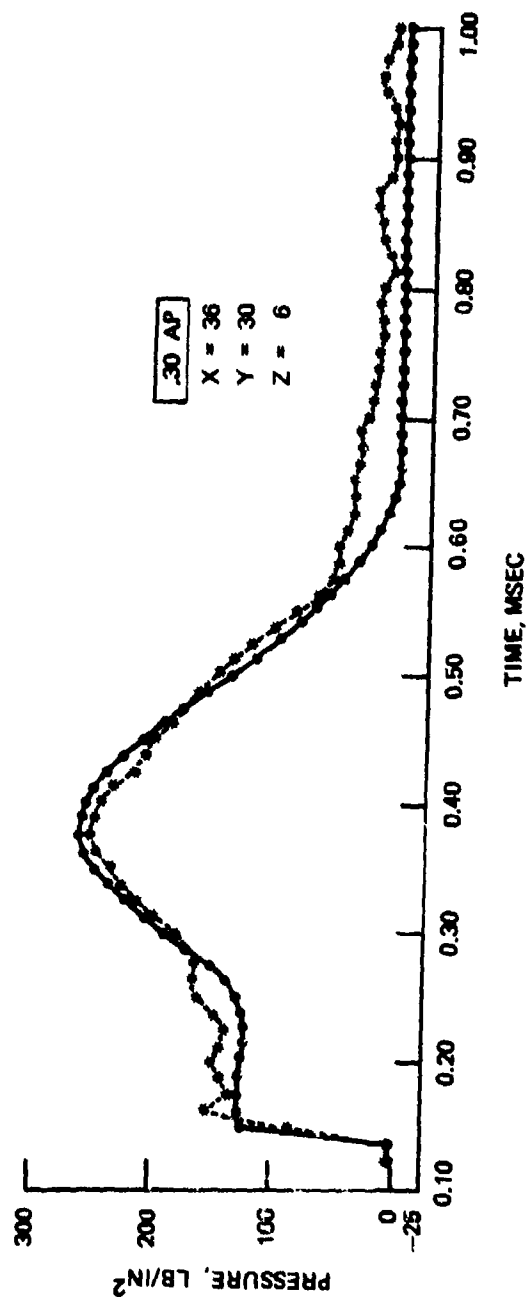


Figure 55. Pressure Versus Time Plot for Shot 4HR3 (Sheet 1 of 4).

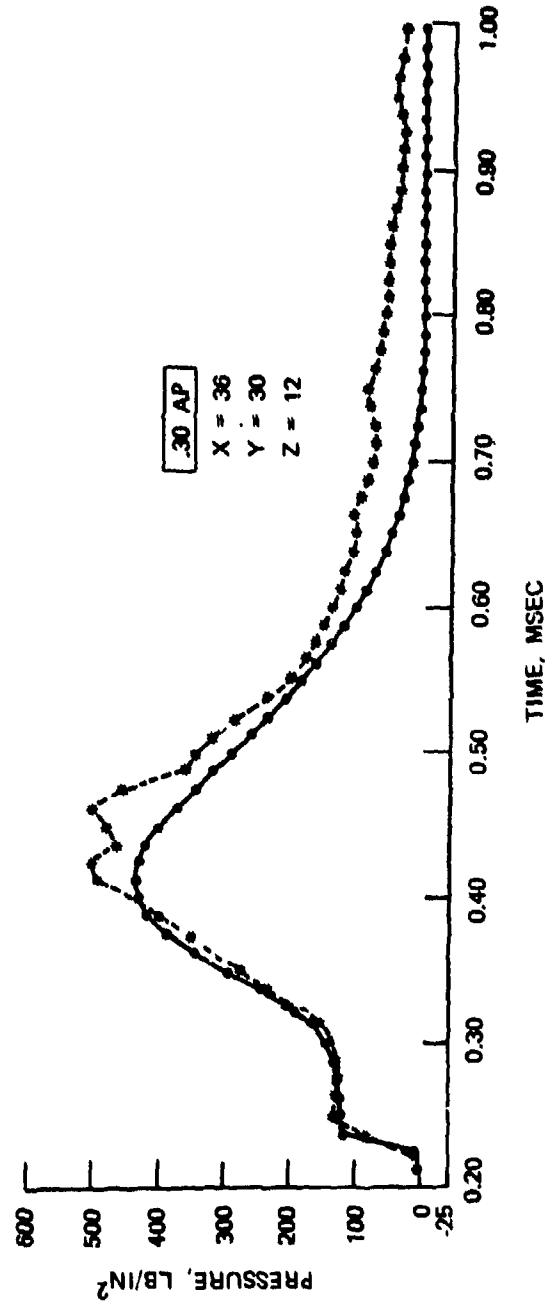


Figure 55. Pressure Versus Time Plot for Shoi 4HR3 (Sheet 2 of 4).



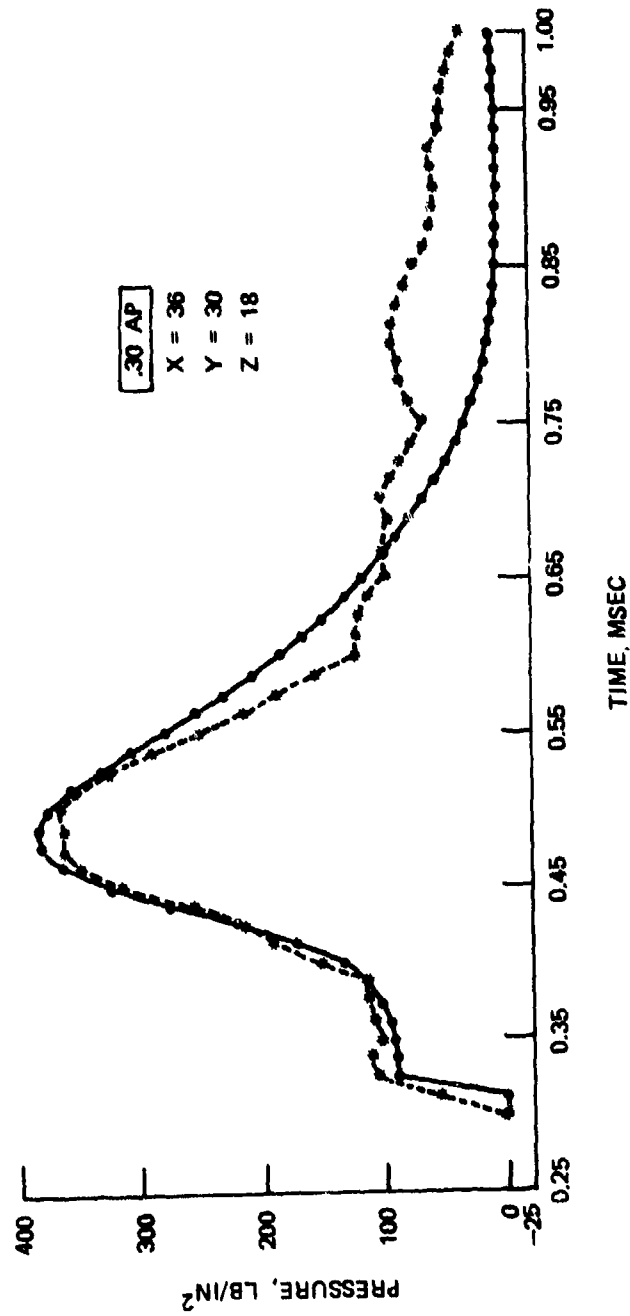


Figure 55. Pressure Versus Time Plot for Shot 4HR3 (Sheet 3 of 4).

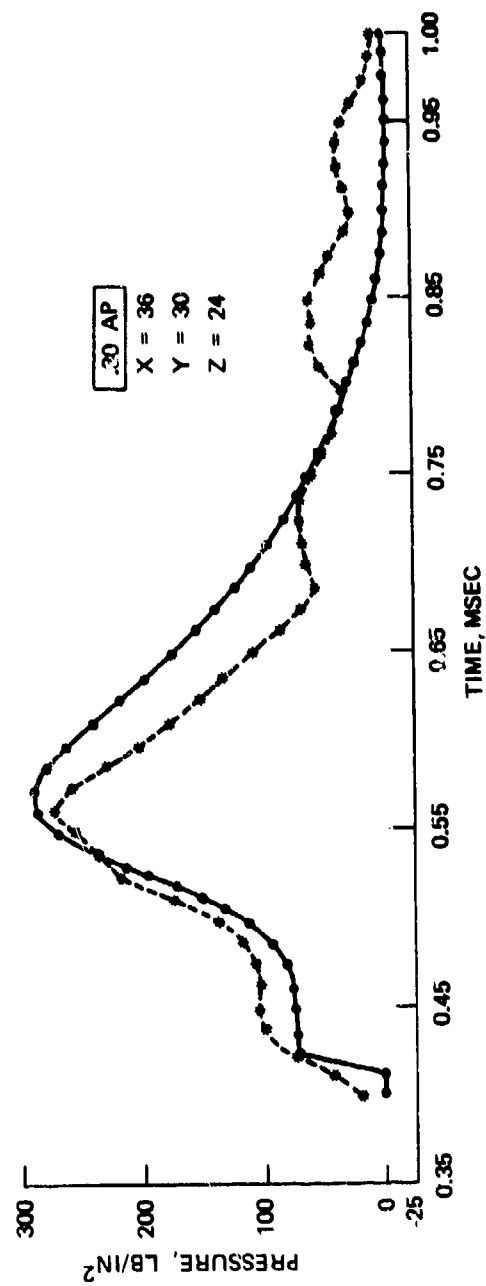


Figure 55. Pressure Versus Time Plot for Shot 4HR3 (Sheet 4 of 4).

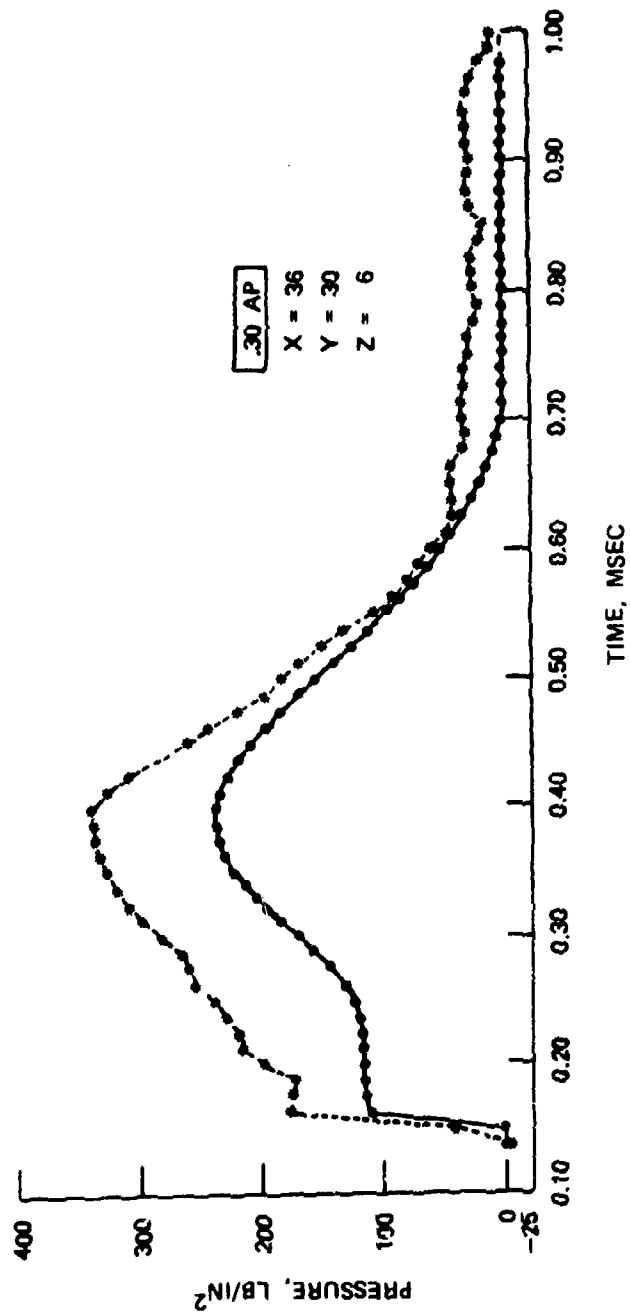


Figure 56. Pressure Versus Time Plot for Shot 4HR5 (Sheet 1 of 4).

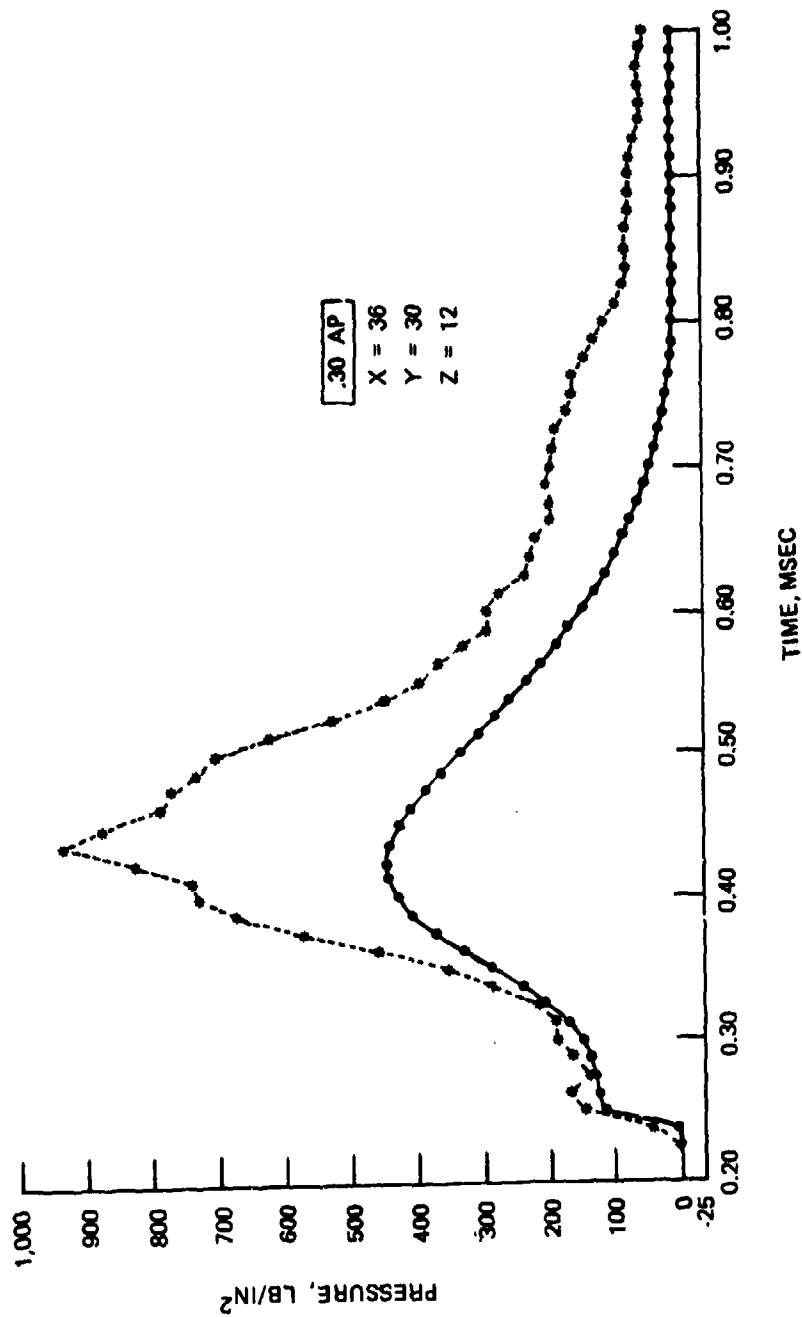


Figure 56. Pressure Versus Time Plot for Shot 4HR5 (Sheet 2 of 4).

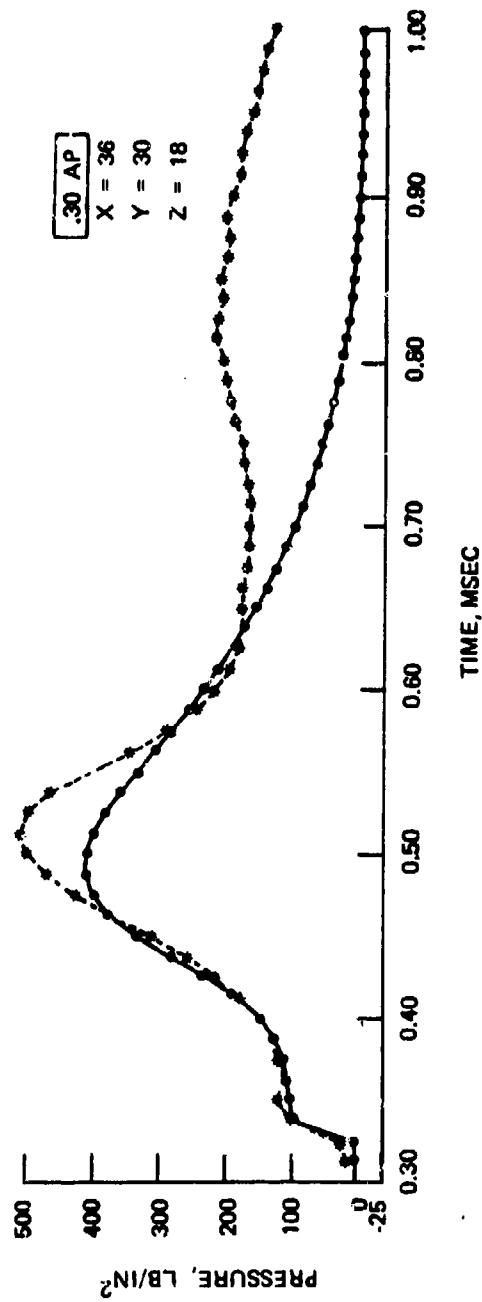


Figure 56. Pressure Versus Time Plot for Shot 4HR5 (Sheet 3 of 4).

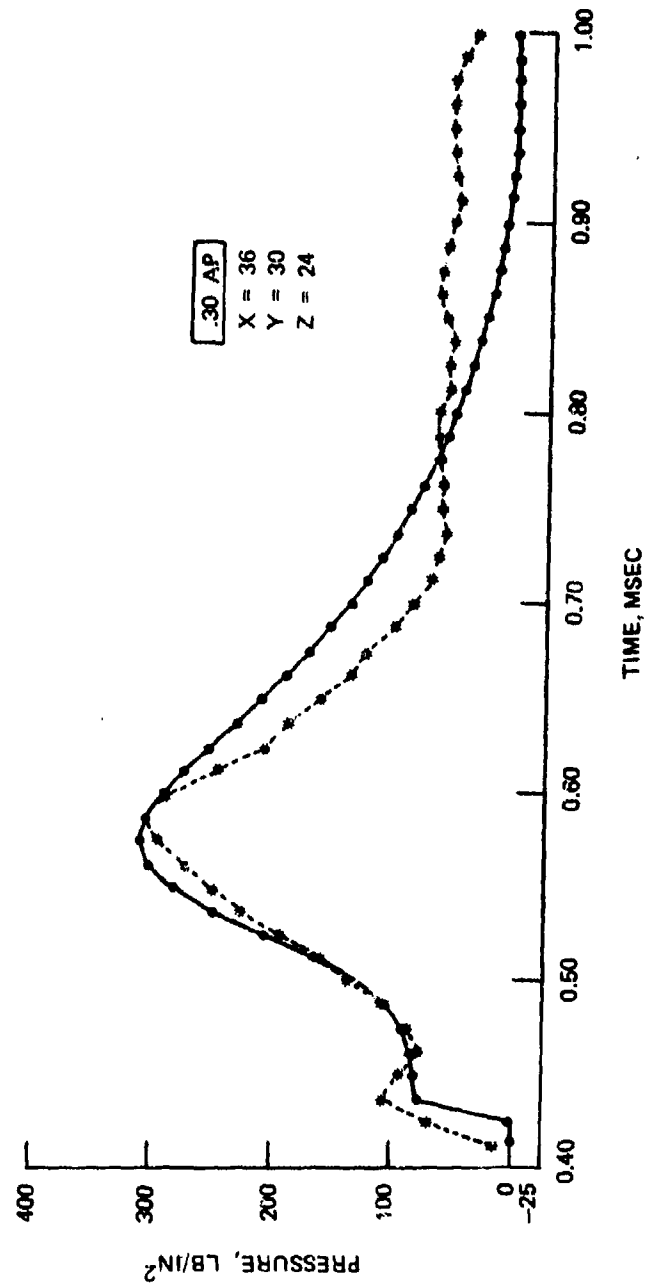


Figure 56. Pressure Versus Time Plot for Shot 4HR5 (Sheet 4 of 4).

## CONCLUSIONS AND RECOMMENDATIONS

An error was detected in the equations for the pressure field derived in *Fluid Dynamic Analysis of Hydraulic Ram*, see Footnote 1, page 1. To maintain consistent definitions of the source strength in equations 18 and 19, equation 19 must be modified to read  $U = \frac{2F}{W}$ . The result of this additional factor of 2 is that equations 37, 38, and 39 must also be multiplied by a factor of 2.

The hydraulic ram model, as modified in this report, gives an adequate description of the pressure field for the 0-degree obliquity shots. The theory consistently underestimated the pressure resulting from shots impacting the tank at 30- and 45-degree obliquities. Experiments at nonzero obliquity should be repeated with more appropriate instrumentation and tank geometry. A thin plastic sheet was used in the present work to obtain the coordinates of a point on the trajectory. This concept worked quite well except the sheet was placed too far from the impact point to be of value. Further experiments at nonzero obliquities should include one or more of these sheets placed closer to the impact point to obtain bullet deflection data.

The straight line trajectory assumption used in this work is satisfactory for most applications. However, to obtain a more accurate modeling of specific experiments, the trajectory could be described in terms of two or more straight line segments.

The hydraulic ram model can be applied easily to fragments with a velocity less than approximately 90% of the sound speed in the fluid. Experiments are required to obtain the drag coefficient of the fragments.

It was concluded that tumbling distances decrease with increased impact obliquity angle. No influence of the entrance panel material or thickness on the tumbling distances was observed. It was postulated that such a dependence could occur at bullet velocities nearer the ballistic limit of the panel. Tests were performed at full muzzle velocity of the round. Further experiments are desirable to check the velocity effect on the pressure field which is predicted by the hydraulic ram model. It is also anticipated that the tumbling behavior of the penetrating bullets will be affected by the initial velocity.

The foregoing recommendations deal only with the pressure wave generation model. The accuracy of this model was sufficiently verified so it is recommended that it be used as a basis for modeling the structural response of the tank walls to the fluid pressure.

JTCG/AS-74-T-015

INITIAL DISTRIBUTION

Aeronautical Systems Division (AFSC)

Wright-Patterson AFB, OH 45433

Attn: ASD/ENFEF (D.C. Wight)  
Attn: ASD/ENFTV (LT COL J.N. McCready)  
Attn: ASD/ENFTV (D.J. Wallick)  
Attn: ASD/XRHD (G.B. Bennett)  
Attn: ASD/XRHP (S.E. Tate)

Aerospace Medical Research Laboratories

Wright-Patterson AFB, OH 45433

Attn: AMRL/EMT (C.N. Day)

Air Force Aero Propulsion Laboratory

Wright-Patterson AFB, OH 45433

Attn: AFAPL/SFH (G.T. Beery)  
Attn: AFAPL/SFH (R.G. Clodfelter)  
Attn: AFAPL/SFH (A.J. Ferrenberg)  
Attn: AFAPL/SFH (G. Gandee)  
Attn: AFAPL/SFH (F.L. Sheldon)

Air Force Armament Laboratory

Eglin AFB, FL 32542

Attn: AFATL/DLYA (V.D. Thornton)

Air Force Flight Dynamics Laboratory

Wright-Patterson AFB, OH 45433

Attn: AFFDL/FER (C.V. Mayrand)  
Attn: AFFDL/FES (G.W. Ducker)  
Attn: AFFDL/FES (C.W. Harris)  
Attn: AFFDL/FES (J. Hodges)  
Attn: AFFDL/FES (R.W. Lauzze)  
Attn: AFFDL/FES (MAJ J.W. Mansur)  
Attn: AFFDL/FES (D.W. Voys)  
Attn: AFFDL/PTS (CDIC)  
Attn: AFFDL/TST (Library)

Air Force Materials Laboratory

Wright-Patterson AFB, OH 45433

Attn: AFML/LC (G.H. Griffith)  
Attn: AFML/MXE (A. Olevitch)

Air Force Test and Evaluation Center

Kirtland AFB, NM 87115

Attn: AFTEC-JT (MAJ Palmer)



Air Force Weapons Laboratory  
Kirtland AFB, NM 87117  
Attn: AFWL/PGV (CAPT D.J. Evans)  
Attn: AFWL/SATL (A.F. Gunther)

Armament Development and Test Center  
Eglin AFB, FL 32542  
Attn: ADTC/TS (M.H. Forbragd)

Army Air Mobility R&D Laboratory  
Eustis Directorate  
Fort Eustis, VA 23604  
Attn: SAVDL-EU-MOS (H.W. Holland)  
Attn: SAVDL-EU-MOS (J.D. Ladd)  
Attn: SAVDL-EU-MOS (C.M. Pedriani)  
Attn: SAVDL-EU-MOS (S. Pociluyko)  
Attn: SAVDL-EU-MOS (J.T. Robinson)  
Attn: SAVDL-EU-TAP

Army Aviation Systems Command  
P.O. Box 209  
St. Louis, MO 63166  
Attn: DRCPM-ASE (J. Keaton)  
Attn: DRCPM-ASE-TM (E.F. Branhof)  
Attn: DRCPM-ASE-TM (MAJ Schwend)  
Attn: DRCPM-ASH (R.J. Braun)  
Attn: DRSAB-ASE-TM (R.M. Tyson)  
Attn: DRSAB-EI (CAPT W.D. Wolfinger)  
Attn: DRSAB-EQP (F. Reed)  
Attn: DRSAB-EXH (J.C. Butler)

Army Ballistic Research Laboratories  
Aberdeen Proving Ground, MD 21005  
Attn: DRXBR-TB (J.T. Frasier)  
Attn: DRXBR-VL (R.G. Bernier)  
Attn: DRXBR-VL (A.J. Hoffman)  
Attn: DRXBR-VL (J.R. Jacobson)  
Attn: DRXBR-VL (O.T. Johnson)  
Attn: DRXBR-VL (R. Mayerhofer)  
Attn: DRXBR-VL (D.L. Rigotti)  
Attn: DRXBR-VL (W.S. Thompson)

Army Electronics Command  
Fort Monmouth, NJ 07703  
Attn: DRSEL-GG-EM (C. Goldy)

JTCG/AS-74-T-015

Army Materials and Mechanics Research Center  
Watertown, MA 02172

Attn: DRXMR-EM (A.A. Anctil)  
Attn: DRXMR-ER (F.C. Quigley)  
Attn: DRXMR-K (S.V. Arnold)  
Attn: DRXMR-MI (C.F. Hickey, Jr.)  
Attn: DRXMR-PL (M.M. Murphy)  
Attn: DRXMR-R (G.R. Thomas)  
Attn: DRXMR-RD (R.W. Lewis)  
Attn: DRXMR-TE (J. Adachi)  
Attn: DRXMR-XC (E.S. Wright)

Army Materiel Systems Analysis Activity  
Aberdeen Proving Ground, MD 21005

Attn: DRXSY-AA (Director)  
Attn: DRXSY-AAM (R.F. Mathias)  
Attn: DRXSY-AD (H.X. Peaker)  
Attn: DRXSY-J (J.J. McCarthy)

Army Missile Command  
Redstone Arsenal, AL 35809  
Attn: DRSMI-CS (R.B. Clem)

Chief of Naval Operations  
Washington, D.C. 20350  
Attn: OP-987 (Director)

Defense Documentation Center  
Cameron Station, Bldg. 5  
Alexandria, VA 22314  
Attn: DDC-TRS-1, 2 copies

Department of Transportation - FAA  
2100 Cond St., SW, Rm. 1400C  
Washington, D.C. 20591  
Attn: ARD-520 (R.A. Kirsch)

Deputy Chief of Staff (AIR)  
Marine Corps Headquarters  
Washington, D.C. 20380  
Attn: AAW-61 (LT COL F.C. Regan)

FAA/NAFEC  
Atlantic City, NJ 08405  
Attn: ANA-430 (L.J. Garodz)  
Attn: ANA-64 (NAFEC Library)

JTCG/AS-74-T-015

Foreign Technology Division (AFSC)  
Wright-Patterson AFB, OH 45433  
Attn: FTD/NICD

Marine Corps Development Center  
Quantico, VA 21134  
Attn: D-042 (MAJ W. Waddell)  
Attn: D-091 (LT COL J. Givan)

NASA - Ames Research Center  
Mail Stop 223-6  
Moffett Field, CA 94035  
Attn: SC (R.L. Altman)  
Attn: SC (J. Parker)

NASA - Ames Research Center  
Army Air Mobility R&D Laboratory  
Mail Stop 207-5  
Moffett Field, CA 94035  
Attn: SAVDL-AS (V.L.J. Di Rito)  
Attn: SAVDL-AS-X (F.H. Immen)

NASA - Johnson Spacecraft Center  
Houston, TX 77058  
Attn: JM6  
Attn: ES-5 (F.S. Dawn)

NASA - Lewis Research Center  
21000 Brookpark Rd.  
Mail Stop 500-202  
Cleveland, OH 44135  
Attn: Library (D. Morris)

National Bureau of Standards  
Building 225, Rm. A62  
Washington, D.C. 20234  
Attn: I.A. Benjamin

Naval Air Development Center  
Warminster, PA 18974

Attn: Code 063 (MAJ W. Boeck)  
Attn: Code 2043 (L.M. Rakszawski)  
Attn: Code 30C (R.A. Ritter)  
Attn: Code 30P72 (F.F. Borriello)  
Attn: Code 30212 (A.A. Conte, Jr.)  
Attn: Code 30231 (R.E. Trabocco)  
Attn: Code 303 (E.J. McQuillen)  
Attn: Code 3033 (S.L. Huang)  
Attn: Code 40A (D.A. Mancinelli)  
Attn: Code 402 (L. Hitchcock)  
Attn: Code 5422 (R.H. Beliveau)  
Attn: Code 5422 (F. Gonzalez)  
Attn: Code 5422 (M.C. Mitchell)  
Attn: Code 5422 (C.E. Murrow)  
Attn: Code 5422 (D.G. Tauras)  
Attn: Code 5422 (B. Vafakos)  
Attn: Code 5423 (B.L. Cavallo)

Naval Air Propulsion Test Center  
Trenton, NJ 08628  
Attn: PE3A (J. Mendrala)

Naval Air Systems Command  
Washington, D.C. 20361  
Attn: AIR-03PAF (CDR R.C. Gibson)  
Attn: AIR-03PA4 (T.S. Momiyama)  
Attn: AIR-330B (E.A. Lichtman)  
Attn: AIR-360D (R. Thyberg)  
Attn: AIR-503W1 (E.A. Thibault)  
Attn: AIR-5203 (R. Schmidt)  
Attn: AIR-5204  
Attn: AIR-5204A (D. Atkinson)  
Attn: AIR-5204J (LT COL R.T. Remers)  
Attn: AIR-53031 (R.O. Lutz)  
Attn: AIR-530313 (R.D. Hume)  
Attn: AIR-531  
Attn: AIR-5323  
Attn: AIR-53242 (C.F. Magee)  
Attn: AIR-5363  
Attn: AIR-53632E (C.D. Johnson)

Naval Material Command  
Washington, D.C. 20360  
Attn: MAT-0331 (H.G. Moore)

Naval Ordnance Station  
Indian Head, MD 20640  
Attn: Code 5123F (D.H. Brooks)

Naval Postgraduate School  
Monterey, CA 93948  
Attn: Code 57BP (R.E. Ball)  
Attn: Code 57BT (M.H. Bank)

Naval Research Laboratory  
4555 Overlook Ave. SW  
Washington, D.C. 20375  
Attn: Code 2627  
Attn: Code 5367 (D.L. Ringwalt)  
Attn: Code 6000 (A.I. Schindler)  
Attn: Code 6360 (R.W. Rice)  
Attn: Code 8430 (J.M. Krafft)  
Attn: Code 8432 (H.L. Smith)

Naval Sea Systems Command  
Washington, D.C. 20362  
Attn: SEA-03511 (C.H. Pohler)

Naval Ship Engineering Center  
Hyattsville, MD 20782  
Attn: Code 6105D

Naval Ship R&D Center  
Annapolis, MD 21402  
Attn: Code 2831 (R.W. McQuaid)  
Attn: Code 2851 (R.O. Foernsler)  
Attn: Code 2851 (J.R. Lugar)

David W. Taylor Naval Ship R&D Center  
Bethesda, MD 20084  
Attn: Code 1740.2 (F.J. Fisch)  
Attn: Code 1740.2 (O.F. Hackett)

Naval Surface Weapons Center  
Dahlgren Laboratory  
Dahlgren, VA 22448  
Attn: DF-52 (W.S. Lenzi)  
Attn: DG-10 (S. Hock)  
Attn: DG-10 (T.L. Wasmund)  
Attn: DG-104 (T.H. McCants)  
Attn: DK-23 (B.W. Montrief)  
Attn: DT-51 (J.F. Horton)  
Attn: Library (A.D. Hopkins)

Naval Surface Weapons Center  
White Oak Laboratory  
Silver Spring, MD 20910  
Attn: WA-11 (L.C. Dixon)  
Attn: WA-11 (E.F. Kelton)  
Attn: WU-41 (J.C. Hetzler)

JTCG/AS-74-T-015

Naval Weapons Center

China Lake, CA 93555

Attn: Code 35033 (W.W. West)  
Attn: Code 40 (M.M. Rogers)  
Attn: Code 40701 (M.H. Keith)  
Attn: Code 408 (W.T. Burt)  
Attn: Code 408 (H. Drake)  
Attn: Code 408 (C. Padgett)  
Attn: Code 4081 (C.B. Sandberg)  
Attn: Code 4083 (G. Moncsko)  
Attn: Code 4085 (C. Driussi)  
Attn: Code 5123 (R.R. Wahler)

Naval Weapons Support Center

Crane, IN 47522

Attn: Code 502 (N.L. Papke)  
Attn: Code 5041 (D.K. Sanders)

Office of Naval Research

Arlington, VA 22217

Attn: Code 474 (N. Perrone)

Pacific Missile Test Center

Point Mugu, CA 93042

Attn: Code 1264 (D.L. Hendrix)  
Attn: Code 1332 (J.R. Bok)  
Attn: Code 1332 (W.E. Chandler)  
Attn: Code 1332 (B.E. Nofrey)

Picatinny Arsenal

Dover, NJ 07801

Attn: SARPA-AD-C (S.K. Einbinder)

Rock Island Arsenal

Rock Island, IL 61201

Attn: DRSAR-PPV (D.K. Kotecki)

San Antonio Air Logistics Center

Kelly AFB, TX 78241

Attn: ALC/MMSRE

Warner Robins Air Logistics Center

Robins AFB, GA 31098

Attn: WRALC/MMET (LT COL G.G. Dean)

Aeroquip Corp.

Subsidiary of Libbey-Owens Ford Co.

300 S. East Ave.

Jackson, MI 49203

Attn: E.R. Steinert  
Attn: R. Rogers

Armament Systems, Inc.  
712-F North Valley  
Anaheim, CA 92801  
Attn: J. Musch

AVCO Corp.  
Lycoming Division  
550 So. Main St.  
Stratford, CT 06497  
Attn: R. Cuny  
Attn: H.F. Grady

Battelle Memorial Institute  
505 King Ave.  
Columbus, OH 43201  
Attn: J.H. Brown, Jr.

Beech Aircraft Corp.  
9709 E. Central Ave.  
Wichita, KS 67201  
Attn: Engineering Library (T.R. Hales)  
Attn: R.J. Wood

Bell Helicopter Co.  
A Textron Co.  
P.O. Box 482  
Fort Worth, TX 76101  
Attn: J.R. Johnson  
Attn: J.F. Jagers  
Attn: E.A. Morris

Boeing Vertol Company  
A Division of The Boeing Co.  
P.O. Box 16858  
Philadelphia, PA 19142  
Attn: J.E. Gonsalves, M/S P32-19

Calspan Corp.  
P.O. Box 235  
Buffalo, NY 14221  
Attn: Library (V.M. Young)

CDI Corp.  
M & T Co.  
2130 Arch St.  
Philadelphia, PA 19103  
Attn: E.P. Lorge  
Attn: R.L. Hall

Cessna Aircraft Co.  
Wallace Division  
P.O. Box 1977  
Wichita, KS 67201  
Attn: B.B. Overfield

E-Systems Inc.  
Greenville Division  
P.O. Box 1056  
Greenville, TX 75401  
Attn: C.H. Hall, 8-55200C  
Attn: Librarian (J. Moore)

Fairchild Industries, Inc.  
Fairchild Republic Co.  
Conklin St.  
Farmingdale, L.I., NY 11735  
Attn: J.A. Arrighi  
Attn: Engineering Library (G.A. Mauter)

Falcon Research and Development Co.  
696 Fairmount Ave.  
Baltimore, MD 21204  
Attn: W.J. Douglass, Jr.

Falcon Research and Development Co.  
601 San Pedro NE, Suite 205  
Albuquerque, NM 87108  
Attn: W.L. Baker

Fiber Science, Inc.  
245 East 157th St.  
Gardena, CA 90248  
Attn: E. Abildskov

Fiber Science, Inc.  
7006 Sea Cliff Rd.  
McLean, VA 22101  
Attn: R.N. Flath

Firestone Coated Fabrics Co.  
P.O. Box 864  
Magnolia, AR 71753  
Attn: L.T. Reddick

General Dynamics Corp.  
Convair Division  
P.O. Box 80877  
San Diego, CA 92138  
Attn: Research Library (U.J. Sweeney)  
Attn: J.P. Waszczak



General Dynamics Corp.  
Fort Worth Division  
Grants Lane, P.O. Box 748  
Fort Worth, TX 76101  
Attn: P.R. deTonnancour/G.W. Bowen

General Electric Co.  
Aircraft Engine Group  
1000 Western Ave.  
West Lynn, MA 01905  
Attn: E.L. Richardson  
Attn: J.M. Wannemacher

General Electric Co.  
Aircraft Engine Group  
Evendale Plant  
Cincinnati, OH 45215  
Attn: AEG Technical Information Center (J.J. Brady)

General Research Corp.  
Science and Technology Division  
5383 Hollister Ave.  
P.O. Box 3587  
Santa Barbara, CA 93105  
Attn: R. Rodman

Goodyear Aerospace Corp.  
1210 Massillon Rd.  
Akron, OH 44315  
Attn: J.R. Wolfersberger, D/152G  
Attn: J.E. Wells, D/959  
Attn: H.D. Smith, D/490G  
Attn: T.L. Shubert, D/910

Grumman Aerospace Corp.  
South Oyster Bay Rd.  
Bethpage, NY 11714  
Attn: J.P. Archey, D/662  
Attn: R.W. Harvey, D/661  
Attn: H.L. Henze, D/471  
Attn: Technical Information Center (J. Davis)

Hughes Helicopters  
A Division of Summa Corp.  
Centinela & Teale St.  
Culver City, CA 90230  
Attn: R.E. Rohtert (15T288)  
Attn: Library (2/T2124, D.K. Goss)

JTCG/AS-74-T-015

ITT Research Institute  
10 West 35th Street  
Chicago, IL 60616  
Attn: K. McKee  
Attn: I. Pincus

JG Engineering Research Associates  
3831 Menlo Dr.  
Baltimore, MD 21215  
Attn: J.E. Greenspon

Kamen Aerospace Corporation  
Old Winsor Rd.  
Bloomfield, CT 06002  
Attn: H.E. Showalter

Lockheed - California Co.  
A Division of Lockheed Aircraft Corp.  
Burbank, CA 91503  
Attn: Technological Information Center (84-40, U-35, A-1)

Lockheed - California Co.  
A Division of Lockheed Aircraft Corp.  
P.O. Box 551  
Burbank, CA 91520  
Attn: C.W. Cook  
Attn: L.E. Channel

Lockheed - Georgia Co.  
A Division of Lockheed Aircraft Corp.  
86 S. Cobb Drive  
Marietta, GA 30063  
Attn: C.K. Bauer  
Attn: D.R. Scarbrough

LTV Aerospace Corporation  
Vought Systems Division  
P.O. Box 5907  
Dallas, TX 75222  
Attn: G. Gilder, Jr.  
Attn: Unit 2-54244 (D.M. Reedy)

Martin-Marietta Corp.  
Orlando Division  
P.O. Box 5837  
Orlando, FL 32805  
Attn: Library (M.C. Griffith)

McDonnell Aircraft Co.  
McDonnell Douglas Corp.  
P.O. Box 516  
St. Louis, MO 63166  
Attn: R.D. Detrich  
Attn: R.A. Eberhard  
Attn: Library  
Attn: M. Meyers

McDonnell Douglas Corp.  
3855 Lakewood Blvd.  
Long Beach, CA 90846  
Attn: Technical Library (Cl 290/36-84)

New Mexico Institute of Mining and Technology  
Socorro, NM 87801  
Attn: TERA

Northrop Corp.  
Aircraft Division  
3901 W. Broadway  
Hawthorne, CA 90250  
Attn: Code 3680/35 (J.H. Bach)  
Attn: V.B. Bertagna  
Attn: Mgr. Library Services (H.W. Jones)  
Attn: Code 3680/35 (W. Hohlenhoff)  
Attn: Code 3628/33 (J.R. Oliver)  
Attn: Code 3628/33 (J.F. Paris)

Northrop  
Ventura Division  
1515 Rancho Conejo Blvd.  
Newbury Park, CA 91320  
Attn: M. Raine

Parker Hannifin Corp.  
18321 Jamboree Rd.  
Irvine, CA 92664  
Attn: C.L. Kimmel  
Attn: J.E. Lowes

Potomac Research, Inc.  
7655 Old Springhouse Rd.  
Westgate Research Park  
McLean, VA 22101  
Attn: D.E. Wegley

JTCG/AS-74-T-015

PRC Technical Applications, Inc.  
7600 Old Springhouse Rd.  
McLean, VA 22101  
Attn: G.E. Monroe

Protective Materials Co.  
York St.  
Andover, MA 01810  
Attn: M.H. Miller

Rockwell International Corp.  
4300 E. Fifth Ave.  
P.O. Box 1259  
Columbus, OH 43216  
Attn: Technical Information Center (D.Z. Cox)

Rockwell International Corp.  
Los Angeles Aircraft Division  
B-1 Division  
International Airport  
Los Angeles, CA 90009  
Attn: W.L. Jackson  
Attn: R. Moonan, AB78  
Attn: S.C. Mellin  
Attn: W.H. Hatton, BB-18

Rockwell International Corp.  
B-1 Division  
5701 Imperial Highway  
Los Angeles, CA 90009  
Attn: R. Hurst, BB33

Russell Plastics Tech.  
521 W. Hoffman Ave.  
Lindenhurst, NY 11757  
Attn: J.C. Hebron

Sikorsky Aircraft  
A Division of United Aircraft Corp.  
Main Street  
Stratford, CT 06602  
Attn: D. Fansler/S. Okarma  
Attn: J.B. Faulk

Southwest Research Institute  
8500 Culebra Rd.  
P.O. Drawer 28510  
San Antonio, TX 78284  
Attn: Bussuy-02  
Attn: W.D. Weatherford

Teledyne CAE  
1330 Laskey Rd.  
Toledo, OH 43697

Attn: Librarian (M. Dowdell)  
Attn: Librarian (M. Dowdell/W.Q. Wagner)  
Attn: Librarian (M. Dowdell/A.E. Kirschmann)

Teledyne Ryan Aeronautical  
2701 Harbor Dr.  
San Diego, CA 92112

Attn: Technical Information Services (W.E. Ebner)  
Attn: P. Kleyn  
Attn: N.S. Sakamoto

The BDM Corp.  
1920 Aline Ave.  
Vienna, VA 22180  
Attn: J.W. Milanski

The Boeing Co.  
Wichita Division  
3801 S. Oliver St.  
Wichita, KS 67210  
Attn: H.E. Corner, M/S K21-57  
Attn: D.Y. Sink, M/S K16-14  
Attn: Library

The Boeing Co.  
Aerospace Corp.  
P.O. Box 3999  
Seattle, WA 98124  
Attn: J.G. Avery, M/S 41-37  
Attn: R.G. Blaisdell, M/S 8C-42  
Attn: R.J. Helzer, M/S 13-66

Uniroyal, Inc.  
Mishawaka Plant  
407 N. Main St.  
Mishawaka, IN 46544  
Attn: J.D. Galloway

Uniroyal, Inc.  
Government Affairs  
1700 K. St., NW  
Washington, D.C. 20006  
Attn: D. Gillett

# ABSTRACT CARD

Naval Weapons Center

*Fluid Dynamic Analysis of Hydraulic Ram III (Result of Analysis)*, by E. A. Lundstrom and W. K. Fung. China Lake, CA, for Joint Technical Coordinating Group/Aircraft Survivability, September 1976, 134 pp. (Report JTCG/AS-74-T-015, publication UNCLASSIFIED.)

This report presents an analysis of the tests results of pressure waves generated by a penetrating projectile in fluid and verifies a theory modeling the pressure waves. The method of data reduction and verification also is presented.

Card UNCLASSIFIED

1 card, 8 copies



Naval Weapons Center

*Fluid Dynamic Analysis of Hydraulic Ram III (Result of Analysis)*, by E. A. Lundstrom and W. K. Fung. China Lake, CA, for Joint Technical Coordinating Group/Aircraft Survivability, September 1976, 134 pp. (Report JTCG/AS-74-T-015, publication UNCLASSIFIED.)

This report presents an analysis of the tests results of pressure waves generated by a penetrating projectile in fluid and verifies a theory modeling the pressure waves. The method of data reduction and verification also is presented.

Card UNCLASSIFIED

1 card, 8 copies



Naval Weapons Center

*Fluid Dynamic Analysis of Hydraulic Ram III (Result of Analysis)*, by E. A. Lundstrom and W. K. Fung. China Lake, CA, for Joint Technical Coordinating Group/Aircraft Survivability, September 1976, 134 pp. (Report JTCG/AS-74-T-015, publication UNCLASSIFIED.)

This report presents an analysis of the tests results of pressure waves generated by a penetrating projectile in fluid and verifies a theory modeling the pressure waves. The method of data reduction and verification also is presented.

Card UNCLASSIFIED

1 card, 8 copies



Naval Weapons Center

*Fluid Dynamic Analysis of Hydraulic Ram III (Result of Analysis)*, by E. A. Lundstrom and W. K. Fung. China Lake, CA, for Joint Technical Coordinating Group/Aircraft Survivability, September 1976, 134 pp. (Report JTCG/AS-74-T-015, publication UNCLASSIFIED.)

This report presents an analysis of the tests results of pressure waves generated by a penetrating projectile in fluid and verifies a theory modeling the pressure waves. The method of data reduction and verification also is presented.

Card UNCLASSIFIED

1 card, 8 copies



JTCG/AS-74-T-015

United Technologies Corp.  
United Technologies Research Center  
Silver Lane, Gate 5R  
East Hartford, CT 06108  
Attn: UTC Library

University of Denver  
Denver Research Institute  
University Part  
Denver, CO 80210  
Attn: R.F. Recht

Williams Research Corp.  
2280 W. Maple Rd.  
Walled Lake, MI 48088  
Attn: Library